Characterisation of beech wood pyrolysis oil: chemical and physical properties and decomposition kinetics

Maximilian Dammann[a,b,c,*], Fabian Hüsing[a,b], Ulrike Santo[b], David Böning[b], Marco Mancini[c], Thomas Kolb[a,b]

[a] *Karlsruhe Institute of Technology (KIT), Engler-Bunte-Institute, Fuel Technology (EBI ceb), Engler-Bunte-Ring 1, 76131 Karlsruhe, Germany*
[b] *Karlsruhe Institute of Technology (KIT), Institute for Technical Chemistry, Gasification Technology (ITC vgt), Hermann-von-Helmholtz-Platz 1, 76344 Eggenstein-Leopoldshafen, Germany*
[c] *Clausthal University of Technology, Institute for Energy Process Engineering and Fuel Technology (IEVB), Agricolastraße 4, 38678 Clausthal-Zellerfeld, Germany*

Abstract

Biogenic and anthropogenic pyrolysis oils can be used as renewable feedstocks in combustion and entrained flow gasification processes. The design, evaluation and scale-up of these processes can be done using process and CFD models. However, this requires comprehensive and consistent data sets for the chemical and thermo-physical properties and the decomposition kinetics. Such data sets have not yet been compiled for research or for commercial pyrolysis oils. Therefore, this study characterised an industrial beech wood pyrolysis oil using (i) proximate, ultimate and heating value analyses, (ii) gas chromatography-mass spectrometry (GC-MS), gel permeation chromatography (GPC) and thermogravimetric (TG) analyses, (iii) vacuum and Engler distillations and (iv) measurements of density, dynamic viscosity, thermal conductivity, specific heat capacity and surface tension under atmospheric-pressure and low-temperature conditions. The chemical analyses demonstrated significant uncertainties in the sampling and the analysis methods, which strongly affect the design and evaluation of pilot-scale entrained flow gasification experiments. The vacuum distillations provided representative samples of the vaporisable

*Corresponding author.
ORCID: https://orcid.org/0000-0002-2851-7787.

and non-vaporisable components to a large extent. The TG analyses showed the superposition of vaporisation and decomposition based on separate analyses of the vacuum distillate and the vacuum distillation residue. Furthermore, thermo-physical property models were developed for the beech wood pyrolysis oil, the vacuum distillate and the vacuum distillation residue. Finally, thermogravimetric kinetics were derived based on multi-reaction Arrhenius law models and multi first-order reaction Gauss distributed activation energy models. Single-particle predictions based on these kinetics indicated that multi first-order reaction Gauss distributed activation energy models should be preferred for extrapolation to high heating rates in the absence of kinetics based on drop-tube reactor experiments.

Keywords: Pyrolysis oil, Bio oil, Properties, Kinetics, Entrained flow, Gasification

---

Nomenclature

Latin symbols

C	coefficient
$\hat{C}_p$	specific isobaric heat capacity
$\overline{E}_\mathrm{a}$	molar activation energy
$\overline{\boldsymbol{E}}_\mathrm{a}$	molar activation energy vector
f	probability density function
g	auxiliary function in Merrick model
$\dot{H}$	enthalpy flow rate
k_0	pre-exponential factor
$\boldsymbol{k}_0$	pre-exponential factor vector
$\dot{m}$	mass flow rate
M	molar mass
n	reaction order

$\boldsymbol{n}$	reaction order vector
N	number of parallel reactions
p	pressure
P_{th}	thermal input
$\dot{Q}$	heat flow rate
r	volume fraction
$\overline{R}$	molar gas constant
s	uncertainty
t	time
T	temperature
w	mass fraction
$\boldsymbol{w}$	mass fraction vector
X	conversion
Greek symbols	
β	heating rate
η	dynamic viscosity
λ	stoichiometric ratio
λ	thermal conductivity
μ	expectation
$\boldsymbol{\mu}$	expectation vector
ρ	density
σ	standard deviation
$\boldsymbol{\sigma}$	standard deviation vector
σ	surface tension
φ	parameter in Maxwell mixing rule

Subscripts and superscripts

af	on ash-free basis
ash	of ash
asr	on as-received basis
d	on dry basis
eq	equilibrium
$\overline{E}_\mathrm{a}$	of the Gaussian distribution of the molar activation energy
i	of reaction i
i	of species i
j	of (mixture) j, in (mixture) j
m	mass-weighted mean
max	maximum
n	number-weighted mean
ng	of natural gas
oil	of the beech wood pyrolysis oil
op	operating
part	particle
slurry	of slurry
solid	of solid compounds
steam	of steam
tot	total
vd	of the vacuum distillate
vdr	of the vacuum distillation residue
0	initial
β	recovered

Acronyms

bioliq EFG	bioliq Entrained Flow Gasifier
CDF	cumulative distribution function
CFD	computational fluid dynamics
CGE	cold gas efficiency
DTG	differential thermogravimetric
EXT I, II or III	external laboratory I, II or III
FID	flame ionisation detector
GC-MS	gas chromatography-mass spectrometry
GPC	gel permeation chromatography
HCR	atomic hydrogen/carbon ratio
HHV	higher heating value
KIT	Karlsruhe Institute of Technology
KIT I, II or III	KIT laboratory I, II or III
LHV	lower heating value
MFORALM	multi first-order reaction Arrhenius law model
MFORGDAEM	multi first-order reaction Gauss distributed activation energy model
MRALM	multi-reaction Arrhenius law model
PD	polydispersity
PDF	probability density function
SMOD	specific minimum oxygen demand
TG	thermogravimetric
UV	ultraviolet

1. Introduction

Biogenic pyrolysis oils, also known as bio-oils, are the liquid products of the thermal decomposition of biogenic substances in the absence of oxygen [1]. Substances, such as cellulose, hemicellulose and lignin, decompose into numerous liquid and solid components depending on the raw material and the pretreatment process employed [2–7]. Industrial pyrolysis oils are mainly produced using fast pyrolysis processes. These processes are operated at moderate temperatures ($\sim$ 500 K), high heating rates ($\sim$ 10^4-10^5 K/s) and short residence times ($<$ 2 s) [1] and provide pyrolysis oils that can be applied as alternative feedstocks in both combustion and entrained flow gasification processes. Production processes, experimental characterisation methods and applications of pyrolysis oils have therefore been investigated and reviewed in numerous studies [1, 8–13].

1.1. Experimental studies

Biogenic pyrolysis oils are typically characterised through (i) the analysis of elemental, solid, water and ash contents, (ii) the analysis of heating values, flash points, ambient density and ambient dynamic viscosity, (iii) the gas chromatography-mass spectrometry (GC-MS) analysis and (iv) the analysis of long-term and thermal stability and miscibility. The ranges of the chemical and physical properties derived from such analyses are given in Tables 1 and 7.

Table 1: Carbon contents (dry) $w_{\mathrm{C,oil,d}}$, hydrogen contents (dry) $w_{\mathrm{H,oil,d}}$, oxygen contents (dry) $w_{\mathrm{O,oil,d}}$, nitrogen contents (dry) $w_{\mathrm{N,oil,d}}$, sulphur contents (dry) $w_{\mathrm{S,oil,d}}$, ash contents (dry) $w_{\mathrm{ash,oil,d}}$, water contents (as received) $w_{\mathrm{H_2O,oil,asr}}$ and higher heating values (as received) $\mathrm{HHV}_{\mathrm{oil,asr}}$ of biogenic pyrolysis oils based on previous studies [8, 14].

$\frac{w_{\mathrm{C,oil,d}}}{\%}$	$\frac{w_{\mathrm{H,oil,d}}}{\%}$	$\frac{w_{\mathrm{O,oil,d}}}{\%}$	$\frac{w_{\mathrm{N,oil,d}}}{\%}$	$\frac{w_{\mathrm{S,oil,d}}}{\%}$	$\frac{w_{\mathrm{ash,oil,d}}}{\%}$	$\frac{w_{\mathrm{H_2O,oil,asr}}}{\%}$	$\frac{w_{\mathrm{solid,oil,asr}}}{\%}$	$\frac{\mathrm{HHV}_{\mathrm{oil,asr}}}{\mathrm{MJ/kg}}$
38.1-62.9	4.6-10.3	29.8-51.4	0-0.2	0-0.01	0-0.2	5-45	0.2-1	16-25

Measurements of further chemical and physical properties have been conducted less frequently for biogenic pyrolysis oils. In particular, previous

studies have rarely measured (i) density and dynamic viscosity at moderate temperatures, (ii) vapour pressure, thermal conductivity, specific heat capacity and refractive index and (iii) distillation curves and molar mass distribution curves. Bakhshi and Adjaye [15] determined vapour pressure curves, and atmospheric and vacuum distillation curves of commercial Ensyn pyrolysis oils. Peacocke et al. [16] measured densities, viscosities, thermal conductivities, specific heat capacities and refractive indices of Ensyn pyrolysis oils mainly between 293 K and 343 K under both inert and oxygen-rich conditions to study the impact of ageing. Elliott et al. [17] determined the density and the dynamic viscosity of three biomass fast pyrolysis oils and correlated both properties with the water content.

More efforts (see Table S1) have been made to study the conversion of biogenic pyrolysis oils under inert or combustion conditions. Thermogravimetric (TG) analyses, differential scanning calorimetry (DSC) experiments, batch or drop-tube furnace experiments and single-droplet experiments were employed to investigate decomposition steps, kinetics and products as well as yields, reactivity, morphology and atomisation quality [3–5, 18–32]. Specifically, TG analyses were used to assign characteristic temperature ranges to the decompositions steps [3, 18]. The vaporisation of light volatiles (e. g. water and acetic acid) and heavy volatiles (e. g. furans and carbohydrates), the formation of secondary char, the low-temperature cracking and the release of gaseous decomposition products (CH_4, C_xH_y, CO, CO_2 and H_2O) was primarily observed below 600 K [3, 18], whereas the heterogeneous combustion of secondary char mainly took place above 600 K in the presence of oxygen [3, 18]. In addition, TG analyses were applied to develop decomposition kinetics using multi-reaction Arrhenius law models with 3-8 parallel reactions [4, 20, 21, 24]. The kinetics were derived from TG and DTG curves at various heating rates assuming unique sets of pre-exponential factors, activation energies and reaction orders for each biogenic pyrolysis oil [4, 20, 21]. However, the kinetics were mainly developed for combustion conditions [4, 20, 21], i. e. the decomposition was superposed by oxidation. Moreover, TG analyses

were combined with DSC experiments, GC-MS analyses and gel permeation chromatography (GPC) analyses [5, 21, 24]. The results showed that the peaks of the TG and DSC curves can be identified at similar positions (between 683 K and 723 K) in the presence of oxygen [24] and that similar compositions in terms of macro-families (water, monolignols, polar components, sugars, etc.) can be derived from thermogravimetric and molar mass distribution curves by proportionate superposition of the corresponding curves of the macro-families [5].

Furthermore, thermogravimetric analysers, differential scanning calorimeters, batch furnaces and drop-tube furnaces were used to study the yields of gas, condensates and char. The results showed that, with higher reactor temperature, the gas yield increases and the yields of char and condensates decrease, while a higher heating rate increases the condensates yield and decreases the char yield at an almost constant gas yield [26, 27, 29]. In addition to that, a higher content of vaporisables and a higher pressure increase the char yield [25, 31], whereas a higher ash content decreases the gas yield and increases the char yield and also shifts the gas composition to more CO_2 and less CH_4 and CO [29]. Thus, lower temperatures, lower heating rates (due to longer reaction times), higher ash contents and higher pressures (due to higher boiling temperatures) favour the thermal re-polymerisation (typically between 523 K and 773 K) and the production of char. The char yield is between 1 % at high heating rates and atmospheric pressures and 40 % at low heating rates and elevated pressures [26, 27, 29, 32]. In addition, an increase in heating rate from $\sim$ 1 K/min to $\geq$ 10^5 K/min reduces the char yield from 30 % to 8 % [26], while an increase in pressure from 1 bar to 40 bar doubles the char yield from 20 % to 40 % in a differential scanning calorimeter [32]. Furthermore, the results showed that the char residues from drop-tube experiments have hollow-spherical structures, compositions similar to graphite, reactivities similar to biomass chars and sizes that are similar to the original droplets [26, 27, 32]. The char reactivities decrease when exposing chars to higher temperatures [26]. In contrast, chars from thermogravimetric

analyses have compact glossy surfaces and high hydrogen and oxygen contents due to pronounced devolatilisation [28]. The decomposition kinetics of the latter chars can be described using four-reaction Arrhenius law models [28].

Previous studies also showed that analysis and measurement results are affected by high uncertainties. This is because of (i) fuel complexity, variability and inhomogeneity, (ii) long-term and thermal fuel instability and (iii) the lack of standardised analysis methods. In particular, the heterogeneous composition of biogenic pyrolysis oils as well as the handling, storage and ageing of samples have challenged the comparability of analysis and measurement results [11, 16, 27, 33]. Therefore, several studies [8, 10, 11, 34] reviewed and standardised the analysis methods, while inter-laboratory round robin tests [35–39] were carried out to investigate the influence of individual laboratory methods on the experimental results. Moreover, Brigdwater et al. [33] provided recommendations for the analysis of elemental and water contents and concluded, based on various test reports, that carbon and hydrogen contents can be reproduced with good accuracy. Furthermore, Harman-Ware and Ferrel [34] recommended GPC analysis for determining the molar mass distributions but suggested improvements to enable the use of GPC analysis for a wide range of biogenic pyrolysis oils.

1.2. Modelling studies

Chemical and physical properties at initial and intermediate conversion states as well as reaction kinetics are essential for describing the conversion of biogenic pyrolysis oils in both combustion and entrained flow gasification processes. However, in the absence of appropriate data and models, the conversion of biogenic pyrolysis oils has mainly been modelled using the surrogate vaporisation approach. Zhang and Kong [40], Saha et al. [41], Sallevelt et al. [42], Mahmoudi et al. [43] and Sital [44] defined surrogates with up to ten volatile components based on GC-MS data reported for bio-oils [2, 3]. However, major organic components seldom have mass fractions of more than 2 %, and biogenic pyrolysis oils, in contrast to liquid fossil fuels,

contain components from various chemical classes. The surrogate vaporisation approach thus strongly simplifies the conversion. Instead of the surrogate vaporisation approach, Hallet and Clark [45] suggested the continuous thermodynamics approach, wherein gamma probability density functions were assumed for acids, aldehydes/ketones, alcohols, water and lignin. It was shown that the probability density functions (in particular of water and lignin) can significantly affect the vaporisation predictions. Furthermore, the surrogate vaporisation approach and the continuous thermodynamics approach were combined with decomposition reaction kinetics. Sital [44] used the mechanism of Houminer et al. [46] for the thermal polymerisation of levoglucosan. Hallet and Clark [45] described the decomposition of lignin using an Arrhenius law model with reaction parameters proposed for cellulose.

The physical property models incorporated in previous studies [40–45] were mainly based on group contribution methods (Joback [47, 48], Constantinou and Gani [49], and Ruzicka and Domalski [50]) and corresponding-states methods. Specific physical property models were seldom used or developed for biogenic pyrolysis oils. So far, Yang et al. [51] derived empirical equations for the molar enthalpy of formation and the molar physical enthalpy as a function of the H/C and O/C ratios in order to estimate the enthalpy of pyrolysis for bio-oils.

1.3. Objectives

Numerous studies have investigated the chemical and physical properties and the conversion of biogenic pyrolysis oil. However, these studies have focussed on specific analyses due to the natural origin of bio-oils and the necessary experimental expenditures. For example, Branca et al. [3, 4, 20, 21] conducted proximate, ultimate, GC-MS and TG analyses, whereas Peacocke et al. [16] derived by far the most comprehensive physical property data sets, but without providing the chemical property data. Thus, there is a lack of comprehensive and consistent data sets for (i) the design, evaluation and scale-up of combustion or gasification experiments with biogenic pyrolysis oils

using process models and (ii) the mathematical description of atomisation and conversion of biogenic pyrolysis oils using CFD models. As part of the bioliq project [52], biogenic (and anthropogenic) pyrolysis oils are converted to synthesis gas in both laboratory-scale and pilot-scale entrained flow gasifiers at Karlsruhe Institute of Technology (KIT) [53–56]. In addition, flow-sheet models [55, 57] and CFD models [58–64] are under development for detailed investigation of sub-processes and for process optimisation and scale-up. Therefore, this study derived chemical and physical property data and decomposition kinetics for an industrial beech wood pyrolysis oil. This bio-oil was produced in the commercial fast pyrolysis plant of proFagus [65] and was used as feedstock in high-pressure entrained flow gasification experiments at the bioliq Entrained Flow Gasifier (bioliq EFG) plant for the production of high-quality synthesis gas and liquid fuels [55, 56]. In this context, samples of the beech wood pyrolysis oil were characterised using (i) proximate, ultimate and heating value analyses, (iv) GC-MS, GPC and TG analyses, (iii) vacuum and Engler distillations and (vi) measurements of density, dynamic viscosity, thermal conductivity, specific heat capacity and surface tension. The TG analyses were applied to derive decomposition kinetics based on multi-reaction Arrhenius law models and multi first-order reaction Gauss distributed activation energy models. The vacuum distillations were used to separate the vaporisable from the non-vaporisable components, whereas the Engler distillations were carried out to determine the boiling behaviour. Furthermore, samples of the vacuum distillates were analysed for boiling behaviour, TG behaviour, density, thermal conductivity and specific heat capacity, and samples of the vacuum distillation residues were analysed for TG behaviour and dynamic viscosity. The measured thermo-physical properties of both the beech wood pyrolysis oil and the vacuum distillate were finally used to derive the density, thermal conductivity and specific heat capacity of the vacuum distillation residue. The possible applications of the measured and derived data are summarised in Section 2. Then, the methods and the results of the analyses and measurements are presented in Sections 3

and 4 and are discussed in Section 5. Finally, the conclusions are given in Section 6.

2. Possible applications

This study derived pyrolysis oil data and models for process, single-particle, RANS based and large-eddy simulations in the course of the entrained flow gasification research at KIT. The process simulations are primarily employed for the design, evaluation and scale-up of experiments (see Section 5.1 and [55]). This requires reliable elemental, water and ash contents and heating values (see Sections 3.2 and 4.1) as well as low-temperature correlations for density and specific heat capacity (see Sections 3.9.2 and 4.8.1). The single-particle simulations, in turn, are applied to develop, test and validate sub-models for describing the conversion of biogenic or anthropogenic (slurry) particles (see Sections 5.4 and [63, 66]). The compositions of such particles are typically based on the elemental, water and ash contents (see Sections 3.2 and 4.1). In addition, the density, thermal conductivity and heat capacity (see Sections 3.9.2 and 4.8.1) and the thermo-chemical conversion (see Sections 3.8, 4.7 and 5.4) can be described using customised models. Moreover, surrogates (see Section S4) can be defined using GC-MS data (see Sections 3.3 and 4.2), Engler distillation data (see Sections 3.6 and 4.5) and thermo-physical property data of vacuum distillates (see Sections 3.9.2 and 4.8.1). Resolved single-particle-models might also account for the molar mass distribution (see Sections 3.4 and 4.3) and the impact of diffusion based on viscosity models (see Sections 3.9.5, 4.8.3 and S5).

The RANS based simulations (see [59, 62, 63]) and the large eddy simulations (see [67]) are finally used (i) to describe the local stoichiometry and the local temperatures in entrained flow gasification processes and (ii) to determine heat extraction, local slag behaviour and conversion. Based on the temperature distribution of a bioliq EFG experiment, the possible conversion of pyrolysis oil droplets is shown in Fig. 1. The conversion is described using a multi first-order reaction Arrhenius model (see Section 5.4), while the heat capacity is based on a

simplified approach (see Section S3). Large eddy simulations can also be used to describe the atomisation of pyrolysis oils at ambient temperatures (see [58, 60]), based on density, viscosity and surface tension data (see Sections 3.9.2, 3.9.4, 3.9.5, 4.8).

3. Methods

This section describes the experimental and mathematical methods used to derive the chemical and physical property data and the thermogravimetric kinetics.

3.1. Preparation

Samples of the beech wood pyrolysis oil, produced by proFagus [65] in 2020, were collected from the storage tanks of the bioliq EFG plant [55, 56]. The pyrolysis oil was continuously stirred in these tanks and additionally pumped in closed circuits for intensive mixing. Therefore, the collected samples can be assumed to be homogeneous and representative mixtures of the original charge. After sampling, some samples were sent to external laboratories, while the other samples were stored in glass bottles of 1 l and kept refrigerated at temperatures below 258 K to suppress composition changes due to ageing and vaporisation. Before their use in internal laboratory experiments, each bottle was warmed up in a water bath at room temperature and was homogenised through stirring the sample.

3.2. Chemical analyses

Chemical analyses were used to determine elemental, ash and water contents as well as lower and higher heating values of the beech wood pyrolysis oil.

The elemental, ash and water contents of the beech wood pyrolysis oil were determined at the internal laboratories KIT I, KIT II and KIT III as well as the external laboratories EXT I and EXT II. In the absence of specific standards for biogenic pyrolysis oils, the analyses of carbon, hydrogen, nitrogen, ash and

water contents were conducted using the standards that were suggested by the laboratories and are summarised in Tables S3 and S4. The oxygen contents were determined by difference, while the ash contents were obtained using an ashing temperature of 823 K at the laboratory EXT I or using an ashing temperature of 1088 K at the laboratories KIT I and KIT III. The lower ashing temperature was suggested in accordance with the standards for biomass, whereas the higher ashing temperature is more realistic for ashing under entrained flow gasification conditions. The water contents were determined using Karl-Fischer titration at the laboratories EXT I, EXT II and KIT II and using xylene distillation at the laboratories KIT I and KIT III.

The lower heating values and the higher heating values of the beech wood pyrolysis oil were determined at the laboratories KIT I, KIT II, KIT III and EXT I according to DIN 51900-2:2003 [68]. Moreover, higher heating values were calculated using the elemental and water contents and the Boie correlation [69]. The ratios of the calculated higher heating values to the measured higher heating values provided the Boie ratios. Following previous studies [55, 70], these ratios were used to evaluate the accuracy of the chemical analyses data for process calculations (see Section 5.1), where ratios around 100 % can indicate superior chemical property data.

Furthermore, reproducibility limits were extracted for the carbon, hydrogen and nitrogen contents from DIN 51732:2007 [71], for the water content from DIN 51777:2020 [72] and for the higher heating value from DIN 51900-1:2000 [73]. Assuming rectangular probability distributions, these limits were used to determine uncertainties s for various variables Y in the course of process calculations (see Section 5.1), i. e. the equilibrium temperature T_{eq} and the equilibrium species mole fractions $x_{\mathrm{CO,eq}}$, $x_{\mathrm{CO_2,eq}}$, $x_{\mathrm{H_2,eq}}$ and $x_{\mathrm{H_2O,eq}}$. The uncertainties s_Y are given by

$$s_Y = \left(\sum_{i=\mathrm{C,H,H_2O}} \left(\frac{\mathrm{d}Y}{\mathrm{d}w_{i,\mathrm{asr}}} \, s_{w_{i,\mathrm{asr}}} \right)^2 + \left(\frac{\mathrm{d}Y}{\mathrm{dHHV_{asr}}} \, s_{\mathrm{HHV_{asr}}} \right)^2 \right)^{0.5} \tag{1}$$

where $s_{w_{\mathrm{C,asr}}} = 0.0185/\sqrt{3}$, $s_{w_{\mathrm{H,asr}}} = 0.004/\sqrt{3}$ and $s_{w_{\mathrm{H_2O,asr}}} = 0.067\, w_{\mathrm{H_2O,asr}}/\sqrt{3}$ are the uncertainties of the mass fractions and $s_{\mathrm{HHV_{asr}}} = 400/\sqrt{3}\,\mathrm{kJ/kg}$ is the uncertainty of the higher heating value.

3.3. GC-MS analyses

GC-MS/FID analyses were used to investigate the contents of the vaporisable components of the beech wood pyrolysis oil. Two measurements were carried out using a commercial gas chromatograph system (Agilent 6890 with a VF-1701ms column ($60\,\mathrm{m} \times 0.25\,\mathrm{mm}, \mathrm{ID} \times 0.25\,\mathrm{mm}$)) at the laboratory EXT II. The initial oven temperature of 318 K was held for 4 min and was then increased to 553 K at a heating rate of 3 K/min. The final oven temperature was held constant for 20 min. The maximum injection temperature of the FID was 523 K with a split mode of 15:1. The mass fractions of the components were quantified through a comparison with calibration lines.

3.4. GPC analyses

GPC analyses were conducted to determine the molar mass distribution of the beech wood pyrolysis oil using the principle of size exclusion chromatography. Two measurements were performed using a commercial liquid chromatograph system (Agilent 1100 Series with an Agilent PolarGel-LGuard pre-column (50 mm × 7.5 mm) and two Varian PolarGel-L columns (300 mm × 7.5 mm)) at the laboratory EXT II. The UV detector had a wavelength of 254 nm. Nine polyethylene glycol standards (with molar masses of 194 g/mol, 420 g/mol, 615 g/mol, 1010 g/mol, 1970 g/mol, 3930 g/mol, 7920 g/mol, 12140 g/mol and 21030 g/mol) were used for the calibration. The injection volumes of the samples were 100 µl. The number-weighted mean molar mass M_{n}, the mass-weighted mean molar mass M_{m} and the polydispersity PD were derived from each molar mass distribution. The polydispersity PD is a measure of the width of the molar mass distribution and is given by

$$\mathrm{PD} = \frac{M_{\mathrm{m}}}{M_{\mathrm{n}}}\,. \tag{2}$$

3.5. Vacuum distillations

Vacuum distillations were used to separate the beech wood pyrolysis oil into vaporisable and non-vaporisable components. The laboratory setup consisted of (i) an electrically heated round bottom flask with a volume of 1000 ml, (ii) a Vigreux column with a length of 300 mm, (iii) a reflux condenser at the top of the separation column, (iv) a condenser with a connection to a vacuum pump and (v) a second flask for collecting the distillate. The beech wood pyrolysis oil sample was continuously homogenised with a stirring bar during the vacuum distillation, while a high reflux ratio of the condenser and a long separation column ensured the separation of the volatile components according to their boiling points. Two type K thermocouples tracked the liquid and gas temperatures. One thermocouple was placed at the bottom of the round bottom flask, while the other was positioned at the condenser inlet and the top of the separation column. Both condensers were operated at 293 K. The absolute operating pressure was 40 mbar, which was the lowest value that ensured constant pressure throughout the distillation process and kept the loss of the volatile components to a minimum.

The temperature in the flask could be increased up to 523 K, while white fumes indicated thermal decomposition reactions at higher temperatures. 523 K was therefore used to separate the vaporisable from the non-vaporisable components and to produce vacuum distillates of the beech wood pyrolysis oil for Engler distillations (see Sections 3.6 and 4.5), TG analyses (see Section 3.7 and 4.6) and measurements of thermo-physical properties (see Sections 3.9 and 4.8). Furthermore, the batch distillations were stopped at four temperatures (373 K, 423 K, 473 K, 508 K) below 523 K (i) to determine the recovered mass fractions at different liquid temperatures and (ii) to obtain different vacuum distillation residues (see Sections 3.9.5 and 4.8.3). Each distillation was performed three times. The recovered fractions at specific temperatures are reported as mean values with corresponding standard deviations.

3.6. Engler distillations

Engler distillations were conducted to determine the boiling-point curves of both the beech wood pyrolysis oil and the vacuum distillate. Three measurements each were carried out following ASTM D86-20a [74] and using modified temperature measurements. The default mercury thermometer was replaced by two type J thermocouples based on previous recommendations [75, 76] in order to track both the liquid temperature and the gas temperature. Both thermocouples were calibrated in the temperature range between 273 K and 673 K. The initial sample volumes in the Engler flask and the recovered distillate volumes were recorded at 293 K to ensure reliable and accurate measurement data. The measured temperatures were finally used to determine mean values and standard deviations for the boiling-point curves.

3.7. TG analyses

TG analyses of the beech wood pyrolysis oil, the vacuum distillate and the vacuum distillation residue were performed using a commercial device (Netzsch TG 209 F1). The analyses of the beech wood pyrolysis oil were carried out using constant heating rates of 2 K/min, 5 K/min, 10 K/min, 20 K/min and 50 K/min, while the analyses of the vacuum distillate and the vacuum distillation residue were conducted using a constant heating rate of 20 K/min only. The initial sample masses were between 70 mg and 100 mg. The temperature was measured using a thermocouple positioned in the gas phase below the sample crucible. In contrast to previous recommendations to use the position close to the sample bottom [3, 20], this was performed in accordance with the fixed setup of the analytical instrument. Nitrogen was applied as inert gas using volume flow rates of approximately 100 ml/min. Concentrations of the decomposition products were not measured, whereas TG and DTG curves, representing the relative mass loss w and the derivative of the relative mass loss $\mathrm{d}w/\mathrm{d}t$, were mainly determined three times (only twice for the beech wood pyrolysis oil at 50 K/min). The measured TG and DTG curves of each heating-rate condition were averaged using linear interpolation.

3.8. TG kinetics

TG kinetics were derived from the averaged TG and DTG curves of the beech wood pyrolysis oil using either multi-reaction Arrhenius law models or multi-reaction distributed activation energy models. For both modelling approaches, the temperature T, the mass fraction w, the time derivative of the mass fraction $\mathrm{d}w/\mathrm{d}t$ and the temperature derivative of the mass fraction $\mathrm{d}w/\mathrm{d}T$ are given by [4, 20, 21, 77]

$$T = \begin{cases} T_0 + \beta\, t\,, & \text{if} \quad 0 < t < \dfrac{T_{\max} - T_0}{\beta} \\ T_{\max}\,, & \text{if} \quad t > \dfrac{T_{\max} - T_0}{\beta} \end{cases} \,, \tag{3}$$

$$w = 1 - \sum_{i=1}^{N} w_{i,0} + \sum_{i=1}^{N} w_i\,, \tag{4}$$

$$\frac{\mathrm{d}w}{\mathrm{d}t} = \sum_{i=1}^{N} \frac{\mathrm{d}w_i}{\mathrm{d}t}\,, \tag{5}$$

$$\frac{\mathrm{d}w}{\mathrm{d}T} = \sum_{i=1}^{N} \frac{\mathrm{d}w_i}{\mathrm{d}T}\,, \tag{6}$$

where T_0 is the initial and ambient temperature, β is the constant heating rate, t is the time, $T_{\max}$ is the maximum temperature, N is the number of parallel reactions, w_i is the mass fraction of reaction i and $w_{i,0}$ is the initial mass fraction of reaction i. The latter is given by [4, 20, 21]

$$w_{i,0} = w_i|_{t=0} = w_i|_{T=T_0}\,. \tag{7}$$

3.8.1. Multi-reaction Arrhenius law models

Multi-reaction Arrhenius law models, as used in this study, are defined by

$$\frac{\mathrm{d}w_i}{\mathrm{d}t} = -k_{0,i}\, \exp\left(-\frac{\overline{E}_{\mathrm{a},i}}{\overline{R}\,T}\right)\, w_i^{n_i}\,, \tag{8}$$

where $k_{0,i}$ is the pre-exponential factor of reaction i, $\overline{E}_{\mathrm{a},i}$ is the molar activation energy of reaction i, $\overline{R}$ is the molar gas constant and n_i is the order of reaction i. In order to determine approximations for the pre-exponential factors $\boldsymbol{k}_0 = (k_{0,i})_{i=1,\ldots,N}$, the molar activation energies $\overline{\boldsymbol{E}}_{\mathrm{a}} = \left(\overline{E}_{\mathrm{a},i}\right)_{i=1,\ldots,N}$, the orders

$\boldsymbol{n} = (n_i)_{i=1,\ldots,N}$ and the initial mass fractions $\boldsymbol{w}_0 = (w_{i,0})_{i=1,\ldots,N}$, regressions of the averaged TG and DTG curves were performed using Eqs. (3)-(8) as well as the *least_squares* and *solve_ivp* methods of SciPy [78, 79]. The differential equations were solved using the LSODA (Adams/BDF) method [80, 81].

3.8.2. Multi-reaction distributed activation energy models

Multi-reaction distributed activation energy models can be developed using various probability distributions and assuming either unity or non-unity reaction orders [77]. Preliminary tests showed that Gaussian distributions and unity reaction orders provide the best approximations for the averaged TG and DTG data. Multi-reaction distributed activation energy models were therefore combined with Gaussian distributions and unity reaction orders. Multi-reaction distributed activation energy models, as used in this study, are defined by [77]

$$w_i = \int_0^\infty \exp\left(-\int_{T_0}^{T} \frac{k_i\left(\overline{E}_\mathrm{a}, \widetilde{T}\right)}{\beta}\,\mathrm{d}\widetilde{T}\right)\, f_i\left(\overline{E}_\mathrm{a}\right)\,\mathrm{d}\overline{E}_\mathrm{a}\,, \tag{9}$$

$$\frac{\mathrm{d}w_i}{\mathrm{d}t} = \beta\,\frac{\mathrm{d}w_i}{\mathrm{d}T}, \tag{10}$$

$$\frac{\mathrm{d}w_i}{\mathrm{d}T} = \int_0^\infty \frac{k_i\left(\overline{E}_\mathrm{a}, T\right)}{\beta}\,\exp\left(-\int_{T_0}^{T} \frac{k_i\left(\overline{E}_\mathrm{a}, \widetilde{T}\right)}{\beta}\,\mathrm{d}\widetilde{T}\right)\, f_i\left(\overline{E}_\mathrm{a}\right)\mathrm{d}\overline{E}_\mathrm{a}\,, \tag{11}$$

where

$$k_i\left(\overline{E}_\mathrm{a}, T\right) = k_{0,i}\,\exp\left(-\frac{\overline{E}_\mathrm{a}}{\overline{R}\,T}\right)\,, \tag{12}$$

is the rate constant and $f_i\left(\overline{E}_\mathrm{a}\right)$ is the probability density function, each of reaction i. The probability density function $f_i\left(\overline{E}_\mathrm{a}\right)$ is given by

$$f_i\left(\overline{E}_\mathrm{a}\right) = \frac{1}{\sqrt{2\,\pi}\,\sigma_{\overline{E}_\mathrm{a},i}}\,\exp\left(-\frac{\overline{E}_\mathrm{a} - \mu_{\overline{E}_\mathrm{a},i}}{2\,\sigma_{\overline{E}_\mathrm{a},i}}\right)\,, \tag{13}$$

where $\mu_{\overline{E}_\mathrm{a},i}$ and $\sigma_{\overline{E}_\mathrm{a},i}$ are the expectation and the standard deviation of the Gaussian distribution for the molar activation energy $\overline{E}_\mathrm{a}$ of reaction i. In order to determine appropriate approximations for the pre-exponential

factors $\boldsymbol{k}_0 = (k_{0,i})_{i=1,\ldots,N}$, the expectations $\boldsymbol{\mu}_{\overline{E}_\mathrm{a}} = \left(\mu_{\overline{E}_\mathrm{a},i}\right)_{i=1,\ldots,N}$, the standard deviations $\boldsymbol{\sigma}_{\overline{E}_\mathrm{a}} = \left(\sigma_{\overline{E}_\mathrm{a},i}\right)_{i=1,\ldots,N}$ and the initial mass fractions $\boldsymbol{w}_0 = (w_{i,0})_{i=1,\ldots,N}$, regressions of the averaged TG and DTG curves were carried out using Eq. (3)-(7) and (9)-(13) as well as the *trapz*, *quadgk*, *fminsearch* and *fmincon SPQ* methods of Matlab [82]. The *trapz* method (trapezoidal quadrature) with 100 equally spaced intervals was applied to the outer integrals, while the *quadgk* method (Gauss-Kronrod quadrature) was used for the inner integrals. The percentiles at 0.0001 and 0.9999 of the Gaussian distributions were used as limits of the outer integrals. The *fminsearch* was used to obtain appropriate initial parameters for the final optimisation using the *fmincon SPQ* method. In the final optimisation, constraints were applied to ensure that the mass fraction w is described properly for $T \to \infty$.

3.9. Thermo-physical properties

Density, thermal conductivity and specific heat capacity were determined for the beech wood pyrolysis oil (see Section 3.9.2), the vacuum distillate (see Section 3.9.2) and the vacuum distillation residue (see Section 3.9.3) under low-temperature conditions. In addition, the surface tension of the beech wood pyrolysis oil was measured under ambient conditions (see Section 3.9.4). Furthermore, the dynamic viscosity of the beech wood pyrolysis oil and three different vacuum distillation residues were determined under low-temperature conditions (see Section 3.9.5). The standards of the experimental methods are summarised in Table S5.

3.9.1. Challenges

The vaporisation of light volatiles, the thermal polymerisation and the decomposition affect measurements under low-temperature conditions. Therefore, three measures were taken to avoid composition changes and ensure reliable and accurate measurement data. Firstly, all measurements were conducted well below 600 K (see Sections 3.9.2 and 3.9.5). Secondly,

comparative measurements were carried out using either different heating behaviour or different set-ups (see Sections 3.9.2 and 3.9.5). Thirdly, some measurements of density, thermal conductivity and specific heat capacity were carried out under pressures of 6 bar to impede the vaporisation of light volatiles (see Section 3.9.2). Possible impacts of the pressurised conditions on the measured data were neglected as pressure effects are considerably smaller than temperature and composition effects for liquids if pressures are moderate and conditions are not close to critical conditions [83].

3.9.2. Density, thermal conductivity and specific heat capacity of the beech wood pyrolysis oil and the vacuum distillate

The density, the thermal conductivity and the specific heat capacity of both the beech wood pyrolysis oil and the vacuum distillate were determined between 293 K and 453 K at the laboratory EXT III. The measurements below 373 K were carried out at atmospheric pressure and, for temperatures above 373 K, at 6 bar. The density was measured according to DIN EN ISO 1183-1:2019 [84] with minor adaptations. The Mohr balance was calibrated using standard calibration substances. The thermal conductivity was obtained using a commercial thermal conductivity meter (flucon LAMBDA) based on the hot wire method according to ASTM D-7896-19 [85]. The measurements were performed using temperature ramps, while stopping at 17 temperatures between 293 K and 453 K and executing each measurement after reaching thermal equilibrium. The specific heat capacity was measured using continuously stirred sample volumes of 100 ml and an adiabatic calorimeter following ASTM D2766-95 [86].

Furthermore, the thermal conductivity and specific heat capacity of the beech wood pyrolysis oil were measured at 373 K and 453 K with fresh samples in single runs to investigate the heating effects. Finally, the density was also determined following ASTM D4052-18a [87] at both KIT and the laboratory EXT I. At KIT, the measurements were conducted between 293 K and 333 K using a commercial density meter (Anton Paar DMA 400). At

EXT I, the measurements were carried out at 288 K using an U-shaped oscillating sample tube.

3.9.3. Density, thermal conductivity and specific heat capacity of the vacuum distillation residue

The density, the thermal conductivity and the specific heat capacity of the vacuum distillation residue were derived from the data measured for the beech wood pyrolysis oil and the vacuum distillate. The density of the vacuum distillation residue ρ_{vdr} and the specific heat capacity of the vacuum distillation residue $\hat{C}_{p,\mathrm{vdr}}$ were determined by

$$\rho_{\mathrm{vdr}} = \frac{1 - w_{\mathrm{vd,oil}}}{\frac{1}{\rho_{\mathrm{oil}}} - \frac{w_{\mathrm{vd,oil}}}{\rho_{\mathrm{vd}}}}\,, \tag{14}$$

$$\hat{C}_{p,\mathrm{vdr}} = \frac{\hat{C}_{p,\mathrm{oil}} - w_{\mathrm{vd,oil}}\,\hat{C}_{p,\mathrm{vd}}}{1 - w_{\mathrm{vd,oil}}}\,, \tag{15}$$

where $w_{\mathrm{vd,oil}}$ is the recovered mass fraction of the vacuum distillate at the maximum liquid temperature, ρ_{oil} is the density of the beech wood pyrolysis oil, ρ_{vd} is the density of the vacuum distillate, $\hat{C}_{p,\mathrm{oil}}$ is the specific heat capacity of the beech wood pyrolysis oil and $\hat{C}_{p,\mathrm{vd}}$ is the specific heat capacity of the vacuum distillate. The thermal conductivity of the vacuum distillation residue λ_{vdr} was calculated using the mass-weighted mixing rule by

$$\lambda_{\mathrm{vdr}} = \frac{\lambda_{\mathrm{oil}} - w_{\mathrm{vd,oil}}\,\lambda_{\mathrm{vd}}}{1 - w_{\mathrm{vd,oil}}} \tag{16}$$

and using the Maxwell mixing rule by

$$\lambda_{\mathrm{vdr}} = \frac{2\,\lambda_{\mathrm{vd}}^2\,(1-\varphi) - \lambda_{\mathrm{oil}}\,\lambda_{\mathrm{vd}}\,(2+\varphi)}{\lambda_{\mathrm{oil}}\,(1-\varphi) - \lambda_{\mathrm{vd}}\,(1+2\,\varphi)}\,, \tag{17}$$

where λ_{oil} is the thermal conductivity of the beech wood pyrolysis oil, λ_{vd} is the thermal conductivity of the vacuum distillate and $\varphi = 1 - w_{\mathrm{vd,oil}}\,\frac{\rho_{\mathrm{oil}}}{\rho_{\mathrm{vdr}}}$.

3.9.4. Surface tension

The surface tension of the beech wood pyrolysis oil was measured at 293 K using a commercial tensiometer (Krüss K20 force) based on the Du Noüy ring method.

3.9.5. Dynamic viscosity

The dynamic viscosity of the beech wood pyrolysis oil and three vacuum distillation residues (obtained after reaching liquid temperatures of 373 K, 423 K and 473 K; see Sections 3.5 and 4.4) were determined between 293 K and 373 K using a commercial rheometer (Anton Paar MCR 302). A concentric cylinder geometry cell was used for the beech wood pyrolysis oil, while a parallel plate setup was applied to the vacuum distillation residues due to their high viscosities and the difficult sample handling. For each measurement point, three measurements were conducted using a shear rate of $40\,\mathrm{s}^{-1}$. For comparison, the dynamic viscosity of the beech wood pyrolysis oil was measured at 293 K, 313 K and 343 K according to DIN EN ISO 3219:1994 [88] at the laboratory EXT I.

4. Results

This section presents the experimental and numerical results of the characterisation of the beech wood pyrolysis oil.

4.1. Chemical analyses

The elemental, ash and water contents of the beech wood pyrolysis oil are given in Tables S6 and S7. The contents range from 0.569 to 0.585 for carbon and from 0.054 to 0.073 for hydrogen. In addition, the nitrogen, sulphur, chlorine and ash contents are below 0.001, and the water contents are between 0.052 and 0.083. The water contents are thus below the ones typical for pyrolysis oils. Moreover, the carbon, hydrogen and nitrogen contents are primarily inside the respective reproducibility limits of ±0.0185, ±0.0040 and ±0.0017 [71], respectively, whereas the water contents are partially outside the reproducibility limits of $\pm 0.067\, w_{\mathrm{H_2O,asr}}$ [72]. Overall, all contents are subject to higher uncertainties and cannot be reproduced with good accuracy, in contrast to previous conclusions [33].

The lower heating values and the higher heating values of the beech wood

pyrolysis oil, based on both measurements and calculations, are given in Table S8. The higher heating values on dry basis are between 25.53 MJ/kg and 26.38 MJ/kg and partially outside the reproducibility limits of ±400 kJ/kg [73]. Thus, similarly to carbon, hydrogen and water contents, the heating values are afflicted with higher uncertainties than should be expected.

Furthermore, the higher heating values based on the Boie correlation [69] as well as the Boie ratios are presented in Table S9. The Boie ratios are close to 100 % for the analysis results of KIT III and EXT I and deviate from 100 % to a greater extent for the analysis results of KIT I and KIT II. As values around 100 % indicate superior fuel data for process calculations [55, 70], the analysis results of KIT III and EXT I are likely superior (see Section 5.1). The analysis results of KIT I and KIT II could deviate due to erroneous sampling and analysis methods if the fuel variability has been low due to intensive mixing (see Section 3.1).

4.2. GC-MS analyses

The GC-MS analyses of the beech wood pyrolysis oil provided repeatable results (see Section S2) and identified 48 organic components from different chemical classes, including acids, non-aromatic ketones, furans, benzenes, lignin derived phenols, methoxy phenols, dimethoxy phenols and carbohydrates. The contents are depicted in Fig. 2 and are listed in Table S10. On average, 44.5 % of the sample mass (including a water content of 5.6 %) could be itemised, where 36.5 % of the total mass was assigned to specific organic components, and 2.4 % of the total mass was linked with an unspecific anhydrosugar. Such values are fairly typical for pyrolysis oils (for example, see [7]) as GC-MS analyses can only detect components that are sufficiently volatile to pass through the injector and the GC column.

Furthermore, organic acids (11.8 % of the sample mass) as well as phenol and phenol derivatives (16.0 % of the sample mass) were identified as major components of the beech wood pyrolysis oil. Thus, in comparison with previous results [2, 3, 89, 90], the beech wood pyrolysis oil is characterised by high

mass fractions of the decomposition products of lignin. Furthermore, the mass fractions of sugars (6.0 %) and ketones (3.7 %), derived from carbohydrates, are quite small for the beech wood pyrolysis oil.

4.3. GPC analyses

The molar mass distributions of the beech wood pyrolysis oil are shown using probability density functions (PDFs) and cumulative distribution functions (CDFs) in Fig. 3. The probability density functions are characterised by a first increase up to a molar mass of 30 g/mol, a strong peak at a molar mass of 60 g/mol, a broad peak between molar masses of 94 g/mol and 210 g/mol, a third peak at a molar mass of 300 g/mol and a largely continuous decrease up to a molar mass of $3 \cdot 10^4$ g/mol. The molar mass distributions up to a molar mass of 210 g/mol are in agreement with the GC-MS data. The first increase can mainly be attributed to the water content, while the first peak is due to the contents of organic acids (acetic acid and propionic acid) and ketones (acetol and 2-cyclopenten-1-one). Moreover, the second peak is due to the high contents of phenol and phenol derivatives. Furthermore, 54.1 % of the pyrolysis oil is characterised by molar masses of up to 210 g/mol, 25.3 % of the pyrolysis oil by molar masses between 210 g/mol and 1000 g/mol, and 20.3 % of the pyrolysis oil by molar masses between 1000 g/mol and $3 \cdot 10^4$ g/mol. The latter contents can be due to oligomeric components derived from lignin or carbohydrates [7], recalling that dimers and trimers have typical molar masses between 210 g/mol and 1000 g/mol.

The characteristic values of both molar mass distributions are shown in Table 2. The beech wood pyrolysis oil has a mean mass-weighted molar mass M_m of 860 g/mol, a mean number-weighted molar mass M_n of 71 g/mol and a mean polydispersity PD of 12. In comparison with previous results [7, 34, 89, 90], the number-weighted molar mass M_n is lower due to higher contents of water and acetic acid, whereas the mass-weighted molar mass M_m is higher due to the broad distribution of molar masses between 18 g/mol and $3 \cdot 10^4$ g/mol. This results in fairly high

polydispersities PD compared to typical polydispersities PD of between 1 and 3 for biogenic pyrolysis oils from a wide range of feedstocks and pyrolysis processes [34].

Table 2: Mass-weighted molar masses M_{m}, number-weighted molar masses M_{n} and polydispersities PD of the beech wood pyrolysis oil based on the GPC analysis results.

Measurement	$\frac{M_{\mathrm{m}}}{\mathrm{g/mol}}$	$\frac{M_{\mathrm{n}}}{\mathrm{g/mol}}$	PD
I	902	71	12.70
II	811	71	11.42

4.4. Vacuum distillations

The vacuum distillations were stopped at five different liquid temperatures. The recovered mass fractions at these temperatures are shown in Table 3.

Table 3: Recovered mass fractions of the vacuum distillates at different liquid temperatures.

~~Liquid temperature / K~~ Liquid	~~Gas temperature / K~~ Gas	Recovered mass fraction / %	
		Total	Differential
293	273	0	0
373	314	9.4 ± 0.7	9.4
423	368	16.4 ± 0.6	7.0
473	433	42.5 ± 0.3	26.1
508	461	55.3 ± 0.2	12.8
523	471	57.7 ± 0.1	2.4

Most of the volatiles, such as phenolic derivatives, were accordingly separated at liquid temperatures between 423 K and 473 K, while 57.7 % of the sample mass was recovered at the maximum liquid temperature of 523 K. Furthermore, 91 % of the sample mass was retrieved as vacuum distillate or vacuum distillation residue, while 9 % of the sample mass was lost. It is expected that the losses

are rather escaped volatiles than uncollected solid residues. Therefore, up to 66.7 % of the sample mass should have been recovered as vacuum distillate at the maximum liquid temperature of 523 K under ideal conditions (see Section 5.2).

4.5. Engler distillations

The Engler distillation curves were determined for both the beech wood pyrolysis oil and the vacuum distillate. The mean gas and mean liquid temperatures are plotted over the recovered volume fraction in Fig. 4. The temperatures are only depicted up to a volume fraction of 60 % in the case of the beech wood pyrolysis oil and up to a volume fraction of 90 % in the case of the vacuum distillate, as decomposition reactions were observed at higher volume fractions.

The gas temperatures of the beech wood pyrolysis oil are largely congruent with those of the vacuum distillate. The initial boiling temperatures are approximately 373 K due to the transition of water into vapour, and the final boiling temperatures are approximately 550 K. However, the gas temperature curves are distorted due to the different contents and compositions of the volatiles (see Section 4.4), given that the fraction of vaporisable components at ambient conditions is 60 % in volume fractions and 60.4 % in mass fractions.

The liquid temperatures are significantly higher than the gas temperatures and increase to approximately 650 K with increasing recovered volume fraction. In addition, the liquid temperature curves of the beech wood pyrolysis oil and the vacuum distillate diverge above recovered volume fractions of 15 % due to the deviating contents and compositions of the volatiles. The liquid temperature curve of the vacuum distillate also gets quite steep at the end of the Engler distillation as the sample mass in the flask decreased and the constant heat supply could have falsified the measured data. Furthermore, solid organic residues were formed during the Engler distillation of the vacuum distillate. This indicates that vacuum distillation up to 523 K separated some components that decompose rather than vaporise under atmospheric-pressure conditions (see Section 5.2).

4.6. TG analyses

The TG and DTG curves that were obtained for the beech wood pyrolysis oil at five heating rates between 303 K and 1273 K are shown in Fig. 5. Firstly, the curves exhibit similar shapes indicating similar decomposition behaviour at the various heating rates. The mass decrease shifts to higher temperatures with an increase in heating, while the total mass decrease (up to 90 %) increases with faster heat-up. Secondly, the mass mainly decreases between 373 K and 723 K, where the maximum mass decrease is between 470 K and 600 K. Above 723 K, the mass varies only slightly. The mass decreases are in qualitative agreement with previous studies [2, 3, 18, 26, 29] (see Section 5.3) and the results obtained through vacuum distillation and Engler distillation. Thirdly, the mass decrease at lower temperatures was due to the vaporisation of light volatiles, while the mass decrease at higher temperatures was due to the vaporisation of heavy volatiles and the release of gases. At the heating rate of 2 K/min, water and very light components (15 % of the mass) evaporated below 423 K, while heavy volatiles vaporised between 423 K and 523 K. About 60 % of the mass was lost at the peak of 473 K. In addition, gaseous decomposition products were released from the non-vaporisable residue at temperatures above 523 K.

The TG and DTG curves of both the vacuum distillate and the vacuum distillation residue, determined at the heating rate of 20 K/min, are compared with the corresponding TG and DTG curves of the beech wood pyrolysis oil in Fig. 6. The TG and DTG curves of both the vacuum distillate and the vacuum distillation residue were weighted by their mass fractions (as determined by vacuum distillation up to the maximum liquid temperature) to demonstrate the contributions of the vaporisable and the non-vaporisable fractions to the thermogravimetric conversion of the beech wood pyrolysis oil. The TG curves of the vacuum distillate and the vacuum distillation residue show that the mass of the vacuum distillate was almost completely converted between 350 K and 650 K, whereas the mass of the vacuum distillation residue started to decrease at 520 K. About 25 % of the initial mass of the vacuum distillation residue remained at the end, which is in agreement with the

residues of approximately 10 % observed in the TG analyses of the beech wood pyrolysis oil. In addition, the DTG curves of the vacuum distillate and the vacuum distillation residue demonstrate the superposition of vaporisation and decomposition in the conversion of the beech wood pyrolysis oil between 500 K and 650 K.

Furthermore, cumulated TG and DTG curves were obtained from the respective curves of the vacuum distillate and the vacuum distillation residue. These curves are shown in Fig. 6 and are in good agreement with the curves of the beech wood pyrolysis oil (see Section 5.2).

4.7. TG kinetics

The approximations of the TG and DTG curves using multi-reaction Arrhenius law models with reaction orders bounded between 0.1 and 2 are shown in Fig. 5, while the approximations using multi first-order reaction Arrhenius law models are depicted in Fig. 7. In addition, the approximations using multi first-order reaction Gauss distributed activation energy models are shown in Fig. 8. The parameters of the models are given in Tables 4, 5 and 6. The approximations of all three models are in good agreement with the measurement data. However, the multi-reaction Arrhenius law models provide slightly superior approximations compared to the multi first-order reaction Gauss distributed activation energy models and could provide better predictions at low heating rates (see Section 5.3).

Table 4: Parameters for the calculation of the mass loss w and the derivative of the mass loss $\mathrm{d}w/\mathrm{d}t$ for the beech wood pyrolysis oil using the multi-reaction Arrhenius law model based on Eqs. (3)-(8).

i	$\frac{k_{0,i}}{1/\mathrm{s}}$	$\frac{\overline{E}_{\mathrm{a},i}}{\mathrm{J/mol}}$	n_i	$w_{0,i}$				
				$2\ \frac{\mathrm{K}}{\mathrm{min}}$	$5\ \frac{\mathrm{K}}{\mathrm{min}}$	$10\ \frac{\mathrm{K}}{\mathrm{min}}$	$20\ \frac{\mathrm{K}}{\mathrm{min}}$	$50\ \frac{\mathrm{K}}{\mathrm{min}}$
1	$4.134 \cdot 10^3$	$4.452 \cdot 10^4$	2.000	$1.861 \cdot 10^{-1}$	$1.787 \cdot 10^{-1}$	$1.947 \cdot 10^{-1}$	$2.170 \cdot 10^{-1}$	$2.769 \cdot 10^{-1}$
2	$1.535 \cdot 10^3$	$5.394 \cdot 10^4$	1.482	$4.072 \cdot 10^{-1}$	$4.593 \cdot 10^{-1}$	$4.954 \cdot 10^{-1}$	$5.452 \cdot 10^{-1}$	$6.254 \cdot 10^{-1}$
3	3.788	$3.728 \cdot 10^4$	2.000	$5.801 \cdot 10^{-2}$	$3.796 \cdot 10^{-2}$	$1.861 \cdot 10^{-2}$	$1.183 \cdot 10^{-2}$	$9.053 \cdot 10^{-3}$
4	$2.530 \cdot 10^5$	$8.189 \cdot 10^4$	2.000	$2.200 \cdot 10^{-1}$	$2.299 \cdot 10^{-1}$	$1.987 \cdot 10^{-1}$	$1.390 \cdot 10^{-1}$	$1.355 \cdot 10^{-2}$

Table 5: Parameters for the calculation of the mass loss w and the derivative of the mass loss $\mathrm{d}w/\mathrm{d}t$ for the beech wood pyrolysis oil using the multi first-order reaction Arrhenius law model based on Eqs. (3)-(8).

i	$\frac{k_{0,i}}{1/\mathrm{s}}$	$\frac{\overline{E}_{\mathrm{a},i}}{\mathrm{J/mol}}$	n_i	$w_{0,i}$				
				$2\ \frac{\mathrm{K}}{\mathrm{min}}$	$5\ \frac{\mathrm{K}}{\mathrm{min}}$	$10\ \frac{\mathrm{K}}{\mathrm{min}}$	$20\ \frac{\mathrm{K}}{\mathrm{min}}$	$50\ \frac{\mathrm{K}}{\mathrm{min}}$
1	7.440	$3.653 \cdot 10^4$	1	$3.818 \cdot 10^{-1}$	$5.139 \cdot 10^{-1}$	$5.289 \cdot 10^{-1}$	$4.342 \cdot 10^{-1}$	$3.237 \cdot 10^{-2}$
2	$1.842 \cdot 10^1$	$3.449 \cdot 10^4$	1	$1.414 \cdot 10^{-1}$	$1.687 \cdot 10^{-1}$	$2.658 \cdot 10^{-1}$	$4.373 \cdot 10^{-1}$	$8.531 \cdot 10^{-1}$
3	2.209	$3.858 \cdot 10^4$	1	$3.033 \cdot 10^{-1}$	$1.925 \cdot 10^{-1}$	$9.171 \cdot 10^{-2}$	$2.187 \cdot 10^{-2}$	$2.927 \cdot 10^{-2}$
4	1.259	$5.387 \cdot 10^4$	1	$4.275 \cdot 10^{-2}$	$2.745 \cdot 10^{-2}$	$1.828 \cdot 10^{-2}$	$1.720 \cdot 10^{-2}$	$7.817 \cdot 10^{-3}$

Table 6: Parameters for the calculation of the mass loss w and the derivative of the mass loss $\mathrm{d}w/\mathrm{d}t$ for the beech wood pyrolysis oil using the multi first-order reaction Gauss distributed activation energy model based on Eqs. (3)-(7) and (9)-(13).

i	$\frac{k_{0,i}}{1/\mathrm{s}}$	$\frac{\mu_{\overline{E}_{\mathrm{a}},i}}{\mathrm{J/mol}}$	$\frac{\sigma_{\overline{E}_{\mathrm{a}},i}}{\mathrm{J/mol}}$	$w_{0,i}$				
				$2\ \frac{\mathrm{K}}{\mathrm{min}}$	$5\ \frac{\mathrm{K}}{\mathrm{min}}$	$10\ \frac{\mathrm{K}}{\mathrm{min}}$	$20\ \frac{\mathrm{K}}{\mathrm{min}}$	$50\ \frac{\mathrm{K}}{\mathrm{min}}$
1	$7.736 \cdot 10^3$	$1.056 \cdot 10^5$	$2.917 \cdot 10^4$	$4.708 \cdot 10^{-2}$	$3.825 \cdot 10^{-2}$	$2.595 \cdot 10^{-2}$	$2.519 \cdot 10^{-2}$	$2.160 \cdot 10^{-2}$
2	7.778	$3.961 \cdot 10^4$	$5.998 \cdot 10^3$	$4.819 \cdot 10^{-1}$	$3.541 \cdot 10^{-1}$	$2.305 \cdot 10^{-1}$	$1.185 \cdot 10^{-1}$	0
3	$1.147 \cdot 10^4$	$6.371 \cdot 10^4$	$7.014 \cdot 10^3$	$3.424 \cdot 10^{-1}$	$5.136 \cdot 10^{-1}$	$6.510 \cdot 10^{-1}$	$7.693 \cdot 10^{-1}$	$9.034 \cdot 10^{-1}$

4.8. Thermo-physical properties

The thermo-physical properties of the beech wood pyrolysis oil under ambient conditions are compared with ranges of values obtained in previous studies [8, 11, 12, 14, 16, 91] in Table 7.

Table 7: Density ρ_{oil}, specific heat capacity $\hat{C}_{p,\mathrm{oil}}$, thermal conductivity λ_{oil}, dynamic viscosity η_{oil} and surface tension σ_{oil} of the beech wood pyrolysis oil under ambient conditions in comparison with ranges of values obtained in previous studies [8, 11, 12, 14, 16, 91].

	$\frac{\rho_{\mathrm{oil}}}{\mathrm{kg/m^3}}$	$\frac{\hat{C}_{p,\mathrm{oil}}}{\mathrm{J/(kg\,K)}}$	$\frac{\lambda_{\mathrm{oil}}}{\mathrm{W/(m\,K)}}$	$\frac{\eta_{\mathrm{oil}}}{\mathrm{Pa\,s}}$	$\frac{\sigma_{\mathrm{oil}}}{\mathrm{N/m}}$
Beech wood pyrolysis oil	1201	2062	0.1887	1.19	23.43
Literature values	1100-1300	2600-3500	0.35-0.45	0.02-10	22-37

The measured density, the measured dynamic viscosity and the measured surface tension of the beech wood pyrolysis oil are in the respective ranges of previously measured values, whereas the measured specific heat capacity and the measured thermal conductivity are significantly lower than the literature values. However, comparative data for these thermo-physical properties is scarce and depends on the feedstock and the pyrolysis process. Given that the density and the viscosity of bio-oils decrease with an increase in water content [17], the water content could strongly affect heat capacity and thermal conductivity. When considering the thermo-physical properties of water, it is expected that the heat capacity and the thermal conductivity of biogenic pyrolysis oils increase with an increase in water content. Thus, if the literature data for heat capacity and thermal conductivity has been determined for pyrolysis oils with water contents between 20 % and 35 % (see [3]), the data measured for the beech wood pyrolysis oil is in a reasonable agreement with the literature data.

4.8.1. Density, thermal conductivity and specific heat capacity of the beech wood pyrolysis oil and the vacuum distillate

The measured densities ρ, the measured thermal conductivities λ and the measured specific heat capacities $\hat{C}_p$ of both the beech wood pyrolysis oil and the vacuum distillate are shown in Figs. 9, 10 and 11.

In Fig. 9, the densities of both the beech wood pyrolysis oil and the vacuum distillate decrease linearly by about 12 % when the temperature is increased from 293 K to 453 K. The density of the vacuum distillate is always lower than that of the beech wood pyrolysis oil, as the vacuum distillate only consists of light components. Moreover, the density of the beech wood pyrolysis oil changes by 54 kg/m^3 between 293 K and 353 K, which is in agreement with previous data [16] for Ensyn pyrolysis oil samples (albeit with higher water contents). Furthermore, the densities of the beech wood pyrolysis oil that were measured between 293 K and 343 K at KIT or at 287 K at EXT I are shown in Fig. 9. The measured data of KIT is in excellent agreement with the data of EXT III, whereas the measured data of EXT I is 2 % lower and could be erroneous. Comparative measurements are thus recommended for future studies.

In Fig. 10, the thermal conductivities of both the beech wood pyrolysis oil and the vacuum distillate decrease by 16 % and 12 %, respectively, when increasing the temperature from 293 K to 453 K. The thermal conductivity of the vacuum distillate decreases linearly, whereas that of the beech wood pyrolysis oil decreases more strongly at higher temperatures than at lower ones. The decrease in the thermal conductivity with increasing temperature is in agreement with literature data for water and extracted bio-oils [92], while previous findings for Ensyn pyrolysis oil samples [16] have suggested a slight increase between 303 K and 333 K for thoroughly mixed samples.

In Fig. 11, the specific heat capacities of both the beech wood pyrolysis oil and the vacuum distillate increase linearly by 24 % and 30 %, respectively, when increasing the temperature from 293 K to 453 K. Due to the higher water

content, the measured heat capacities are higher for the vacuum distillate than for the beech wood pyrolysis oil. Moreover, the beech wood pyrolysis oil exhibits a smaller increase in heat capacity between 303 K and 333 K compared to Ensyn pyrolysis oil samples [16], recalling that previous data varied strongly between 2600 J/(kg K) and 3800 J/(kg K) due to various measurement challenges, such as the vaporisation and decomposition of pyrolysis oil components [16].

Furthermore, the measured single-run data of EXT III are shown in Figs. 10 and 11. These single-run values are in good agreement with the previously measured data of EXT III. Thus, heating did not significantly affect the measurements.

The density ρ, the thermal conductivity λ and the specific heat capacity $\hat{C}_p$ were finally approximated by

$$\rho_j = \left(\sum_{i=1}^{2} C_{i,j} \left(\frac{T}{\mathrm{K}} \right)^{i-1} \right) \frac{\mathrm{kg}}{\mathrm{m}^3} \,, \tag{18}$$

$$\lambda_j = \left(\sum_{i=1}^{3} C_{i,j} \left(\frac{T}{\mathrm{K}} \right)^{i-1} \right) \frac{\mathrm{W}}{\mathrm{m\,K}} \,, \tag{19}$$

$$\hat{C}_{p,j} = \left(\sum_{i=1}^{3} C_{i,j} \left(\frac{T}{\mathrm{K}} \right)^{i-1} \right) \frac{\mathrm{J}}{\mathrm{kg\,K}} \,, \tag{20}$$

where $j = \mathrm{oil}, \mathrm{vd}$ refers to the beech wood pyrolysis oil and the vacuum distillate, respectively, C_1, C_2 and C_3 are coefficients and T is the temperature. The coefficients C_1, C_2 and C_3 are given in Tables 8 and 9. The approximations are in good agreement with the measured data.

Table 8: Coefficients for the calculation of the density ρ_{oil} using Eq. (18), the calculation of the thermal conductivity λ_{oil} using Eq. (19) and the calculation of the specific heat capacity $\hat{C}_{p,\mathrm{oil}}$ using Eq. (20), each of the beech wood pyrolysis oil.

i	C_i		
	ρ_{oil}	λ_{oil}	$\hat{C}_{p,\mathrm{oil}}$
1	$1.466\,068 \cdot 10^{3}$	$2.174\,394 \cdot 10^{-1}$	$1.672\,170 \cdot 10^{3}$
2	$-9.008\,656 \cdot 10^{-1}$	$-4.402\,192 \cdot 10^{-5}$	$-2.935\,937 \cdot 10^{-1}$
3	–	$-1.848\,268 \cdot 10^{-7}$	$5.582\,648 \cdot 10^{-3}$

Table 9: Coefficients for the calculation of the density ρ_{vd} using Eq. (18), the calculation of the thermal conductivity λ_{vd} using Eq. (19) and the calculation of the specific heat capacity $\hat{C}_{p,\mathrm{vd}}$ using Eq. (20), each of the vacuum distillate.

i	C_i		
	ρ_{vd}	λ_{vd}	$\hat{C}_{p,\mathrm{vd}}$
1	$1.433\,500 \cdot 10^{3}$	$2.342\,043 \cdot 10^{-1}$	$1.202\,392 \cdot 10^{3}$
2	$-9.733\,561 \cdot 10^{-1}$	$-1.881\,592 \cdot 10^{-4}$	$3.393\,910$
3	–	–	$6.470\,100 \cdot 10^{-8}$

4.8.2. Density, thermal conductivity and specific heat capacity of the vacuum distillation residue

The derived density ρ, the derived thermal conductivity λ and the derived specific heat capacity $\hat{C}_p$ of the vacuum distillation residue are shown in Figs. 9, 10 and 11. The density of the vacuum distillation residue is thus higher than that of the beech wood pyrolysis oil under low-temperature conditions, while the specific heat capacity of the vacuum distillation residue is lower than the specific heat capacity of the beech wood pyrolysis oil. Moreover, the thermal conductivity of the vacuum distillation residue is higher than that of the beech wood pyrolysis oil at temperatures of up to 420 K and lower than the thermal conductivity of the beech wood pyrolysis oil at higher

temperatures. This is in agreement with the deviating slopes of the thermal conductivities of the beech wood pyrolysis oil and the vacuum distillate. In addition, both the mass-weighted mixing rule and the Maxwell mixing rule provide fairly similar predictions for the thermal conductivity of the vacuum distillation residue. The impact of the mixing rule on the derived data is thus rather low. Furthermore, the specific heat capacity of the vacuum distillation residue $\hat{C}_{p,\mathrm{vdr}}$ was approximated using the Einstein/Merrick model with two characteristic temperatures [93] in order to enable a reasonable extrapolation to higher temperatures. The approximation is given by

$$\hat{C}_{p,\mathrm{vdr}} = (1 - w_{\mathrm{ash,oil}})\, \hat{C}_{p,\mathrm{vdr,af}} + w_{\mathrm{ash,oil}}\, \hat{C}_{p,\mathrm{ash}}\,, \tag{21}$$

$$\hat{C}_{p,\mathrm{vdr,af}} = \left(C_1 \left(g\left(C_2 \frac{\mathrm{K}}{T} \right) + 2\, g\left(C_3 \frac{\mathrm{K}}{T} \right) \right) \right) \frac{\mathrm{J}}{\mathrm{kg/K}}\,, \tag{22}$$

$$\hat{C}_{p,\mathrm{ash}} = \left(754 + 0.586 \left(\frac{T}{\mathrm{K}} - 273.15 \right) \right) \frac{\mathrm{J}}{\mathrm{kg/K}}\,, \tag{23}$$

where C_1, C_2 and C_3 are coefficients, given in Table 10, and g is an auxiliary function that is defined by [93]

$$g\,(z) = \frac{\exp\,(z)}{\left(\left(\exp\,(z) - 1\right)/z\right)^2}\,. \tag{24}$$

Table 10: Coefficients for the calculation of the specific heat capacity of the vacuum distillation residue $\hat{C}_{p,\mathrm{vdr}}$ using Eqs. (21)-(24).

i	C_i
1	$1.007\,613 \cdot 10^2$
2	$4.272\,600 \cdot 10^2$
3	$2.322\,618 \cdot 10^3$

4.8.3. Dynamic viscosity

The measured dynamic viscosities of the beech wood pyrolysis oil η_{oil} are shown in Fig. 12. The dynamic viscosity decreases with an increase in temperature and asymptotically approaches a minimum value at high

temperatures. Furthermore, the measurement data is in agreement with the data measured at the laboratory EXT I. However, in comparison with the literature data [11], the measured dynamic viscosities are higher due to the lower water content and the higher fraction of large molecules (see Section 4.3). An accurate approximation is given by

$$\eta_{\mathrm{oil}} = \exp\left(C_1 - C_2 \left(\frac{T}{\mathrm{K}}\right)\right) + \exp\left(C_3 - C_4 \left(\frac{T}{\mathrm{K}}\right)\right) + C_5\,, \tag{25}$$

where the coefficients C_1, C_2, C_3, C_4 and C_5 are given in Table 11.

The measured dynamic viscosities of the vacuum distillation residues, obtained at 373 K, 423 K and 473 K (see Sections 3.5 and 4.4), are shown in Fig. 12. This data was mainly obtained at higher temperatures, as the samples were usually too viscous at lower ones. Furthermore, the dynamic viscosity increases with increasing fraction of non-vaporisable components, while the temperature dependency differs for the various vacuum distillation residues.

Several approximations of the measured dynamic viscosities of the beech wood pyrolysis oil and the vacuum distillation residues were tested in this study. The best possible approximation, which provides both accurate results and reasonable extrapolation behaviour, is shown in Fig. 12 and is given by

$$\begin{aligned}\eta_{\mathrm{vdr}} = {} & (C_1 + C_2\, w_\beta)\, \exp\left(C_3 + C_4\, w_\beta + C_5\, w_\beta^2 - C_6 \left(\frac{T}{\mathrm{K}}\right)\right) \\ & + (C_7 + C_8\, w_\beta)\, \exp\left(C_9 + C_{10}\, w_\beta + C_{11}\, w_\beta^2 - C_{12} \left(\frac{T}{\mathrm{K}}\right)\right) \\ & + \left(C_{13} + C_{14}\, w_\beta + C_{15}\, w_\beta^2\right)\,,\end{aligned} \tag{26}$$

where $C_1, \ldots, C_{15}$ are coefficients, given in Table 11, and w_β is the recovered mass fraction, which is used to include the effect of distillation progress corresponding to the distillation temperature (see Table 3). The approximation slightly overestimates the dynamic viscosity at higher temperatures and may be revised in future studies.

Table 11: Coefficients for the calculation of the dynamic viscosity of the beech wood pyrolysis oil and the vacuum distillation residues using Eq. (26).

i	C_i	
	η_{oil}	η_{vdr}
1	$4.463\,692 \cdot 10^{1}$	$1.373\,277 \cdot 10^{-2}$
2	$1.295\,787 \cdot 10^{-1}$	$3.104\,976$
3	$2.220\,811 \cdot 10^{1}$	$5.463\,751$
4	$5.572\,887 \cdot 10^{-2}$	$6.768\,664$
5	$5.550\,941$	$2.050\,511 \cdot 10^{1}$
6	–	$8.516\,608 \cdot 10^{-1}$
7	–	$9.938\,904 \cdot 10^{-1}$
8	–	$-1.275\,005$
9	–	$2.929\,994 \cdot 10^{1}$
10	–	$2.498\,487 \cdot 10^{2}$
11	–	$-2.738\,196 \cdot 10^{3}$
12	–	$7.705\,428 \cdot 10^{-2}$
13	–	$9.169\,229$
14	–	$1.326\,153 \cdot 10^{3}$
15	–	$5.811\,586 \cdot 10^{3}$

5. Discussion

This section discusses (i) the chemical analysis data in connection with process calculations, (ii) the separation of vaporisable and non-vaporisable components using vacuum distillations, (iii) the TG data and (iv) the extrapolation of the TG kinetics to high-temperature and high-heating-rate conditions.

5.1. Chemical analyses

Chemical analyses conducted at five laboratories provided scattered data mainly within the reproducibility limits of DIN 51732:2007 [71], DIN 51777:2020 [72] and DIN 51900-1:2000 [73]. Process calculations were therefore applied to investigate the impact of the chemical analysis results on the design and the evaluation of the bioliq EFG experiment V105. This experiment was conducted at the bioliq EFG plant [55, 56, 94] with a total thermal input of 4.9 MW and a total pressure of 40 bar. Oxygen and steam were used as gasification media, glass beads were supplied to ensure slag deposition on the refractory material of the cooling screen, and natural gas was used for ignition and flame stabilisation (see [55]). The characteristic operating parameters are given in Table 12, whereas the averaged mass flow rates and corresponding enthalpy flow rates of the feed streams are given in Tables 13 and S11. The total heat extraction was balanced to 652 kW, while peripheral heat losses were neglected following previous assumptions [55]. The molar H/C ratios $\mathrm{HCR_{slurry}}$, the minimum specific oxygen demands $\mathrm{SMOD_{slurry}}$, the stoichiometric ratios λ, the equilibrium compositions in mole fractions $\boldsymbol{x}_{\mathrm{eq}}$, the equilibrium temperatures T_{eq} and the equilibrium cold-gas efficiencies $\mathrm{CGE_{eq}}$ were determined using the chemical analysis results of the laboratories[1], the measured mass flow rates, temperatures and pressures, and the equilibrium model for the bioliq EFG [55].

[1] Heating values were not determined at the laboratory EXT II and were therefore based on the Boie correlation [69].

Table 12: Characteristic operating parameters of the bioliq EFG experiment V105: slurry, thermal input P_{th}, operating pressure p_{op}, ash/slurry mass flow rate ratio $\dot{m}_{\mathrm{ash}}/\dot{m}_{\mathrm{slurry}}$, steam/slurry mass flow rate ratio $\dot{m}_{\mathrm{steam}}/\dot{m}_{\mathrm{slurry}}$, oxygen/slurry mass flow rate ratio $\dot{m}_{\mathrm{O_2}}/\dot{m}_{\mathrm{slurry}}$ and nitrogen/slurry mass flow rate ratio $\dot{m}_{\mathrm{N_2}}/\dot{m}_{\mathrm{slurry}}$.

Experiment	Slurry	$\frac{P_{\mathrm{th}}}{\mathrm{MW}}$	$\frac{p_{\mathrm{op}}}{\mathrm{bar}}$	$\frac{\dot{m}_{\mathrm{ash}}}{\dot{m}_{\mathrm{slurry}}}$	$\frac{\dot{m}_{\mathrm{steam}}}{\dot{m}_{\mathrm{slurry}}}$	$\frac{\dot{m}_{\mathrm{O_2}}}{\dot{m}_{\mathrm{slurry}}}$	$\frac{\dot{m}_{\mathrm{N_2}}}{\dot{m}_{\mathrm{slurry}}}$
V105	Beech wood pyrolysis oil + glass beads	4.9	40	0.045	0.36	0.94	0.26

Table 13: Feed data of the bioliq EFG experiment V105: mass flow rate of slurry $\dot{m}_{\mathrm{slurry}}$, mass flow rate of natural gas $\dot{m}_{\mathrm{ng}}$, mass flow rate of steam $\dot{m}_{\mathrm{steam}}$, mass flow rate of O_2 $\dot{m}_{\mathrm{O_2}}$ and mass flow rate of N_2 $\dot{m}_{\mathrm{N_2}}$ based on measurements.

Experiment	$\frac{\dot{m}_{\mathrm{slurry}}}{\mathrm{kg/h}}$	$\frac{\dot{m}_{\mathrm{ng}}}{\mathrm{kg/h}}$	$\frac{\dot{m}_{\mathrm{steam}}}{\mathrm{kg/h}}$	$\frac{\dot{m}_{\mathrm{O_2}}}{\mathrm{kg/h}}$	$\frac{\dot{m}_{\mathrm{N_2}}}{\mathrm{kg/h}}$
V105	743.9	37.5	267.6	702.5	195.2

The molar H/C ratios $\mathrm{HCR}_{\mathrm{slurry}}$ and the specific minimum oxygen demands $\mathrm{SMOD}_{\mathrm{slurry}}$ based on the five chemical analysis results are given in Table 14. The molar H/C ratios are between 1.1 and 1.5, while the specific minimum oxygen demands $\mathrm{SMOD}_{\mathrm{slurry}}$ are between 1.68 and 1.79. This, in turn, suggests a wide range of stoichiometric ratios λ between 0.496 and 0.525 (based on the specific minimum oxygen demands $\mathrm{SMOD}_{\mathrm{slurry}}$ and the mass flow rates $\dot{m}_{\mathrm{slurry}}$ and $\dot{m}_{\mathrm{O_2}}$).

Table 14: Molar H/C ratios $\mathrm{HCR}_{\mathrm{slurry}}$, minimum specific oxygen demands $\mathrm{SMOD}_{\mathrm{slurry}}$ and stoichiometric ratios λ based on different chemical analysis results.

Laboratory	$\frac{\mathrm{HCR}_{\mathrm{slurry}}}{\mathrm{mol/mol}}$	$\frac{\mathrm{SMOD}_{\mathrm{slurry}}}{\mathrm{kg/kg}}$	λ
KIT I	1.28	1.61	0.525
KIT II	1.40	1.61	0.525
KIT III	1.42	1.69	0.503
EXT I	1.46	1.68	0.506
EXT II	1.65	1.71	0.496

The equilibrium compositions in mole fractions $\boldsymbol{x}_{\mathrm{eq}} = (x_{i,\mathrm{eq}})$ and the equilibrium temperatures T_{eq} based on the five chemical analysis results are shown in Fig. 13. The equilibrium concentrations of H_2 and H_2O and the equilibrium temperature are thus very sensitive to the chemical analysis results, whereas this applies less to the equilibrium concentrations of CO, CO_2 and N_2. Moreover, the uncertainties (see Section 3.2) are shown in Fig. 13. The uncertainties of the equilibrium temperatures are up to $\pm 151\,\mathrm{K}$ if the deviations of the analysis results are inside the reproducibility limits (in particular of the carbon and hydrogen contents). Moreover, the uncertainties of the equilibrium concentrations of H_2 and H_2O are up to ± 0.021, whereas those of the equilibrium concentrations of CO, CO_2 and N_2 are much smaller. Note that the uncertainties of the equilibrium concentrations reflect both the impact of the uncertainties of the elemental contents and the impact of the adjusted equilibrium temperature. The former impact is based on the reproducibility limits, whereas the latter is due to the water-gas shift reaction (see [55]). The uncertainties of the equilibrium concentrations due to the shift of the equilibrium temperature only are up to ± 0.013.

The equilibrium cold gas efficiencies $\mathrm{CGE}_{\mathrm{eq}}$ are compared in Table 15. The equilibrium cold gas efficiency $\mathrm{CGE}_{\mathrm{eq}}$ is in a broad range between 59 % and 65 %. However, similar values were obtained based on the analysis results of the laboratories KIT III, EXT I and EXT II, i. e. the analysis data with Boie ratios of approximately 100 %. This is in agreement with previous recommendations to use fuel data with a Boie ratio close to 100 % for process calculations [55, 70].

Table 15: Equilibrium cold gas efficiencies CGE_{eq} based on different chemical analysis results.

Laboratory	$\frac{CGE_{eq}}{\%}$
KIT I	59.39
KIT II	60.22
KIT III	64.79
EXT I	63.81
EXT II	64.63

In summary, uncertain chemical beech wood pyrolysis oil data strongly affect both the design and the evaluation of entrained flow gasification experiments. This is primarily because the elemental and water contents are strongly linked with the stoichiometries of both slurry and feed. In addition, both the elemental and water contents, and the heating value influence the flow rate, composition and temperature of the synthesis gas in the equilibrium model. In order to reduce the uncertainties of both the carbon, hydrogen and water contents and the heating values (see Section 4.1) and eventually improve the design and evaluation of technical processes, future studies should enhance the sampling and the analysis methods for the chemical properties of pyrolysis oils.

5.2. Vacuum distillations

Vacuum distillations at 40 mbar were applied to separate the beech wood pyrolysis oil into vaporisable and non-vaporisable components, assuming that the vacuum distillate and the vacuum distillation residue can represent the volatile and the non-volatile components of the beech wood pyrolysis oil. However, some comments and comparisons are needed to substantiate this approach:

1. The GC-MS data indicates a lower mass fraction of volatiles (44.5 %) compared to both the vacuum distillation data (57.7 %) and the Engler distillation data (60.4 %). This is reasonable because the GC-MS analyses did not (fully) detect low-volatile components with boiling temperatures

above 523 K (see Sections 3.3 and 4.2). Thus, both vacuum distillates and Engler distillates are better representatives of the vaporisable components than mixtures based on GC-MS data (see also Section S4).

2. The mass fraction of the Engler distillate (60.4 %) is greater than the mass fraction of the vacuum distillate (57.7 %) and less than the maximum possible mass fraction of the vacuum distillate (66.7 %). This is because some volatiles were lost during vacuum distillation (see Section 4.4). In addition to that, some volatiles that decompose rather than vaporise under atmospheric-pressure conditions were released during vacuum distillation (see Section 4.4). Therefore, the vacuum distillate differs from the Engler distillate and is not fully representative of the vaporisable components under atmospheric-pressure conditions. The Engler distillate could be superior to the vacuum distillate.

3. The Engler distillation residue cannot be used for further analysis based on the authors' experiences. Thus, the vacuum distillation residue is likely the most appropriate basis for investigating the chemical and physical properties of the non-vaporisable components.

4. The TG data demonstrates that the TG and DTG curves for the beech wood pyrolysis oil are largely consistent with the mass fraction-weighted and superposed TG and DTG curves of the vacuum distillate and the vacuum distillation residue. Thus, the vacuum distillate and the vacuum distillation residue can reflect the TG behaviour of the beech wood pyrolysis oil.

In summary, vacuum distillation can provide representative samples of the vaporisable and non-vaporisable components to a large extent. Therefore, the thermo-physical properties of the vacuum distillate and the vacuum distillation residue were measured and used to describe the vaporisable and non-vaporisable fractions of the beech wood pyrolysis oil. Future studies may improve upon this approach.

5.3. TG analyses

TG analyses have been conducted for a wide range of biogenic pyrolysis oils. For example, TG curves were determined for four commercial wood pyrolysis oils in the presence of oxygen at a heating rate of 5 K/min and a maximum temperature of 600 K [3]. These oils were derived in the pyrolysis plants of BTG, Dynamotive, Ensyn and Pyrovac, respectively, and exhibited water contents of 30.4 % (BTG), 21.1 % (Dynamotive), 20.3 % (Ensyn) and 15.7 % (Pyrovac) [3]. The TG curves of these four oils are reproduced in Fig. 14 and are compared with the TG data of the (proFagus) beech wood pyrolysis oil for 5 K/min. First, note that the TG curves were determined using different setups. In this study, the temperature was measured below the sample crucible (see Section 3.7), whereas the thermocouple was previously positioned close to the sample bottom [3]. This could limit the comparability of the TG data (see [20]). Then, despite a qualitative agreement, the TG curves differ clearly from each other. The volatiles of the proFagus pyrolysis oil were mainly released between 350 K and 600 K, whereas the sample masses of the other pyrolysis oils mainly decreased between 300 K and 550 K. Moreover, between 300 K and 400 K, the mass decreased more strongly for the BTG pyrolysis oil with the highest water content than for the other oils with lower water contents. The water content thus strongly determines the thermogravimetric conversion, while the impact of other volatiles is less pronounced, as the pyrolysis oils with similar water contents (Dynamotive and Ensyn) have shown similar mass decreases. This is also in line with TG analyses of other proFagus pyrolysis oil charges with slightly different water contents. Furthermore, 23-45 % of the initial sample masses were retrieved as residues at 600 K. The residues were similar for the proFagus, the Ensyn and the BTG pyrolysis oil, while larger residues were obtained for the Dynamotive and the Pyrovac pyrolysis oil. This reflects different contents of (light and heavy) volatiles. In summary, the TG data of the (proFagus) beech wood pyrolysis oil is in accordance with its water content. Therefore, the TG data should not be adopted for other pyrolysis oils with higher water contents. However, future studies may use the TG data for pyrolysis oils with similar water contents in

the absence of experimental data.

5.4. TG kinetics

TG kinetics were derived for the beech wood pyrolysis oil using multi-reaction Arrhenius law models (MRALM), multi first-order reaction Arrhenius law models (MFORALM) and multi first-order reaction Gauss distributed activation energy models (MFORGDAEM). Zero-dimensional particle simulations were subsequently performed using an in-house software in Python to compare the kinetics. Two test cases were considered in this study.

In test case 1, a non-moving spherical droplet with an initial temperature of 300 K and an initial diameter of 100 µm is heated up using a constant heating rate of 50 K/min in an inert non-moving gas. The particle temperature T_{part} was thus prescribed, as shown in Fig. 15 (left), while differential equations were solved for the particle conversion X_{part} using constant time steps of 1 s and assuming constant particle diameters. The simulated particle conversions X_{part} are shown in Fig. 15 (right). The multi-reaction Arrhenius law model and the multi first-order reaction Arrhenius law model provide similar predictions, whereas the conversion based on the multi first-order reaction Gauss distributed activation energy model is initially faster and then slows down in accordance with the numerical approximations (see Section 4.6).

In test case 2, a non-moving spherical droplet with the same initial temperature of 300 K and the same initial diameter of 100 µm is assumed in a non-moving gas consisting of nitrogen with a gas temperature of 1673 K and a gas pressure of 1 bar. Differential equations were solved for the particle temperature T_{part} and the particle conversion X_{part} using constant time steps of 10^{-4} s, assuming constant particle diameters and with an empirical approach for the particle heat capacity (see Section S3). Furthermore, the initial mass fractions $\boldsymbol{w}_0 = (w_i)$ were adjusted for high-heating-rate conditions based on previous observations [29] and SEM images of cenospheres collected in atmospheric-pressure drop-tube reactor experiments and bioliq EFG experiments (see Fig. 16). The adjustment is depicted for the multi first-order

reaction Gauss distributed activation energy model in Fig. 17. The initial mass fractions $\boldsymbol{w}_0$ for high heating rates are given in Table S12.

The simulated particle temperatures T_{part} are shown in Fig. 18 (left) and differ clearly from each other, as the particle temperatures T_{part} are linked with the particle conversion X_{part} through the correlation of the particle heat capacity (see Section S3). The simulated particle conversions X_{part} are shown in Fig. 18 (right). The kinetics provide full conversion at about 0.3 s (MFORGDAEM), 1.6 s (MRALM) and 3.5 s (MFORALM), respectively. First of all, this is in line with the adjusted initial mass fractions $\boldsymbol{w}_0$. Then, the multi first-order reaction Gauss distributed activation energy model provides faster conversion than the multi-reaction Arrhenius law models. This can also be observed for both smaller and larger particles (see Figs. S1 and S2). Moreover, both multi-reaction Arrhenius law models provide deviating predictions. Recalling that the kinetics were derived at low heating rates of between 2 K/min and 50 K/min, this indicates inconsistent extrapolation behaviour of the multi-reaction Arrhenius law models. It also shows that extrapolation of TG kinetics can result in unreliable predictions at high heating rates. Therefore, kinetics from drop-tube reactor experiments should be preferred over TG kinetics for simulations with rapid heating processes. However, in the absence of kinetics based on elaborative drop-tube reactor experiments, kinetics may be developed using the steps described below:

1. TG analyses under inert conditions at heating rates of 2 K/min, 5 K/min, 10 K/min, 20 K/min and 50 K/min up to a maximum temperature of 1273 K
2. Numerical approximation of experimental TG curves under constraints using multi-reaction Gauss distributed activation energy models
3. Numerical extrapolation of TG and DTG curves to heating rates of 10^3 K/min, 10^4 K/min, 10^5 K/min and 10^6 K/min applying multi-reaction Gauss distributed activation energy models with the parameters from the previous numerical approximation but with adjusted initial

mass fractions (corresponding to the expected minimum remaining mass fractions at high heating rates)

4. Calculation of numerical TG and DTG curves at 2 K/min, 5 K/min, 10 K/min, 20 K/min, 50 K/min, 10^3 K/min, 10^4 K/min, 10^5 K/min and 10^6 K/min using multi first-order reaction Gauss distributed activation energy models
5. Numerical approximation using multi-reaction Arrhenius law models or multi first-order reaction Arrhenius law models

In summary, decomposition kinetics for high heating rates may be derived using multi-reaction Arrhenius law models from TG and DTG curves predicted by multi-reaction Gauss distributed activation energy models, where the latter models should be based on experimental TG and DTG curves. This is recommended because (i) multi-reaction Gauss distributed activation energy models could provide better extrapolation behaviour (see [66, 95]) and (ii) decompositions kinetics based on multi-reaction Arrhenius law models are beneficial for CFD simulations of combustion and entrained flow gasification processes due to lower computing times.

The numerical approximations of the numerical TG and DTG curves using multi-reaction Arrhenius law models with unity and non-unity reaction orders are shown in Fig. 19. The approximations based on the multi-reaction Arrhenius law model and non-unity reaction orders are thus slightly superior for high heating rates compared to the approximations based on the multi first-order reaction Arrhenius law model. The parameters of the approximations for the heating rate of 10^6 K/min are presented in Tables 16 and 17.

Table 16: Parameters for the calculation of the mass loss w and the derivative of the mass loss $\mathrm{d}w/\mathrm{d}t$ for the beech wood pyrolysis oil using the multi-reaction Arrhenius law model based on Eqs. (3)-(8).

i	$\frac{k_{0,i}}{1/\mathrm{s}}$	$\frac{\overline{E}_{\mathrm{a},i}}{\mathrm{J/mol}}$	n_i	$\frac{w_{0,i}}{10^6\ \frac{\mathrm{K}}{\mathrm{min}}}$
1	$1.089 \cdot 10^5$	$7.951 \cdot 10^4$	1.552	$8.758 \cdot 10^{-11}$
2	$3.363 \cdot 10^3$	$4.697 \cdot 10^4$	1.228	$3.211 \cdot 10^{-1}$
3	$1.849 \cdot 10^2$	$5.481 \cdot 10^4$	2	$2.215 \cdot 10^{-7}$
4	$1.077 \cdot 10^4$	$6.132 \cdot 10^4$	1.281	$6.982 \cdot 10^{-1}$

Table 17: Parameters for the calculation of the mass loss w and the derivative of the mass loss $\mathrm{d}w/\mathrm{d}t$ for the beech wood pyrolysis oil using the multi first-order reaction Arrhenius law model based on Eqs. (3)-(8).

i	$\frac{k_{0,i}}{1/\mathrm{s}}$	$\frac{\overline{E}_{\mathrm{a},i}}{\mathrm{J/mol}}$	n_i	$\frac{w_{0,i}}{10^6\ \frac{\mathrm{K}}{\mathrm{min}}}$
1	$6.394 \cdot 10^3$	$6.115 \cdot 10^4$	1	$4.839 \cdot 10^{-1}$
2	$6.721 \cdot 10^3$	$7.172 \cdot 10^4$	1	0
3	$4.609 \cdot 10^3$	$5.026 \cdot 10^4$	1	$4.951 \cdot 10^{-1}$
4	1.259	$4.390 \cdot 10^4$	1	0

6. Conclusions

Chemical and physical property data, thermo-physical property models and decomposition kinetics were determined for an industrial beech wood pyrolysis oil with a low water content and a high oligomer content. The investigation included (i) proximate, ultimate, heating value, gas chromatography-mass spectrometry (GC-MS), gel permeation chromatography (GPC) and thermogravimetric (TG) analyses, (ii) vacuum and Engler distillations and (iii) measurements of density, dynamic viscosity, thermal conductivity, specific

heat capacity and surface tension. The data and the models can be used for the design and scale-up of combustion or entrained flow gasification processes using both process and CFD models. The conclusions based on the evaluation of the measured and derived data are summarised below:

1. The uncertainties of the sampling and chemical analysis methods strongly affect the design and the performance evaluation of technical processes.
2. The vaporisable and non-vaporisable fractions of pyrolysis oils can be separated through vacuum distillation to a large extent.
3. The TG data of the vacuum distillate and the vacuum distillation residue can show the superposition of vaporisation and decomposition.
4. The thermal conductivity data and the heat capacity data of pyrolysis oils strongly depend on the water content.
5. Multi-reaction Arrhenius law models have provided slightly superior approximations of the TG data of the beech wood pyrolysis oil compared to multi first-order reaction Gauss distributed activation energy models. The latter models, however, are recommended for the extrapolation to high heating rates in the absence of kinetics based on drop-tube reactor experiments.

Future studies should enhance the sampling and the analysis methods for the chemical properties of pyrolysis oils, including the carbon, hydrogen, oxygen and water contents and the heating values. In the absence of enhanced methods, the chemical analysis data could be assessed using the Boie correlation [69] and the Boie ratio (see [55]), or using measured and balanced process data from laboratory-scale or pilot-scale experiments (see [55]). Due to fuel complexity and variability and the impact of the water content, the chemical and physical property data and kinetics derived in this study could only be used to describe beech wood pyrolysis oils with water contents around 5-10 %. Therefore, future studies may also focus on the comprehensive characterisation of biogenic pyrolysis oils with water contents between 10 % and 30 % and of anthropogenic pyrolysis oils. Such an investigation may analyse whether

pyrolysis oils on dry basis exhibit similar thermo-physical properties. Future studies may also determine the decomposition rates at low and high heating rates as well as under atmospheric- and high-pressure conditions. In addition, gaseous and solid decomposition products may be characterised regarding their chemical and physical properties, as the products determine the temperature distribution and the conversion in technical processes (see [53, 54, 63]). Finally, future studies may incorporate the data and the models for the beech wood pyrolysis oil in detailed combustion or entrained flow gasification models. The chemical analysis data and the thermo-physical property models can be used to describe the chemical and physical properties of pyrolysis oil droplets, while the extrapolated kinetics can be applied to describe the droplet conversion.

Acknowledgements

The authors thank (i) the Helmholtz Association of German Research Centres (HGF) for funding the programmes Energy Efficiency, Materials and Resources (EMR) and Materials and Technologies for the Energy Transition (MTET), (ii) Volker Zibat (Karlsruhe Institute of Technology, Light Technology Institute) for the experimental support and (iii) Hannah Knoch (Karlsruhe Institute of Technology, Institute for Technical Chemistry, Gasification Technology) and Stella Clara Walker (Karlsruhe Institute of Technology, Engler-Bunte-Institute, Fuel Technology and Karlsruhe Institute of Technology, Institute for Technical Chemistry, Gasification Technology) for the constant collaboration.

Figures

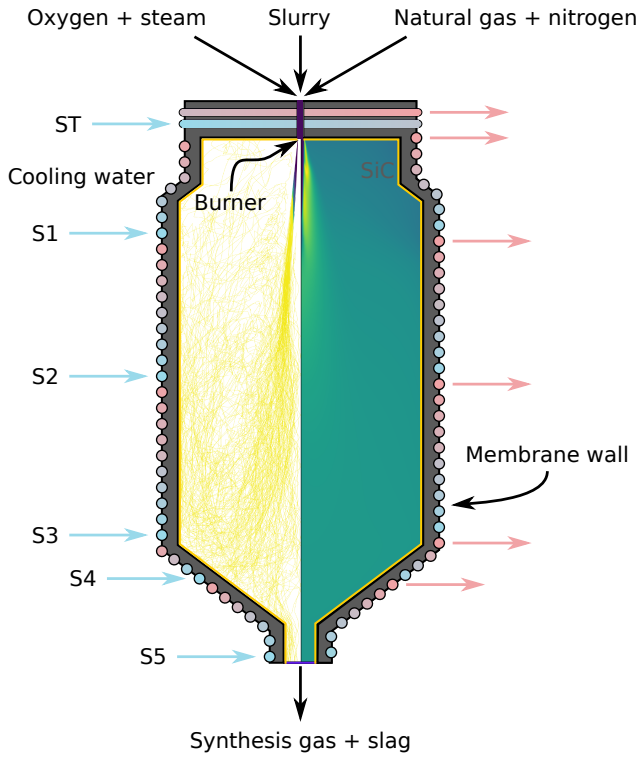

Figure 1: Schematic cross section of the bioliq EFG reactor with the feed and product streams, with the cooling circuits S1, ..., ST, with particle trajectories of pyrolysis oil droplets (left; coloured by conversion; violet: no conversion, yellow: almost full conversion) and with a gas temperature distribution (right).

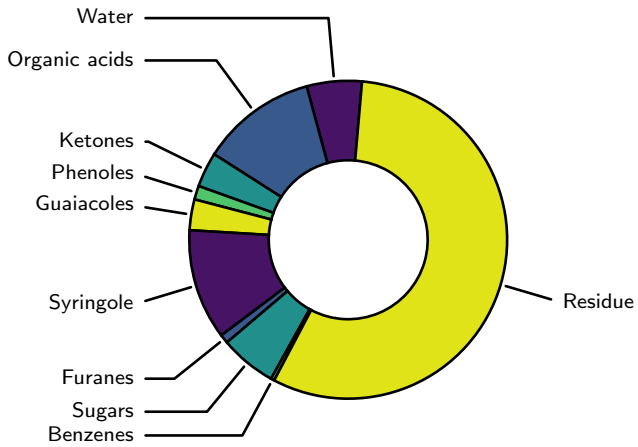

Figure 2: Composition of the beech wood pyrolysis oil based on the GC-MS analyses.

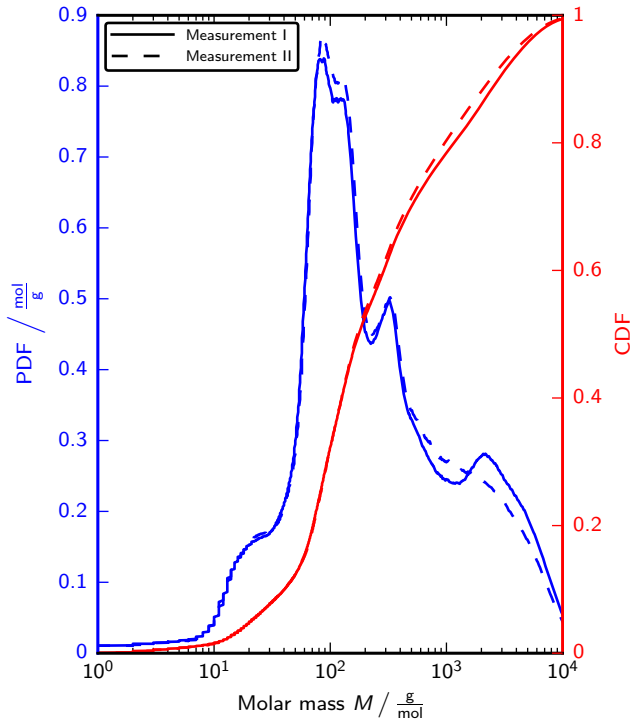

Figure 3: Molar mass distributions of the beech wood pyrolysis oil based on the GPC analyses: probability density function (PDF) and cumulative distribution function (CDF) for two single measurements.

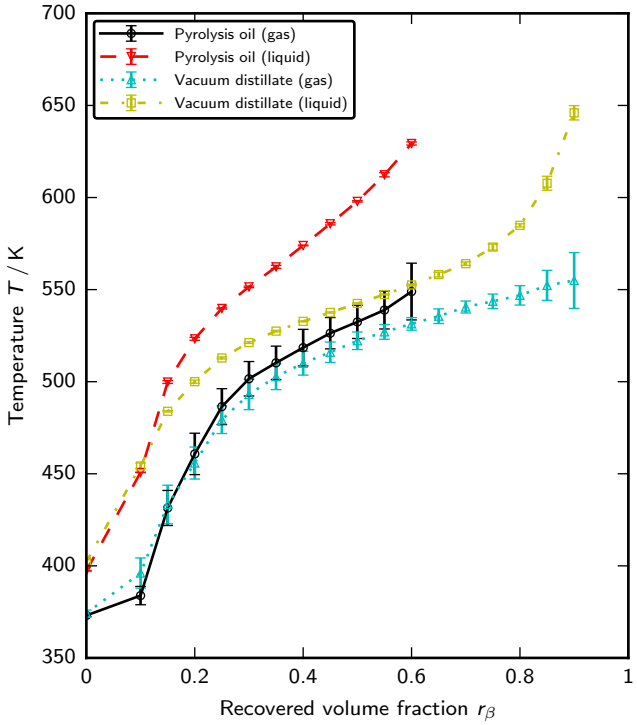

Figure 4: Engler distillation curves of the beech wood pyrolysis oil and the vacuum distillate.

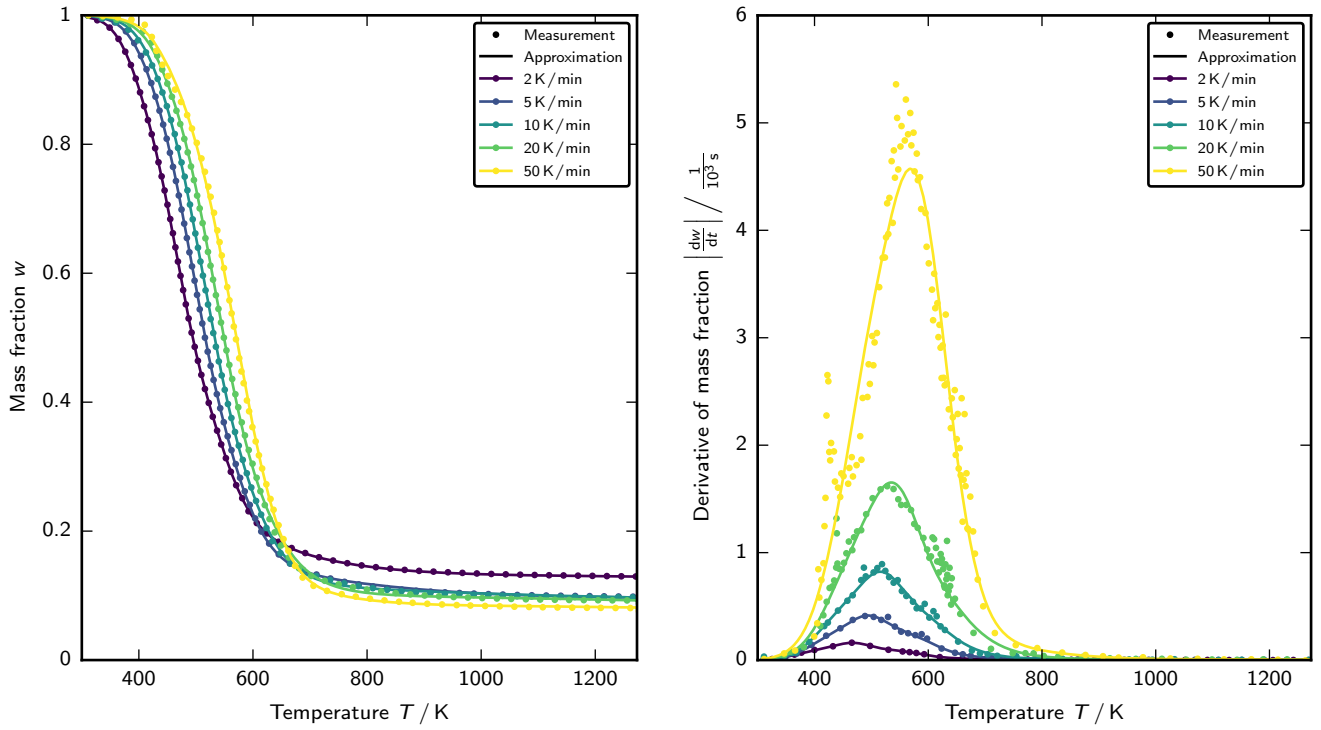

Figure 5: TG and DTG curves of the beech wood pyrolysis oil: comparison of measurement data with numerical approximations based on the multi-reaction Arrhenius law model.

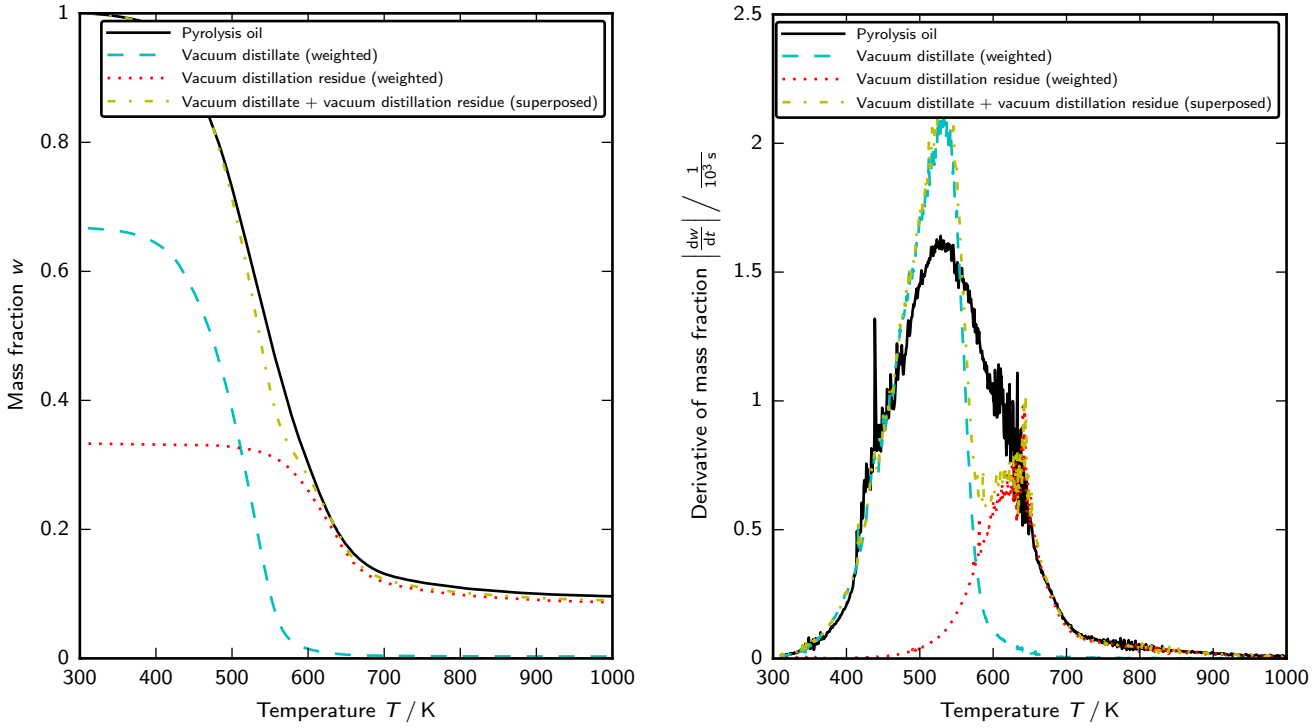

Figure 6: TG and DTG curves of the beech wood pyrolysis oil, the vacuum distillate and the vacuum distillation residue.

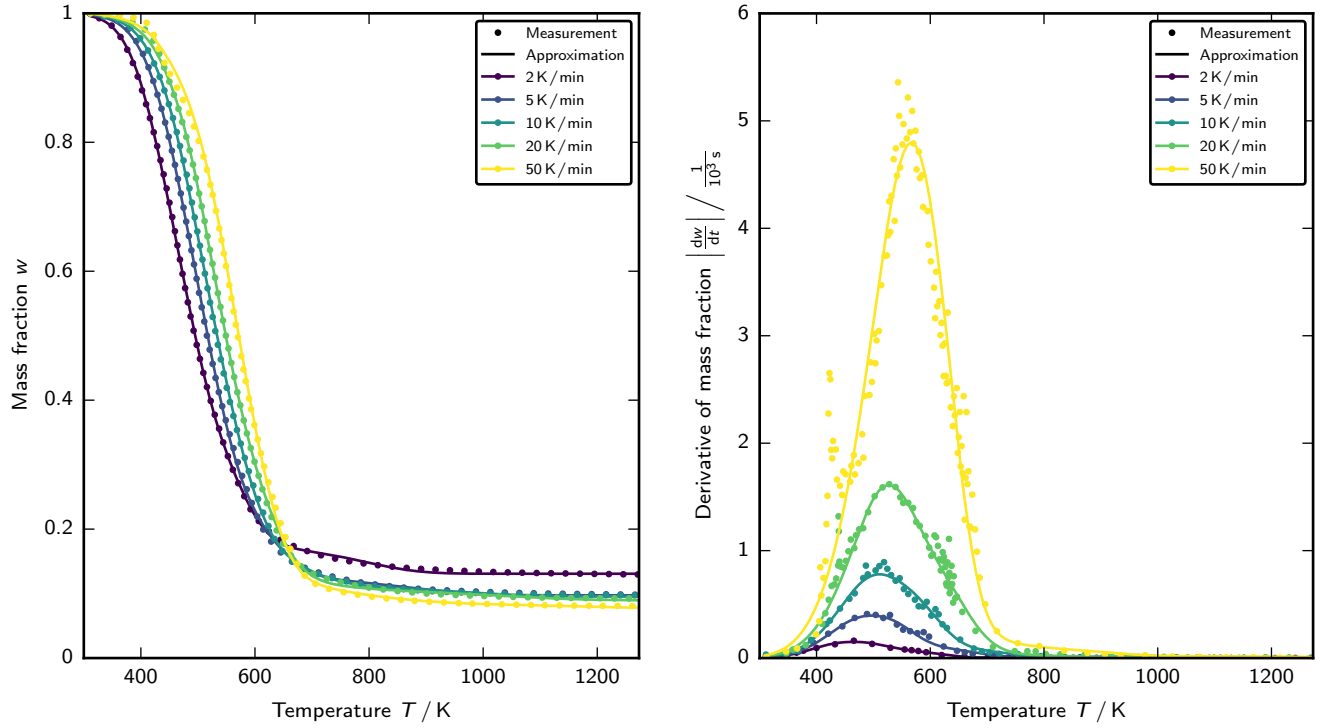

Figure 7: TG and DTG curves of the beech wood pyrolysis oil: comparison of measurement data with numerical approximations based on the multi first-order reaction Arrhenius law model.

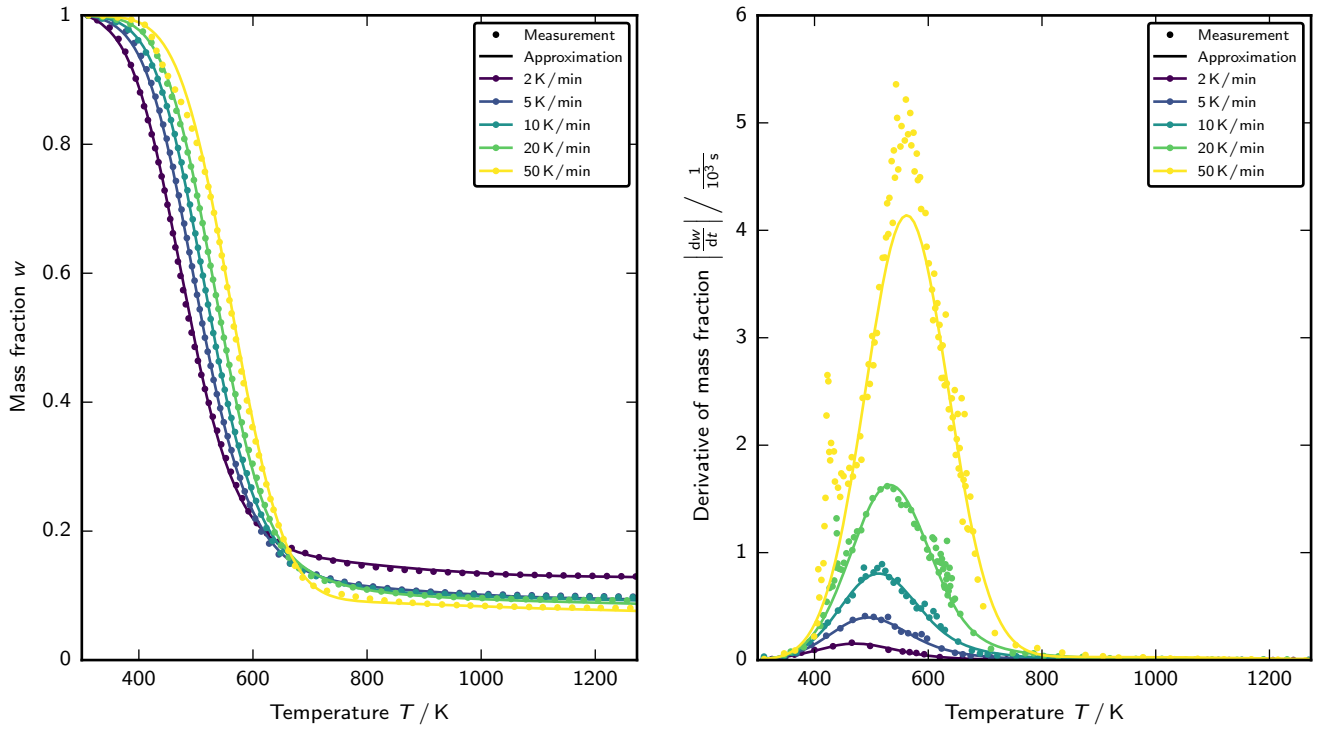

Figure 8: TG and DTG curves of the beech wood pyrolysis oil: comparison of measurement data with numerical approximations based on the multi first-order reaction Gauss distributed activation energy model.

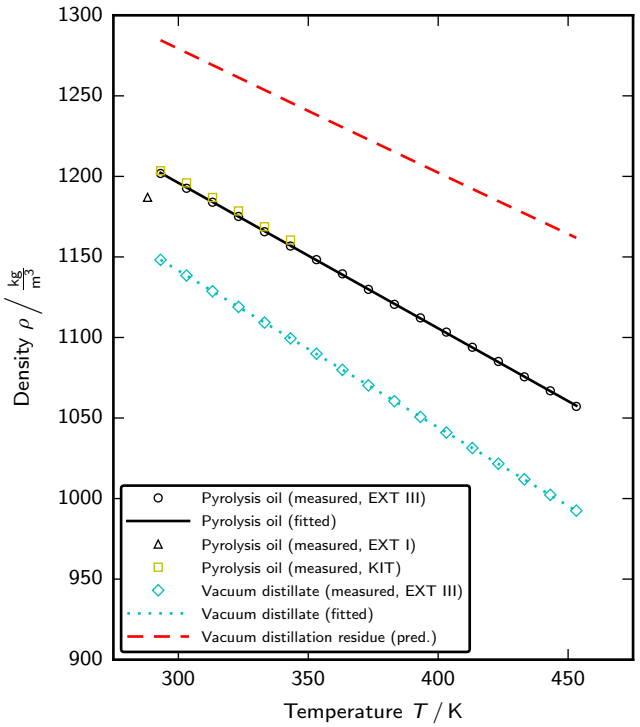

Figure 9: Densities of the beech wood pyrolysis oil, the vacuum distillate and the vacuum distillation residue: comparison of measurement data with numerical approximations. Note the abbreviation: pred.: predicted.

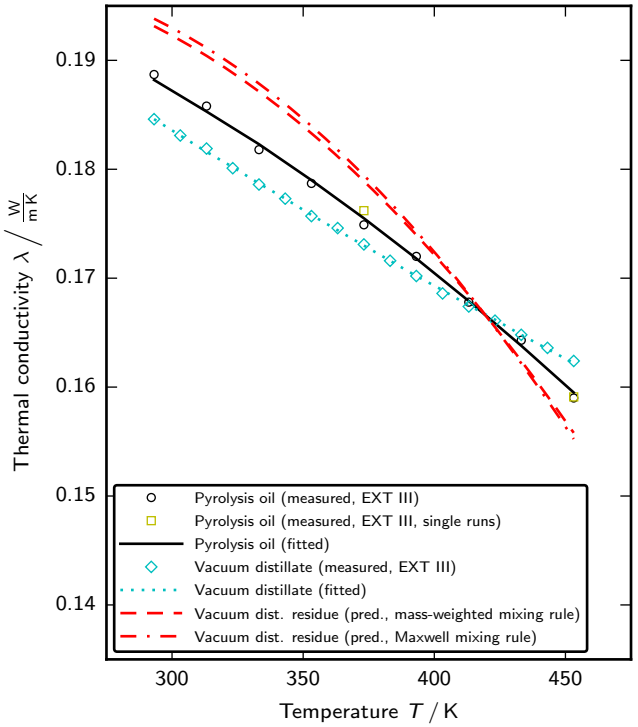

Figure 10: Thermal conductivities of the beech wood pyrolysis oil, the vacuum distillate and the vacuum distillation residue: comparison of measurement data with numerical approximations. Note the abbreviations: dist.: distillation; pred.: predicted.

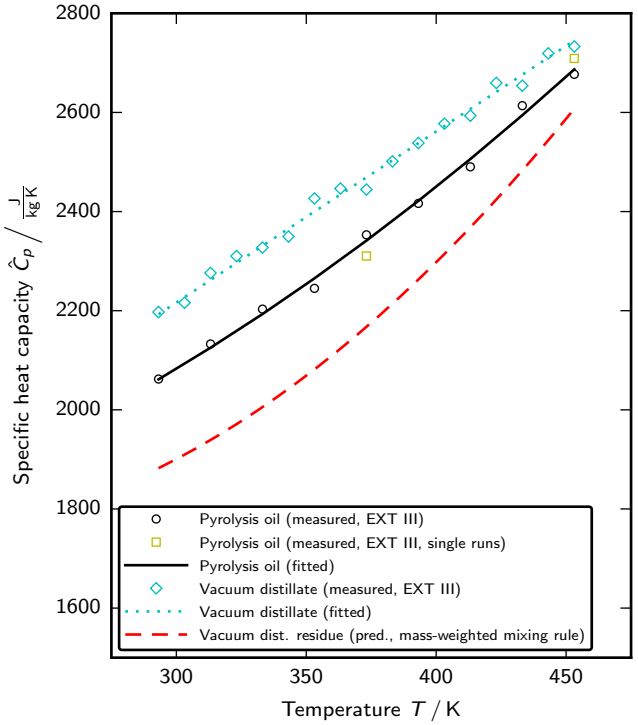

Figure 11: Specific heat capacities of the beech wood pyrolysis oil, the vacuum distillate and the vacuum distillation residue: comparison of measurement data with numerical approximations. Note the abbreviations: dist.: distillation; pred.: predicted.

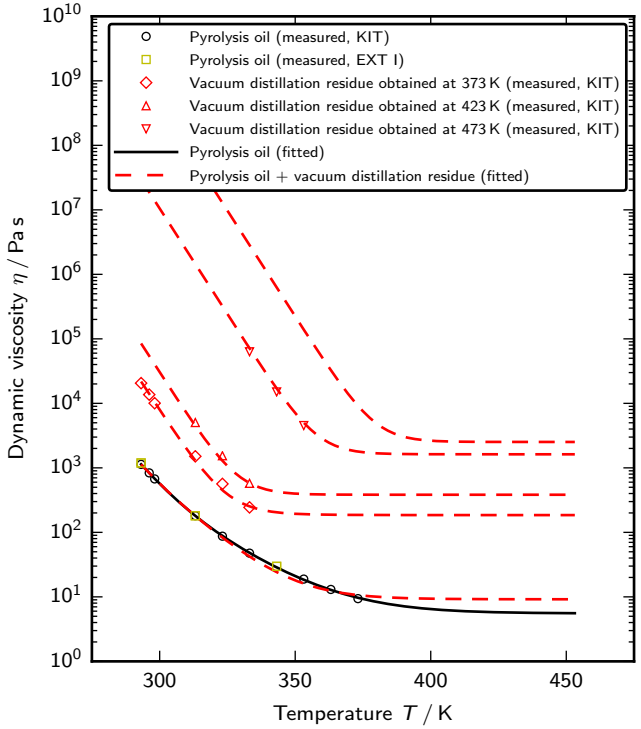

Figure 12: Dynamic viscosity of the beech wood pyrolysis oil and four vacuum distillation residues: comparison of measurement data with numerical approximations.

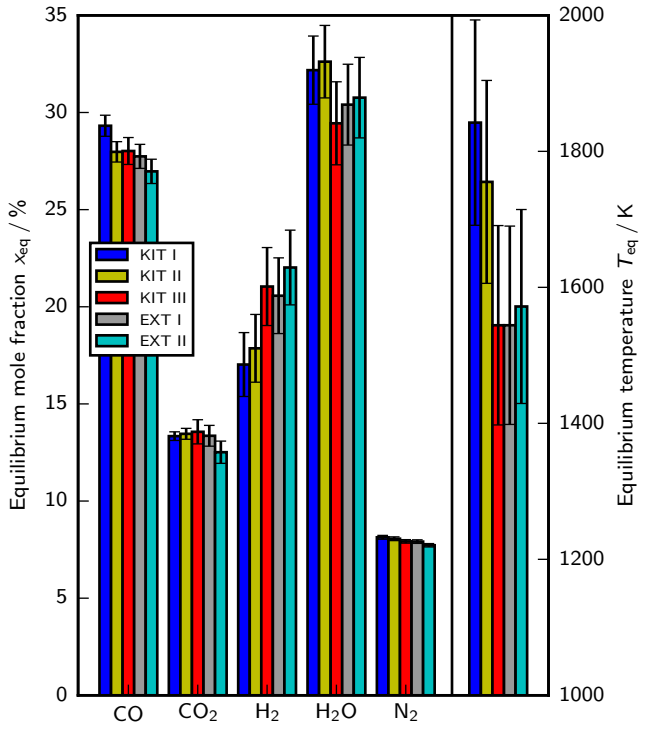

Figure 13: Equilibrium compositions in mole fractions $\boldsymbol{x}_{\mathrm{eq}}$ and equilibrium temperature T_{eq}, based on different chemical analysis results, for the bioliq EFG experiment V105.

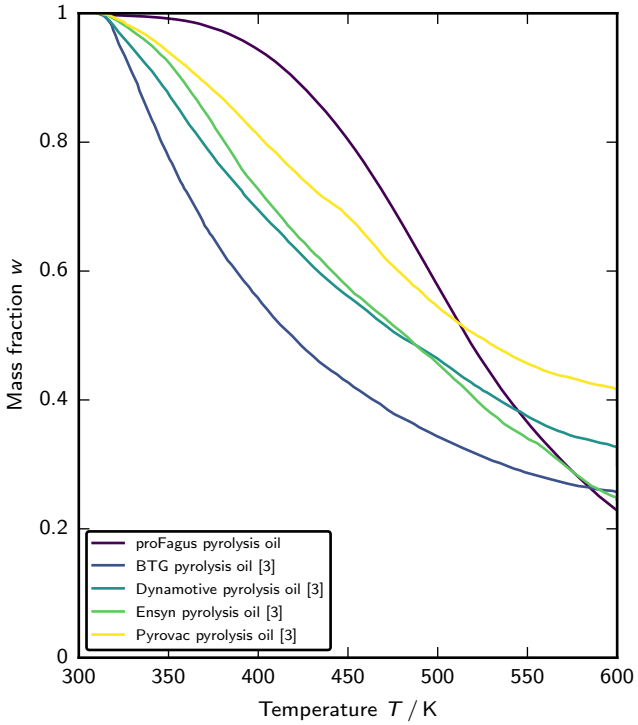

Figure 14: TG curves of the BTG, Dynamotive, Ensyn and Pyrovac pyrolysis oils at 5 K/min [3] in comparison with the TG data of the (proFagus) beech wood pyrolysis oil.

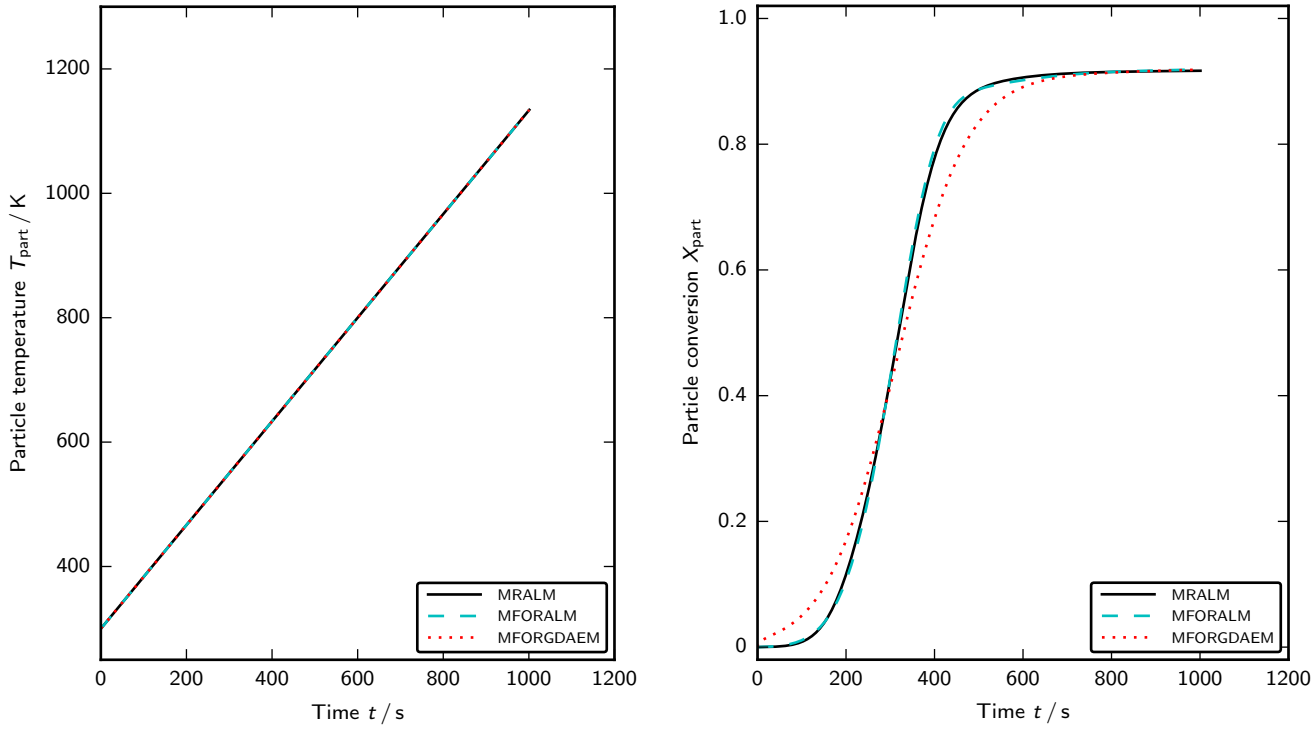

Figure 15: Assumed particle temperatures T_{part} (left) and predicted particle conversions X_{part} (right) using the multi-reaction Arrhenius law model (MRALM), the multi first-order reaction Arrhenius law model (MFORALM) and the multi first-order reaction Gauss distributed activation energy model (MFORGDAEM) for test case 1.

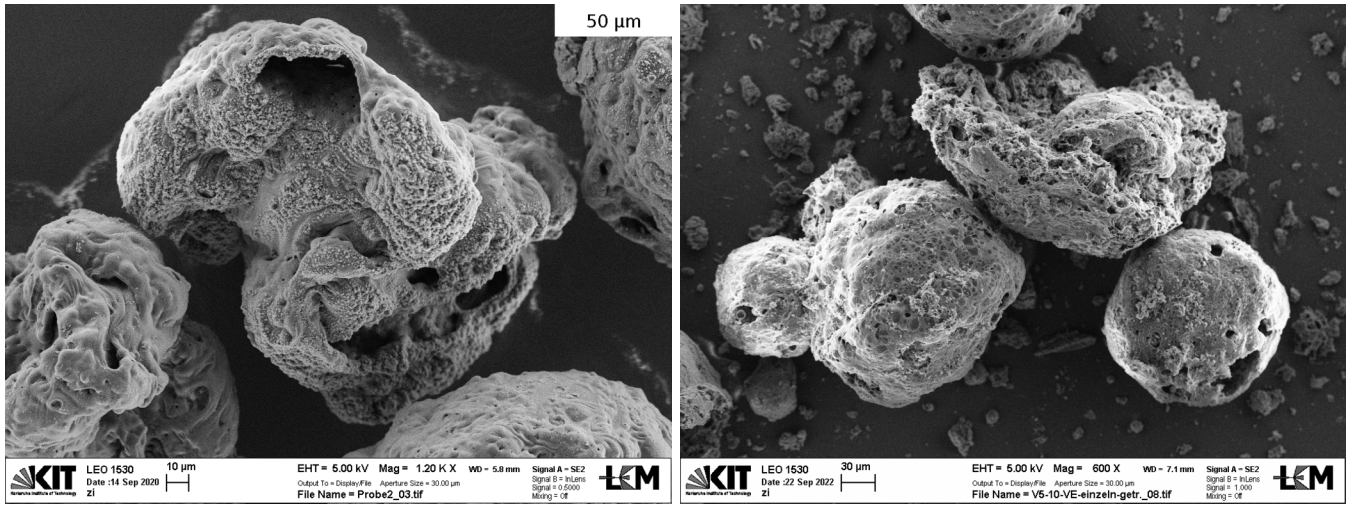

Figure 16: SEM images of cenospheres collected in an atmospheric-pressure drop-tube reactor experiment (1273 K, 1 bar, left) and in a bioliq EFG experiment (1433 K, 40 bar, right), each with (proFagus) beech wood pyrolysis oil.

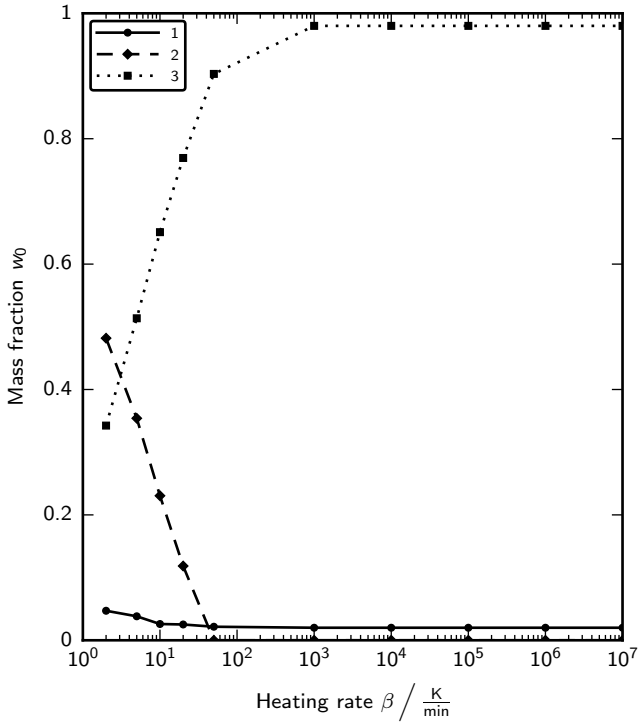

Figure 17: Extrapolation of the initial mass fractions $w_{0,1}$, $w_{0,2}$ and $w_{0,3}$ to high heating rates for the multi first-order reaction Gauss distributed activation energy model. Note that the labels refer to the indices of the initial mass fraction $\boldsymbol{w}_0$.

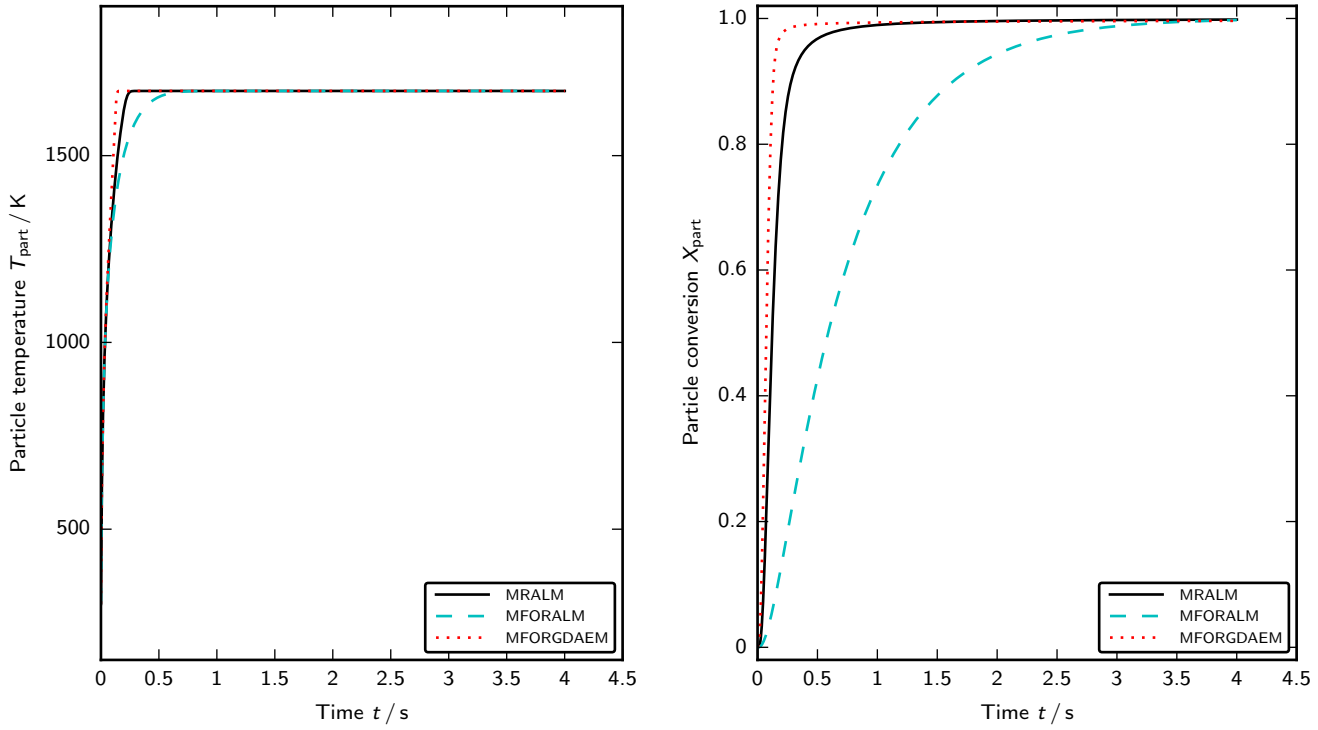

Figure 18: Predicted particle temperatures T_{part} (left) and predicted particle conversions X_{part} (right) using the multi-reaction Arrhenius law model (MRALM), the multi first-order reaction Arrhenius law model (MFORALM) and the multi first-order reaction Gauss distributed activation energy model (MFORGDAEM) for test case 2.

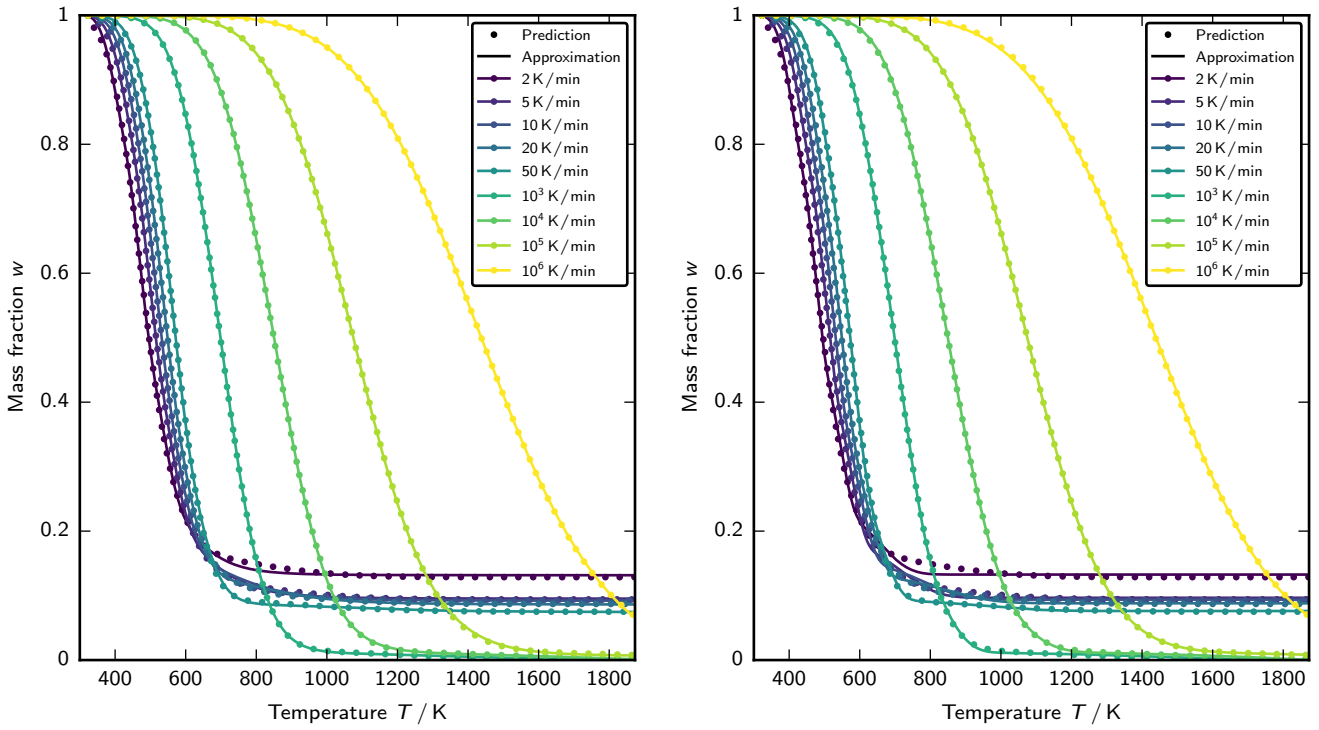

Figure 19: TG curves of the beech wood pyrolysis oil: comparison of predicted data based on the multi first-order reaction Gauss distributed activation energy model with numerical approximations based on the multi-reaction Arrhenius law model (left) and the multi first-order reaction Arrhenius law model (right).

References

[1] D. Mohan, C. U. Pittman, P. H. Steele, Pyrolysis of wood/biomass for bio-oil: a critical review, Energy & Fuels 20 (3) (2006) 848–889. doi:10.1021/ef0502397.
URL https://doi.org/10.1021/ef0502397

[2] C. Branca, P. Giudicianni, C. Di Blasi, GC/MS characterization of liquids generated from low-temperature pyrolysis of wood, Industrial & Engineering Chemistry Research 42 (14) (2003) 3190–3202. doi:10.1021/ie030066d.
URL https://doi.org/10.1021/ie030066d

[3] C. Branca, C. Di Blasi, R. Elefante, Devolatilization and heterogeneous combustion of wood fast pyrolysis oils, Industrial & Engineering Chemistry Research 44 (4) (2005) 799–810. doi:10.1021/ie049419e.
URL https://doi.org/10.1021/ie049419e

[4] C. Branca, C. Di Blasi, Multistep mechanism for the devolatilization of biomass fast pyrolysis oils, Industrial & Engineering Chemistry Research 45 (17) (2006) 5891–5899. doi:10.1021/ie060161x.
URL https://doi.org/10.1021/ie060161x

[5] M. García-Pérez, A. Chaala, H. Pakdel, D. Kretschmer, C. Roy, Characterization of bio-oils in chemical families, Biomass and Bioenergy 31 (4) (2007) 222–242. doi:10.1016/j.biombioe.2006.02.006.
URL https://doi.org/10.1016/j.biombioe.2006.02.006

[6] M. García-Pérez, T. T. Adams, J. W. Goodrum, D. P. Geller, K. C. Das, Production and fuel properties of pine chip bio-oil/biodiesel blends, Energy & Fuels 21 (4) (2007) 2363–2372. doi:10.1021/ef060533e.
URL https://doi.org/10.1021/ef060533e

[7] E.-B. M. Hassan, P. H. Steele, L. Ingram, Characterization of fast pyrolysis bio-oils produced from pretreated pine wood, Applied Biochemistry and

Biotechnology 154 (1-3) (2008) 3–13. doi:10.1007/s12010-008-8445-3.
URL https://doi.org/10.1007/s12010-008-8445-3

[8] S. Czernik, A. V. Bridgwater, Overview of applications of biomass fast pyrolysis oil, Energy & Fuels 18 (2) (2004) 590–598. doi:10.1021/ef034067u.
URL https://doi.org/10.1021/ef034067u

[9] L. Fagernäs, Chemical and physical characterisation of biomass-based pyrolysis oils, Tech. Rep. 1706, VTT Technical Research Centre of Finland, Espoo, Finland (Dec. 1995).
URL https://cris.vtt.fi/en/publications/chemical-and-physical-characterisation-of-biomass-based-pyrolysis

[10] A. Oasmaa, E. Leppämäki, P. Koponen, J. Levander, E. Tapola, Physical characterisation of biomass-based pyrolysis liquids: application of standard fuel oil analyses, Tech. Rep. 306, VTT Technical Research Centre of Finland, Espoo, Finland (1997).
URL https://cris.vtt.fi/en/publications/physical-characterisation-of-biomass-based-pyrolysis-liquids-appl

[11] A. Oasmaa, C. Peacocke, A guide to physical property characterisation of biomass-derived fast pyrolysis liquids, Tech. Rep. 450, VTT Technical Research Centre of Finland, Espoo, Finland (2001).
URL https://cris.vtt.fi/en/publications/a-guide-to-physical-property-characterisation-of-biomass-derived-

[12] Q. Lu, W.-Z. Li, X.-F. Zhu, Overview of fuel properties of biomass fast pyrolysis oils, Energy Conversion and Management 50 (5) (2009) 1376–1383. doi:10.1016/j.enconman.2009.01.001.
URL https://doi.org/10.1016/j.enconman.2009.01.001

[13] M. Staš, D. Kubička, J. Chudoba, M. Pospíšil, Overview of analytical methods used for chemical characterization of pyrolysis bio-oil, Energy &

Fuels 28 (1) (2014) 385–402. doi:10.1021/ef402047y.
URL https://doi.org/10.1021/ef402047y

[14] M. Dammann, U. Santo, D. Böning, H. Knoch, M. Eberhard, T. Kolb, Characterisation of beech wood pyrolysis oil: chemical and physical property data (internal report) (2022).

[15] N. N. Bakhshi, J. D. Adjaye, Properties and characteristics of Ensyn bio-oil, in: Proceedings of the Biomass Pyrolysis Oil Properties and Combustion Meeting, 26-28 September 1994, Estes Park, CO, USA, Estes Park, CO, USA, 1994, pp. 54–66.

[16] G. V. C. Peacocke, P. A. Russell, J. D. Jenkins, A. V. Bridgwater, Physical properties of flash pyrolysis liquids, Biomass and Bioenergy 7 (1-6) (1994) 169–177. doi:10.1016/0961-9534(94)00056-y.
URL https://doi.org/10.1016/0961-9534(94)00056-Y

[17] D. C. Elliott, D. Meier, A. Oasmaa, B. van de Beld, A. V. Bridgwater, M. Marklund, Results of the International Energy Agency round robin on fast pyrolysis bio-oil production, Energy & Fuels 31 (5) (2017) 5111–5119. doi:10.1021/acs.energyfuels.6b03502.
URL https://doi.org/10.1021/acs.energyfuels.6b03502

[18] S. Vitolo, P. Ghetti, Physical and combustion characterization of pyrolytic oils derived from biomass material upgraded by catalytic hydrogenation, Fuel 73 (11) (1994) 1810–1812. doi:10.1016/0016-2361(94)90175-9.
URL https://doi.org/10.1016/0016-2361(94)90175-9

[19] M. J. Wornat, B. G. Porter, N. Y. C. Yang, Single droplet combustion of biomass pyrolysis oils, Energy & Fuels 8 (5) (1994) 1131–1142. doi:10.1021/ef00047a018.
URL https://doi.org/10.1021/ef00047a018

[20] C. Branca, C. Di Blasi, C. Russo, Devolatilization in the temperature range 300-600 K of liquids derived from wood pyrolysis and gasification, Fuel

84 (1) (2005) 37–45. doi:10.1016/j.fuel.2004.07.007.
URL https://doi.org/10.1016/j.fuel.2004.07.007

[21] C. Branca, C. D. Blasi, R. Elefante, Devolatilization of conventional pyrolysis oils generated from biomass and cellulose, Energy & Fuels 20 (5) (2006) 2253–2261. doi:10.1021/ef0601059.
URL https://doi.org/10.1021/ef0601059

[22] M. García-Pérez, P. Lappas, P. Hughes, L. Dell, A. Chaala, D. Kretschmer, C. Roy, Evaporation and combustion characteristics of biomass vacuum pyrolysis oils, IFRF Combustion Journal (200601).
URL https://ifrf.net/research/archive/evaporation-and-combustion-characteristics-of-biomass-vacuum-pyrolysis-oils/

[23] R. Calabria, F. Chiariello, P. Massoli, Combustion fundamentals of pyrolysis oil based fuels, Experimental Thermal and Fluid Science 31 (5) (2007) 413–420. doi:10.1016/j.expthermflusci.2006.04.010.
URL https://doi.org/10.1016/j.expthermflusci.2006.04.010

[24] L. Li, X. Yin, C. Wu, L. Ma, Z. Zhou, Kinetic studies on the pyrolysis and combustion of bio-oil, in: Proceedings of the ISES World Congress 2007, 18-21 September 2007, Beijing, China, Beijing, China, 2007.

[25] R. P. B. Ramachandran, G. van Rossum, W. P. M. van Swaaij, S. R. A. Kersten, Evaporation of biomass fast pyrolysis oil: evaluation of char formation, Environmental Progress & Sustainable Energy 28 (3) (2009) 410–417. doi:10.1002/ep.10388.
URL https://doi.org/10.1002/ep.10388

[26] G. van Rossum, Steam reforming and gasification of pyrolysis oil: reactor and process development for syngas production from biomass, Ph.D. Thesis, College voor Promoties, University of Twente, Enschede, The Netherlands (2009). doi:10.3990/1.9789036528894.
URL https://doi.org/10.3990/1.9789036528894

[27] G. van Rossum, B. M. Güell, B. R. P. Ramachandran, K. Seshan, L. Lefferts, W. P. M. Van Swaaij, S. R. A. Kersten, Evaporation of pyrolysis oil: product distribution and residue char analysis, AIChE Journal (2010) 2200–2210doi:10.1002/aic.12126.
URL https://doi.org/10.1002/aic.12126

[28] C. Branca, C. Di Blasi, Combustion kinetics of secondary biomass chars in the kinetic regime, Energy & Fuels 24 (10) (2010) 5741–5750. doi:10.1021/ef100952x.
URL https://doi.org/10.1021/ef100952x

[29] Y. Chhiti, S. Salvador, J.-M. Commandré, F. Broust, Thermal decomposition of bio-oil: focus on the products yields under different pyrolysis conditions, Fuel 102 (2012) 274–281. doi:10.1016/j.fuel.2012.06.098.
URL https://doi.org/10.1016/j.fuel.2012.06.098

[30] M. Beran, L.-U. Axelsson, Development and experimental investigation of a tubular combustor for pyrolysis oil burning, Journal of Engineering for Gas Turbines and Power 137 (3) (2015) 031508. doi:10.1115/1.4028450.
URL https://doi.org/10.1115/1.4028450

[31] P. Stoesser, J. Ruf, R. Gupta, N. Djordjevic, T. Kolb, Contribution to the understanding of secondary pyrolysis of biomass-based slurry under entrained-flow gasification conditions, Energy & Fuels 30 (8) (2016) 6448–6457. doi:10.1021/acs.energyfuels.6b00935.
URL https://doi.org/10.1021/acs.energyfuels.6b00935

[32] P. Stösser, Investigation of solid-phase processes during the conversion of biogenic slurry in entrained-flow gasifiers, Ph.D. Thesis, Fakultät für Chemieingenieurwesen und Verfahrenstechnik, Karlsruher Institut für Technologie, Karlsruhe, Germany (Mar. 2020).

[33] A. V. Bridgwater (Ed.), Progress in thermochemical biomass conversion,

Wiley, Oxford, UK [et al.], 2001. doi:10.1002/9780470694954.
URL https://doi.org/10.1002/9780470694954

[34] A. E. Harman-Ware, J. R. Ferrell, Methods and challenges in the determination of molecular weight metrics of bio-oils, Energy & Fuels 32 (9) (2018) 8905–8920. doi:10.1021/acs.energyfuels.8b02113.
URL https://doi.org/10.1021/acs.energyfuels.8b02113

[35] A. Oasmaa, D. Meier, Norms and standards for fast pyrolysis liquids, Journal of Analytical and Applied Pyrolysis 73 (2) (2005) 323–334. doi:10.1016/j.jaap.2005.03.003.
URL https://doi.org/10.1016/j.jaap.2005.03.003

[36] D. C. Elliott, A. Oasmaa, F. Preto, D. Meier, A. V. Bridgwater, Results of the IEA round robin on viscosity and stability of fast pyrolysis bio-oils, Energy & Fuels 26 (6) (2012) 3769–3776. doi:10.1021/ef300384t.
URL https://doi.org/10.1021/ef300384t

[37] D. C. Elliott, A. Oasmaa, D. Meier, F. Preto, A. V. Bridgwater, Results of the IEA round robin on viscosity and aging of fast pyrolysis bio-oils: long-term tests and repeatability, Energy & Fuels 26 (12) (2012) 7362–7366. doi:10.1021/ef301607v.
URL https://doi.org/10.1021/ef301607v

[38] J. W. McKinley, R. P. Overend, D. C. Elliott, The ultimate analysis of biomass liquefaction products: the results of the IEA round robin, in: Proceedings of the Biomass Pyrolysis Oil Properties and Combustion Meeting, 26-28 September 1994, Estes Park, CO, USA, National Renewable Energy Laboratory, Estes Park, CO, USA, 1994, pp. 34–53.

[39] D. Meier, New methods for chemical and physical characterization and round robin testing, in: S. Czernik, J. Diebold, D. Meier, A. Oasmaa, C. Peacocke, J. Piskorz, D. Radlein, A. V. Bridgwater (Eds.), Fast pyrolysis of biomass: a handbook, CPL Press, Newbury, UK, 1999, pp. 92–101.

[40] L. Zhang, S.-C. Kong, Multicomponent vaporization modeling of bio-oil and its mixtures with other fuels, Fuel 95 (2012) 471–480. doi:10.1016/j.fuel.2011.12.009.
URL https://doi.org/10.1016/j.fuel.2011.12.009

[41] K. Saha, E. Abu-Ramadan, X. Li, Multicomponent evaporation model for pure and blended biodiesel droplets in high temperature convective environment, Applied Energy 93 (2012) 71–79. doi:10.1016/j.apenergy.2011.05.034.
URL https://doi.org/10.1016/j.apenergy.2011.05.034

[42] J. L. H. P. Sallevelt, A. K. Pozarlik, G. Brem, Numerical study of pyrolysis oil combustion in an industrial gas turbine, Energy Conversion and Management 127 (2016) 504–514. doi:10.1016/j.enconman.2016.09.029.
URL https://doi.org/10.1016/j.enconman.2016.09.029

[43] A. H. Mahmoudi, A. K. Pozarlik, E. van der Weide, S. R. A. Kersten, S. Luding, G. Brem, Effect of char on the combustion process of multicomponent bio-fuel, Chemical Engineering Science 175 (2018) 286–295. doi:10.1016/j.ces.2017.09.053.
URL https://doi.org/10.1016/j.ces.2017.09.053

[44] C. Sital, Pyrolysis oil evaporation including liquid phase polymerization reaction, Master's Thesis, Faculty of Mechanical, Maritime and Materials Engineering, Process & Energy Department, Delft University of Technology, Delft, The Netherlands (Oct. 2018).
URL http://resolver.tudelft.nl/uuid:0f355e41-1dab-4369-b83e-f4f5e7379a6c

[45] W. L. H. Hallett, N. A. Clark, A model for the evaporation of biomass pyrolysis oil droplets, Fuel 85 (4) (2006) 532–544. doi:10.1016/j.fuel.2005.08.006.
URL https://doi.org/10.1016/j.fuel.2005.08.006

[46] Y. Houminer, S. Patai, Thermal polymerization of levoglucosan, Journal of Polymer Science, Part A-1: Polymer Chemistry 7 (10) (1969) 3005–3014. doi:10.1002/pol.1969.150071020.
URL https://doi.org/10.1002/pol.1969.150071020

[47] K. G. Joback, A unified approach to physical property estimation using multivariate statistical techniques, Ph.D. Thesis, Department of Chemical Engineering, Massachusetts Institute of Technology, Cambridge, MA, USA (Jun. 1984).
URL http://hdl.handle.net/1721.1/15374

[48] K. G. Joback, R. C. Reid, Estimation of pure-component properties from group-contributions, Chemical Engineering Communications 57 (1-6) (1987) 233–243. doi:10.1080/00986448708960487.
URL https://doi.org/10.1080/00986448708960487

[49] L. Constantinou, R. Gani, New group contribution method for estimating properties of pure compounds, AIChE Journal 40 (10) (1994) 1697–1710. doi:10.1002/aic.690401011.
URL https://doi.org/10.1002/aic.690401011

[50] V. Růžička, E. S. Domalski, Estimation of the heat capacities of organic liquids as a function of temperature using group additivity. I. Hydrocarbon compounds, Journal of Physical and Chemical Reference Data 22 (3) (1993) 597–618. doi:10.1063/1.555923.
URL https://doi.org/10.1063/1.555923

[51] H. Yang, S. Kudo, H.-P. Kuo, K. Norinaga, A. Mori, O. Mašek, J.-i. Hayashi, Estimation of enthalpy of bio-oil vapor and heat required for pyrolysis of biomass, Energy & Fuels 27 (5) (2013) 2675–2686. doi:10.1021/ef400199z.
URL https://doi.org/10.1021/ef400199z

[52] Karlsruhe Institute of Technology, bioliq (2021).
URL https://www.bioliq.de

[53] S. Fleck, U. Santo, C. Hotz, T. Jakobs, G. Eckel, M. Mancini, R. Weber, T. Kolb, Entrained flow gasification. Part 1: gasification of glycol in an atmospheric-pressure experimental rig, Fuel 217 (2018) 306–319. doi:10.1016/j.fuel.2017.12.077.
URL https://doi.org/10.1016/j.fuel.2017.12.077

[54] M. Haas, M. Dammann, S. Fleck, T. Kolb, Entrained flow gasification: impact of fuel spray distribution on reaction zone structure, Fuel 334 (2023) 126572. doi:10.1016/j.fuel.2022.126572.
URL https://doi.org/10.1016/j.fuel.2022.126572

[55] M. Dammann, U. Santo, D. Böning, H. Knoch, M. Eberhard, T. Kolb, Entrained flow gasification: pilot-scale experimental, balancing and equilibrium data for model validation, Fuel, Part A 382 (2025) 132809. doi:10.1016/j.fuel.2024.132809.
URL https://doi.org/10.1016/j.fuel.2024.132809

[56] M. Eberhard, U. Santo, B. Michelfelder, A. Günther, P. Weigand, J. Matthes, P. Waibel, V. Hagenmeyer, T. Kolb, The bioliq® Entrained Flow Gasifier: a model for the German Energiewende, ChemBioEng Reviews 7 (4) (2020) 106–118. doi:10.1002/cben.202000006.
URL https://doi.org/10.1002/cben.202000006

[57] U. Santo, D. Böning, M. Eberhard, H. Schmid, T. Kolb, Entrained flow gasification: experiments and balancing for design and scale-up, in: Proceedings of the 30th Deutscher Flammentag: für nachhaltige Verbrennung, 28-29 September 2021, Hannover-Garbsen, Germany, Deutsche Vereinigung für Verbrennungsforschung and The Combustion Institute Deutsche Sektion, Hannover-Garbsen, Germany, 2021. doi:10.5445/IR/1000139705.
URL https://doi.org/10.5445/IR/1000139705

[58] T. Müller, A. Sänger, P. Habisreuther, T. Jakobs, D. Trimis, T. Kolb, N. Zarzalis, Simulation of the primary breakup of a high-viscosity liquid

jet by a coaxial annular gas flow, International Journal of Multiphase Flow 87 (2016) 212–228. doi:10.1016/j.ijmultiphaseflow.2016.09.008.
URL https://doi.org/10.1016/j.ijmultiphaseflow.2016.09.008

[59] M. Mancini, M. Alberti, M. Dammann, U. Santo, G. Eckel, T. Kolb, R. Weber, Entrained flow gasification. Part 2: mathematical modeling of the gasifier using RANS method, Fuel 225 (2018) 596–611. doi:10.1016/j.fuel.2018.03.100.
URL https://doi.org/10.1016/j.fuel.2018.03.100

[60] F. Zhang, T. Zirwes, T. Müller, S. Wachter, T. Jakobs, P. Habisreuther, N. Zarzalis, D. Trimis, T. Kolb, Effect of elevated pressure on air-assisted primary atomization of coaxial liquid jets: basic research for entrained flow gasification, Renewable and Sustainable Energy Reviews 134 (2020) 110411. doi:10.1016/j.rser.2020.110411.
URL https://doi.org/10.1016/j.rser.2020.110411

[61] M. Dammann, M. Mancini, R. Weber, T. Kolb, Entrained flow gasification: mathematical modelling based on RANS for design and scale-up, in: Proceedings of the 30th Deutscher Flammentag: für nachhaltige Verbrennung, 28-29 September 2021, Hannover-Garbsen, Germany, Deutsche Vereinigung für Verbrennungsforschung and The Combustion Institute Deutsche Sektion, Hannover-Garbsen, Germany, 2021. doi:10.5445/IR/1000140359.
URL https://doi.org/10.5445/IR/1000140359

[62] M. Dammann, M. Mancini, T. Kolb, R. Weber, Thermal radiation at high-temperature and high-pressure conditions: comparison of models for design and scale-up of entrained flow gasification processes, Thermal Sciences and Engineering Progress 40 (2023) 101772. doi:10.1016/j.tsep.2023.101772.
URL https://doi.org/10.1016/j.tsep.2023.101772

[63] M. Dammann, Numerical modelling and simulation of atmospheric

entrained flow gasification of surrogate fuels, Ph.D. Thesis, Fakultät für Chemieingenieurwesen und Verfahrenstechnik, Karlsruher Institut für Technologie, Karlsruhe, Germany (2024). doi:10.5445/IR/1000172116.
URL https://doi.org/10.5445/IR/1000172116

[64] S. Wachter, T. Jakobs, T. Kolb, Effect of solid particles on droplet size applying the time-shift method for spray investigation, Applied Sciences 10 (21) (2020) 7615. doi:10.3390/app10217615.
URL https://doi.org/10.3390/app10217615

[65] proFagus (2021). [link].
URL https://profagus.de

[66] M. Dammann, S. C. Walker, M. Mancini, T. Kolb, Devolatilisation of beech wood char: kinetics from thermogravimetric and drop-tube reactor experiments, Fuel 375 (2024) 131967. doi:10.1016/j.fuel.2024.131967.
URL https://doi.org/10.1016/j.fuel.2024.131967

[67] G. Eckel, P. Le Clercq, T. Kathrotia, A. Saenger, S. Fleck, M. Mancini, T. Kolb, M. Aigner, Entrained flow gasification. Part 3: insight into the injector near-field by large eddy simulation with detailed chemistry, Fuel 223 (2018) 164–178. doi:10.1016/j.fuel.2018.02.176.
URL https://doi.org/10.1016/j.fuel.2018.02.176

[68] DIN Deutsches Institut für Normung, DIN 51900-2:2003-03. Prüfung fester und flüssiger Brennstoffe. Bestimmung des Brennwertes mit dem Bomben-Kalorimeter und Berechnung des Heizwertes. Teil 2: Verfahren mit isoperibolem oder static-jacket Kalorimeter (Mar. 2003).

[69] W. Boie, Vom Brennstoff zum Rauchgas: feuerungstechnisches Rechnen mit Brennstoffkenngrössen und seine Vereinfachung mit Mitteln der Statistik, Teubner, Leipzig, Germany, 1957.

[70] C. Higman, M. van der Burgt, Gasification, 2nd Edition, Gulf Professional Publishing, Burlington, MA, USA, 2008. doi:10.1016/

b978-0-7506-8528-3.x0001-6.
URL https://doi.org/10.1016/b978-0-7506-8528-3.x0001-6

[71] DIN Deutsches Institut für Normung, DIN 51732:2007-08. Prüfung fester Brennstoffe. Bestimmung des Gesamtgehaltes an Kohlenstoff, Wasserstoff und Stickstoff. Instrumentelle Methoden (Aug. 2007).

[72] DIN Deutsches Institut für Normung, DIN 51777:2020-04. Mineralölerzeugnisse. Bestimmung des Wassergehaltes durch Titration nach Karl Fischer (Apr. 2020).

[73] DIN Deutsches Institut für Normung, DIN 51900-1:2000-04. Prüfung fester und flüssiger Brennstoffe. Bestimmung des Brennwertes mit dem Bomben-Kalorimeter und Berechnung des Heizwertes. Teil 1: Allgemeine Angaben, Grundgeräte, Grundverfahren (Apr. 2000).

[74] ASTM International, ASTM D86-20a. Standard test method for distillation of petroleum products and liquid fuels at atmospheric pressure (2020). doi:10.1520/D0086-20A.
URL https://doi.org/10.1520/D0086-20A

[75] T. J. Bruno, Improvements in the measurement of distillation curves. 1. A composition-explicit approach, Industrial & Engineering Chemistry Research 45 (12) (2006) 4371–4380. doi:10.1021/ie051393j.
URL https://doi.org/10.1021/ie051393j

[76] A. M. Ferris, D. A. Rothamer, Methodology for the experimental measurement of vapor-liquid equilibrium distillation curves using a modified ASTM D86 setup, Fuel 182 (2016) 467–479. doi:10.1016/j.fuel.2016.05.099.
URL https://doi.org/10.1016/j.fuel.2016.05.099

[77] J. Cai, W. Wu, R. Liu, An overview of distributed activation energy model and its application in the pyrolysis of lignocellulosic biomass, Renewable and Sustainable Energy Reviews 36 (2014) 236–246. doi:10.1016/j.rser.

2014.04.052.
URL https://doi.org/10.1016/j.rser.2014.04.052

[78] P. Virtanen, R. Gommers, T. E. Oliphant, M. Haberland, T. Reddy, D. Cournapeau, E. Burovski, P. Peterson, W. Weckesser, J. Bright, S. J. van der Walt, M. Brett, J. Wilson, K. J. Millman, N. Mayorov, A. R. J. Nelson, E. Jones, R. Kern, E. Larson, C. J. Carey, İ. Polat, Y. Feng, E. W. Moore, J. VanderPlas, D. Laxalde, J. Perktold, R. Cimrman, I. Henriksen, E. A. Quintero, C. R. Harris, A. M. Archibald, A. H. Ribeiro, F. Pedregosa, P. van Mulbregt, SciPy 1.0 Contributors, SciPy 1.0: fundamental algorithms for scientific computing in Python, Nature Methods 17 (2020) 261–272. doi:10.1038/s41592-019-0686-2.
URL https://doi.org/10.1038/s41592-019-0686-2

[79] SciPy Developers, SciPy. Release 1.5.1, https://pypi.org/project/scipy/ (2021).
URL https://pypi.org/project/scipy/

[80] A. C. Hindmarsh, ODEPACK, a systematized collection of ODE solvers, IMACS Transactions of Scientific computing 1 (1983) 55–64.

[81] L. Petzold, Automatic selection of methods for solving stiff and nonstiff systems of ordinary differential equations, SIAM Journal on Scientific and Statistical Computing 4 (1) (1983) 136–148. doi:10.1137/0904010.
URL https://doi.org/10.1137/0904010

[82] MathWorks, MATLAB. Release 2019b (2019).

[83] B. E. Poling, J. M. Prausnitz, J. P. O'Connell, The properties of gases and liquids, 5th Edition, McGraw-Hill, New York, NY, USA, 2001.

[84] DIN Deutsches Institut für Normung, DIN EN ISO 1183-1:2019-09. Kunststoffe. Verfahren zur Bestimmung der Dichte von nicht verschäumten Kunststoffen. Teil 1: Eintauchverfahren, Verfahren

mit Flüssigkeitspyknometer und Titrationsverfahren (ISO 1183-1:2019, korrigierte Fassung 2019-05) (Sep. 2019).

[85] ASTM International, ASTM D7896-19. Standard test method for thermal conductivity, thermal diffusivity, and volumetric heat capacity of engine coolants and related fluids by transient hot wire liquid thermal conductivity method (2019). doi:10.1520/D7896-19.
URL https://doi.org/10.1520/D7896-19

[86] ASTM International, ASTM D2766-95. Standard test method for specific heat of liquids and solids (2017). doi:10.1520/D2766-95.
URL https://doi.org/10.1520/D2766-95

[87] ASTM International, ASTM D4052-18a. Standard test method for density, relative density, and API gravity of liquids by digital density meter (2018). doi:10.1520/D4052-18A.
URL https://doi.org/10.1520/D4052-18A

[88] DIN Deutsches Institut für Normung, DIN EN ISO 3219:1994-10. Kunststoffe/Polymere/Harze in flüssigem, emulgiertem oder dispergiertem Zustand. Bestimmung der Viskosität mit einem Rotationsviskosimeter bei definiertem Geschwindigkeitsgefälle (Oct. 1994).

[89] Y. S. Choi, P. A. Johnston, R. C. Brown, B. H. Shanks, K.-h. Lee, Detailed characterization of red oak-derived pyrolysis oil: Integrated use of GC, HPLC, IC, GPC and Karl-Fischer, Journal of Analytical and Applied Pyrolysis 110 (2014) 147–154. doi:10.1016/j.jaap.2014.08.016.
URL http://dx.doi.org/10.1016/j.jaap.2014.08.016

[90] L. Ingram, D. Mohan, M. Bricka, P. Steele, D. Strobel, D. Crocker, B. Mitchell, J. Mohammad, K. Cantrell, C. U. Pittman, Pyrolysis of wood and bark in an auger reactor: physical properties and chemical analysis of the produced bio-oils, Energy & Fuels 22 (1) (2007) 614–625. doi:10.1021/ef700335k.
URL https://doi.org/10.1021/ef700335k

[91] L. Jampolski, M. T. Morgano, H. Seifert, T. Kolb, N. Willenbacher, Flow behavior and aging of pyrolysis oils from different feedstocks, Energy & Fuels 31 (5) (2017) 5165–5173. doi:10.1021/acs.energyfuels.7b00196.
URL https://doi.org/10.1021/acs.energyfuels.7b00196

[92] A. Turgut, I. Tavman, S. Tavman, Measurement of thermal conductivity of edible oils using transient hot wire method, International Journal of Food Properties 12 (4) (2009) 741–747. doi:10.1080/10942910802023242.
URL https://doi.org/10.1080/10942910802023242

[93] D. Merrick, Mathematical models of the thermal decomposition of coal. 2. Specific heats and heats of reaction, Fuel 62 (5) (1983) 540–546. doi:10.1016/0016-2361(83)90223-5.
URL https://doi.org/10.1016/0016-2361(83)90223-5

[94] N. Dahmen, J. Abeln, M. Eberhard, T. Kolb, H. Leibold, J. Sauer, D. Stapf, B. Zimmerlin, The bioliq process for producing synthetic transportation fuels, WIREs Energy and Environment 6 (3). doi:10.1002/wene.236.
URL https://doi.org/10.1002/wene.236

[95] K. Miura, T. Maki, A simple method for estimating f(E) and k0(E) in the distributed activation energy model, Energy & Fuels 12 (5) (1998) 864–869. doi:10.1021/ef970212q.
URL https://doi.org/10.1021/ef970212q

Characterisation of beech wood pyrolysis oil: chemical and physical properties and decomposition kinetics

Maximilian Dammann[a,b,c,*], Fabian Hüsing[a,b], Ulrike Santo[b], David Böning[b], Marco Mancini[c], Thomas Kolb[a,b]

[a] *Karlsruhe Institute of Technology (KIT), Engler-Bunte-Institute, Fuel Technology (EBI ceb), Engler-Bunte-Ring 1, 76131 Karlsruhe, Germany*
[b] *Karlsruhe Institute of Technology (KIT), Institute for Technical Chemistry, Gasification Technology (ITC vgt), Hermann-von-Helmholtz-Platz 1, 76344 Eggenstein-Leopoldshafen, Germany*
[c] *Clausthal University of Technology, Institute for Energy Process Engineering and Fuel Technology (IEVB), Agricolastraße 4, 38678 Clausthal-Zellerfeld, Germany*

Nomenclature

Latin symbols

A	coefficient
$\hat{C}_p$	specific isobaric heat capacity
D	diffusion coefficient
$\dot{H}$	enthalpy flow rate
M	molar mass
n	coefficient
p	generic physical property
$\dot{Q}$	heat flow rate
r	volume fraction
T	temperature
$\overline{V}$	molar volume
w	mass fraction

*Corresponding author.
ORCID: https://orcid.org/0000-0002-2851-7787.

$\boldsymbol{w}$	mass fraction vector
X	conversion
Greek symbols	
η	dynamic viscosity
λ	thermal conductivity
ρ	density
ϕ	association factor
Subscripts and superscripts	
ash	of ash
asr	on as-received basis
Boie	based on the Boie correlation
boil	boiling
d	on dry basis
i	of species i
j	of (mixture) j, in (mixture) j
ng	of natural gas
oil	of the beech wood pyrolysis oil
part	particle
S1, S2 or S3	of surrogate S1, S2 or S3
slurry	of slurry
steam	of steam
tot	total
0	initial
β	recovered
Acronyms	

bdl	below detection limit
CAS	Chemical Abstracts Service
DTG	differential thermogravimetric
EXT I, II or III	external laboratory I, II or III
GC-MS	gas chromatography-mass spectrometry
GPC	gel permeation chromatography
HHV	higher heating value
KIT	Karlsruhe Institute of Technology
KIT I, II or III	KIT laboratory I, II or III
LHV	lower heating value
MFORALM	multi first-order reaction Arrhenius law model
MFORGDAEM	multi first-order reaction Gauss distributed activation energy model
MRALM	multi-reaction Arrhenius law model
TG	thermogravimetric

S1. Supplementary data

S1.1. Introduction

Table S1: Previous studies on conversion of biogenic pyrolysis oils.

Study	Details
Vitolo and Ghetti [1]	TG analyses (25 K/min, up to 1273 K) of unhydrogenated and hydrogenated biogenic pyrolysis oils under nitrogen and air atmospheres to investigate the impact of hydrogenation on the chemical and physical properties
Wornat et al. [2]	Single-droplet experiments (320 µm, 1600 K) with oak and pine pyrolysis oils to investigate single-droplet combustion behaviour
Branca et al. [3, 4, 5, 6, 7]	TG analyses (5-20 K/min, up to 873 K) of several biogenic pyrolysis oils from research and commercial pyrolysis processes under air atmospheres to derive kinetics
García-Pérez et al. [8]	Laminar entrained flow reactor experiments (58-62 µm, 973/1073 K) with softwood bark residue and hardwood bark residue pyrolysis oils and under argon and argon-oxygen atmospheres to analyse the morphology of both the droplets during conversion and the residues
Calabria et al. [9]	Single-droplet experiments (300-1200 µm, 573-1473 K) with forest residue pyrolysis oil to investigate both droplet temperature and droplet diameter during combustion

Study	Details
van Rossum et al. [10, 11]	Experiments in a heated atomisation reactor ($\geq 10^5$ K/min, 88-117 µm, 823-1123 K), a thermogravimetric analyser (1/10/100 K/min, 1073 K) and a batch reactor (823 K) with pine wood pyrolysis oil under inert atmospheres to investigate the impact of the heating rate on the yields of gas, vapour and char and on the reativity of residues
Ramachandran et al. [12]	Experiments in a heated atomisation reactor ($\geq 10^5$ K/min, 88-117 µm, 773-1123 K) and a thermogravimetric analyser (10 K/min, 1073 K) with forest-residue pyrolysis oils to investigate the char yields at different heating rates and different water concentrations
Branca et al. [13]	TG analyses (5-15 K/min, up to 873 K) of milled secondary pyrolysis oil chars under air atmospheres to derive kinetics
Chhiti et al. [14]	Experiments in a tubular reactor (2 K/s, 823 K) and in a high-temperature entrained flow reactor (2000 K/s, 1273 K) under nitrogen atmospheres to study the impact of both the heating rate and the ash content on the yields of gas, tar and char
Beran and Axelsson [15]	Experiments in an atmospheric-pressure tubular combustor with pyrolysis oil to investigate combustion behaviour (e. g. spray quality, emissions)
Stösser et al. [16]	DSC experiments with wood-derived pyrolysis oil at pressures between 1 bar and 40 bar to investigate char yields
Stösser et al. [16]	Drop-tube furnace experiments (1273 K) with wood and straw pyrolysis oils under nitrogen atmospheres to collect solid residues and soot for morphology and reactivity analysis

S1.2. Methods

Table S2: Data derived for the beech wood pyrolysis oil, the vacuum distillate and the vacuum distillation residue.

Data	Beech wood pyrolysis oil	Vacuum distillate of the beech wood pyrolysis oil	Vacuum distillation residue of the beech wood pyrolysis oil
Elemental, ash and water contents	X		
Heating values	X		
Engler distillation curves	X	X	
GC-MS data	X		
GPC data	X		
TG and DTG curves	X	X	X
Density at 288 K	X		
Density up to 453 K	X	X	
Thermal conductivity up to 453 K	X	X	
Specific heat capacity up to 453 K	X	X	
Dynamic viscosity at 293 K	X		
Dynamic viscosity up to 373 K	X		X
Surface tension at 293 K	X		

Table S3: Standards used for the chemical analyses of the beech wood pyrolysis oil at the laboratories EXT I and EXT II.

Analysis	Laboratory EXT I	Laboratory EXT II
C, H, N	DIN 51732:2007 [17]	DIN 51732:2007 [17]
S	DIN EN 15289:2011 [18]	–
Cl	DIN 51727:2001 [19]	–
Water	DIN 51777:2020 [20]	DIN 51777:2020 [20]
Ash	DIN 51719:1997 [21]	–
HHV	DIN 51900-2:2003 [22]	–

Table S4: Standards used for the chemical analyses of the beech wood pyrolysis oil at the laboratories KIT I, KIT II and KIT III.

Analysis	Laboratory KIT I/III	Laboratory KIT II
C, H, N	DIN EN ISO 16948:2015 [23]	DIN EN 15104 [24]
S	DIN EN ISO 16994:2016 [25]	–
Water	DIN ISO 3733:2003 [26]	DIN 51777:2020 [20]
Ash	DIN 51719:1997 [21]	DIN 51719:1997 [21]
HHV	DIN 51900-2:2003 [22]	DIN 51900-2:2003 [22]

Table S5: Standards used for the thermo-physical property measurements of the beech wood pyrolysis oil and the vacuum distillate at the laboratories EXT I and EXT III.

Measurement	Laboratory EXT I	Laboratory EXT III
Density	ASTM D4052-18a [27]	Based on DIN EN ISO 1183-1:2019 [28]
Specific heat capacity	–	ASTM D2766-95 [29]
Thermal conductivity	–	ASTM D7896-19 [30]
Dynamic viscosity	DIN EN ISO 3219:1994 [31]	–

S1.3. Results

Table S6: Compositions of the beech wood pyrolysis oil in mass fractions on as-received basis (asr) based on various chemical analysis results. Repeatability and reproducibility limits are given according to DIN 51732:2007 [17] and DIN 51777:2020 [20].

Laboratory	$w_{\mathrm{C,oil,asr}}$	$w_{\mathrm{H,oil,asr}}$	$w_{\mathrm{N,oil,asr}}$	$w_{\mathrm{S,oil,asr}}$	$w_{\mathrm{Cl,oil,asr}}$	$w_{\mathrm{ash,oil,asr}}$	$w_{\mathrm{H_2O,oil,asr}}$
KIT I	0.5805	0.0544	bdl	bdl	–	–	0.0706
KIT II	0.5690	0.0589	–	–	–	–	0.0700
KIT III	0.5853	0.0603	0.0020	–	–	0.0001	0.0829
EXT I	0.5780	0.0650	0.0016	0.0002	< 0.00005	0.0010	0.0520
EXT II	0.5693	0.0726	0.0021	–	–	–	0.0560
Repeatability limit	±0.0040 (abs.)	±0.0010 (abs.)	±0.0006 (abs.)	–	–	–	±0.0195 (rel.)
Reproducibility limit	±0.0185 (abs.)	±0.0040 (abs.)	±0.0017 (abs.)	–	–	–	±0.067 (rel.)

Table S7: Compositions of the beech wood pyrolysis oil in mass fractions on dry basis (d) based on various chemical analysis results.

Laboratory	$w_{\mathrm{C,oil,d}}$	$w_{\mathrm{H,oil,d}}$	$w_{\mathrm{N,oil,d}}$	$w_{\mathrm{S,oil,d}}$	$w_{\mathrm{Cl,oil,d}}$	$w_{\mathrm{ash,oil,d}}$
KIT I	0.6246	0.0585	bdl	bdl	–	–
KIT II	0.6118	0.0633	–	–	–	–
KIT III	0.6382	0.0658	0.0022	–	–	0.0001
EXT I	0.6097	0.0686	0.0017	0.0002	< 0.00006	0.0010
EXT II	0.6031	0.0769	0.0022	–	–	–

Table S8: Lower heating values and higher heating values of the beech wood pyrolysis oil on as-received basis (asr) and dry basis (d) based on various chemical analysis results. Repeatability and reproducibility limits are given according to DIN 51900-1:2000 [32].

Laboratory	$\frac{\mathrm{LHV_{oil,asr}}}{\mathrm{kJ/kg}}$	$\frac{\mathrm{HHV_{oil,asr}}}{\mathrm{kJ/kg}}$	$\frac{\mathrm{LHV_{oil,d}}}{\mathrm{kJ/kg}}$	$\frac{\mathrm{HHV_{oil,d}}}{\mathrm{kJ/kg}}$
KIT I	22823	24182	24728	26019
KIT II	22392	23848	24261	25643
KIT III	22678	24197	24752	26384
EXT I	22686	24212	24053	25530
EXT II	–	–	–	–
Repeatability limit	–	–	–	±140
Reproducibility limit	–	–	–	±400

Table S9: Lower heating values and higher heating values of the beech wood pyrolysis oil based on the Boie correlation [33] on as-received basis (asr) and Boie ratios $\mathrm{HHV_{Boie,oil,asr}}/\mathrm{HHV_{oil,asr}}$.

Laboratory	$\frac{\mathrm{LHV_{Boie,oil,asr}}}{\mathrm{kJ/kg}}$	$\frac{\mathrm{HHV_{Boie,oil,asr}}}{\mathrm{kJ/kg}}$	$\frac{\mathrm{HHV_{Boie,oil,asr}}}{\mathrm{HHV_{oil,asr}}} \Big/ \%$
KIT I	23344	21972	96.5
KIT II	23418	21949	98.2
KIT III	24481	22950	101.2
EXT I	24415	22855	100.8
EXT II	25017	23820	–

Table S10: Components in the beech wood pyrolysis oil and their mass fractions (related to the sample mass) based on two GC-MS analysis results.

	Group	Component	CAS number	Molecular formula	$\frac{M}{\text{g/mol}}$	w / %	
						I	II
1	Acids	acetic acid	64-19-7	$C_2H_4O_2$	60.05	6.271	6.340
2		propionic acid	79-09-4	$C_3H_6O_2$	74.08	5.473	5.518
3	Non-aromatic ketones	acetol or hydroxyacetone	116-09-6	$C_3H_6O_2$	74.08	1.676	1.809
4		1-hydroxy-2-butanone	5077-67-8	$C_4H_8O_2$	88.11	0.414	0.425
5		1-acetyloxy-propan-2-one	592-20-1	C_5H_6O	116.12	0.079	0.078
6		2-cyclopenten-1-one	930-30-3	C_5H_6O	82.10	0.065	0.068
7		2-methyl-2-cyclopenten-1-one	1120-73-6	C_6H_8O	96.13	0.076	0.083
8		3-methyl-2-cyclopenten-1-one	2758-18-1	C_6H_8O	96.13	0.137	0.144
9		2-hydroxy-1-methyl-1-cyclopenten-3-one	80-71-7	$C_6H_8O_2$	112.13	1.106	1.178
10	Furans	2(5H)-furanone	497-23-4	$C_4H_4O_2$	84.07	0.126	0.135
11		2-furaldehyde	98-01-1	$C_5H_4O_2$	96.08	0.211	0.222
12		2,5-dihydro-3,5-dimethyl-furan-2-one	5584-69-0	$C_6H_8O_2$	112.13	0.203	0.216
13		γ-butyrolactone	96-48-0	$C_4H_6O_2$	86.09	0.419	0.445

	Group	Component	CAS number	Molecular formula	$\frac{M}{\text{g/mol}}$	w / %	
						I	II
14	Benzenes	3,4-dimethoxytoluene	494-99-5	$C_9H_{12}O_2$	152.19	0.038	0.039
15		naphthalene	91-20-3	$C_{10}H_8$	128.17	0.058	0.060
16		1-methylnaphthalene	90-12-0	$C_{11}H_{10}$	142.20	0.194	0.189
17		2-methylnaphthalene	91-57-6	$C_{11}H_{10}$	142.20	0.062	0.059
18	Lignin derived phenols	phenol	108-95-2	C_6H_6O	94.11	0.209	0.219
19		o-cresol	95-48-7	C_7H_8O	108.14	0.348	0.362
20		p-cresol	106-44-5	C_7H_8O	108.14	0.101	0.106
21		m-cresol	108-39-4	C_7H_8O	108.14	0.246	0.325
22		2,5-dimethylphenol	95-87-4	$C_8H_{10}O$	122.16	0.168	0.171
23		2,4-dimethylphenol	105-67-9	$C_8H_{10}O$	122.16	0.084	0.085
24		2,3-dimethylphenol	526-75-0	$C_8H_{10}O$	122.16	0.041	0.044
25		3,5-dimethylphenol	108-68-9	$C_8H_{10}O$	122.16	0.059	0.061
26		3-ethylphenol	620-17-7	$C_8H_{10}O$	122.16	0.127	0.128
27		4-ethylphenol	123-07-9	$C_8H_{10}O$	122.16	0.021	0.021

	Group	Component	CAS number	Molecular formula	$\frac{M}{\text{g/mol}}$	w / %	
						I	II
28	Methoxy phenols	guaiacol	90-05-1	$C_7H_8O_2$	124.14	0.588	0.634
29		3-methylguaiacol	18102-31-3	$C_8H_{10}O_2$	138.16	0.061	0.072
30		4-methylguaiacol	93-51-6	$C_8H_{10}O_2$	138.16	0.706	0.715
31		3-ethylguaiacol	–	$C_9H_{12}O_2$	152.19	0.097	0.093
32		4-ethylguaiacol	2785-89-9	$C_9H_{12}O_2$	152.19	0.569	0.582
33		eugenol or 4-allyl-guaiacol	97-53-0	$C_{10}H_{12}O_2$	164.20	0.101	0.112
34		4-propylguaiacol	2785-87-7	$C_{10}H_{14}O_2$	166.22	0.164	0.176
35		isoeugenol (cis)	97-54-1	$C_{10}H_{12}O_2$	164.20	0.153	0.157
36		isoeugenol (trans)	5932-68-3	$C_{10}H_{12}O_2$	164.20	0.471	0.478
37		guaiacylacetone	2503-46-0	$C_{10}H_{12}O_3$	180.20	0.217	0.244

	Group	Component	CAS number	Molecular formula	M / g/mol	w / %	
						I	II
38	Dimethoxy phenols	syringol	91-10-1	$C_8H_{10}O_3$	154.16	3.460	3.542
39		4-methylsyringol	6638-05-7	$C_9H_{12}O_3$	168.19	2.718	2.754
40		4-ethylsyringol	14059-92-8	$C_{10}H_{14}O_3$	182.22	1.757	1.814
41		4-propylsyringol	6766-82-1	$C_{11}H_{16}O_3$	196.24	1.063	1.085
42		4-cis-1-propenylsyringol	26624-13-5	$C_{11}H_{14}O_3$	194.23	0.278	0.281
43		4-trans-1-propenylsyringol	20675-95-0	$C_{11}H_{14}O_3$	194.23	1.115	1.181
44		acetosyringone	2478-38-8	$C_{10}H_{12}O_4$	196.20	0.246	0.276
45		propiosyringone	5650-43-1	$C_{11}H_{14}O_4$	210.23	0.143	0.148
46		syringylacetone	112468-41-4	$C_{11}H_{14}O_4$	210.23	0.454	0.479
47	Carbohydrates	levoglucosan	498-07-7	$C_6H_{10}O_5$	162.14	2.729	2.916
48		1,4:3,6-dianhydro-α-D-glucopyranose	–	$C_6H_8O_4$	144.13	0.763	0.819
49		anhydrosugar unknown (unspecific spectrum)	–	–	–	2.262	2.487
$\sum$						38.125	39.574

S1.4. Discussion

Table S11: Feed and heat extraction data of the bioliq EFG experiment V105: enthalpy flow rates of slurry $\dot{H}_{\mathrm{slurry}}$, enthalpy flow rates of natural gas $\dot{H}_{\mathrm{ng}}$, enthalpy flow rate of steam $\dot{H}_{\mathrm{steam}}$, enthalpy flow rates of O_2 $\dot{H}_{O_2}$, enthalpy flow rates of N_2 $\dot{H}_{N_2}$ and total heat flow rates $\dot{Q}_{\mathrm{tot}}$ based on measurements and balancing. Reference conditions: 1 bar and 298.15 K.

Experiment	$\frac{\dot{H}_{\mathrm{slurry}}}{\mathrm{kW}}$	$\frac{\dot{H}_{\mathrm{ng}}}{\mathrm{kW}}$	$\frac{\dot{H}_{\mathrm{steam}}}{\mathrm{kW}}$	$\frac{\dot{H}_{O_2}}{\mathrm{kW}}$	$\frac{\dot{H}_{N_2}}{\mathrm{kW}}$	$\frac{\dot{Q}_{\mathrm{tot}}}{\mathrm{kW}}$
V105 (KIT I)	4782.9	|	|	|	|	|
V105 (KIT II)	4429.6	|	|	|	|	|
V105 (KIT III)	4785.8	497.8	31.1	21.7	−2.0	651.9
V105 (EXT I)	4487.7	|	|	|	|	|
V105 (EXT II)	4944.6	|	|	|	|	|

Table S12: Adjusted initial mass fractions $\boldsymbol{w}_0 = (w_i)$ for the multi-reaction Arrhenius law model (MRALM), the multi first-order reaction Arrhenius law model (MFORALM) and the multi first-order reaction Gauss distributed activation energy model (MFORGDAEM) at high heating rates.

i	$w_{0,i}$		
	MRALM	MFORLAM	MFORGDAEM
1	$3.041\,737 \cdot 10^{-1}$	0	$2.0 \cdot 10^{-2}$
2	$6.858\,263 \cdot 10^{-1}$	1	0
3	0	0	$9.8 \cdot 10^{-1}$
4	0	0	–

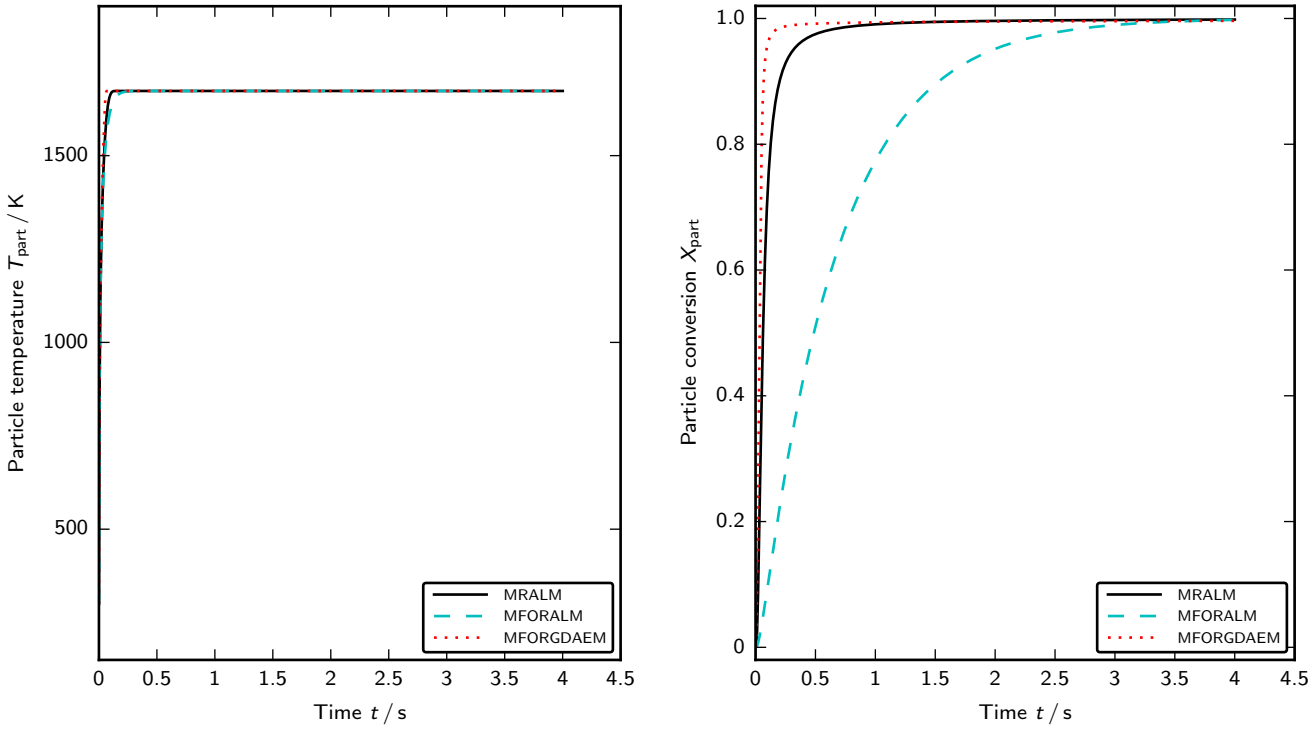

Figure S1: Predicted particle temperatures T_{part} (left) and predicted particle conversions X_{part} (right) using the multi-reaction Arrhenius law model (MRALM), the multi first-order reaction Arrhenius law model (MFORALM) and the multi first-order reaction Gauss distributed activation energy model (MFORGDAEM) for test case 2 but with 50 µm as particle diameter.

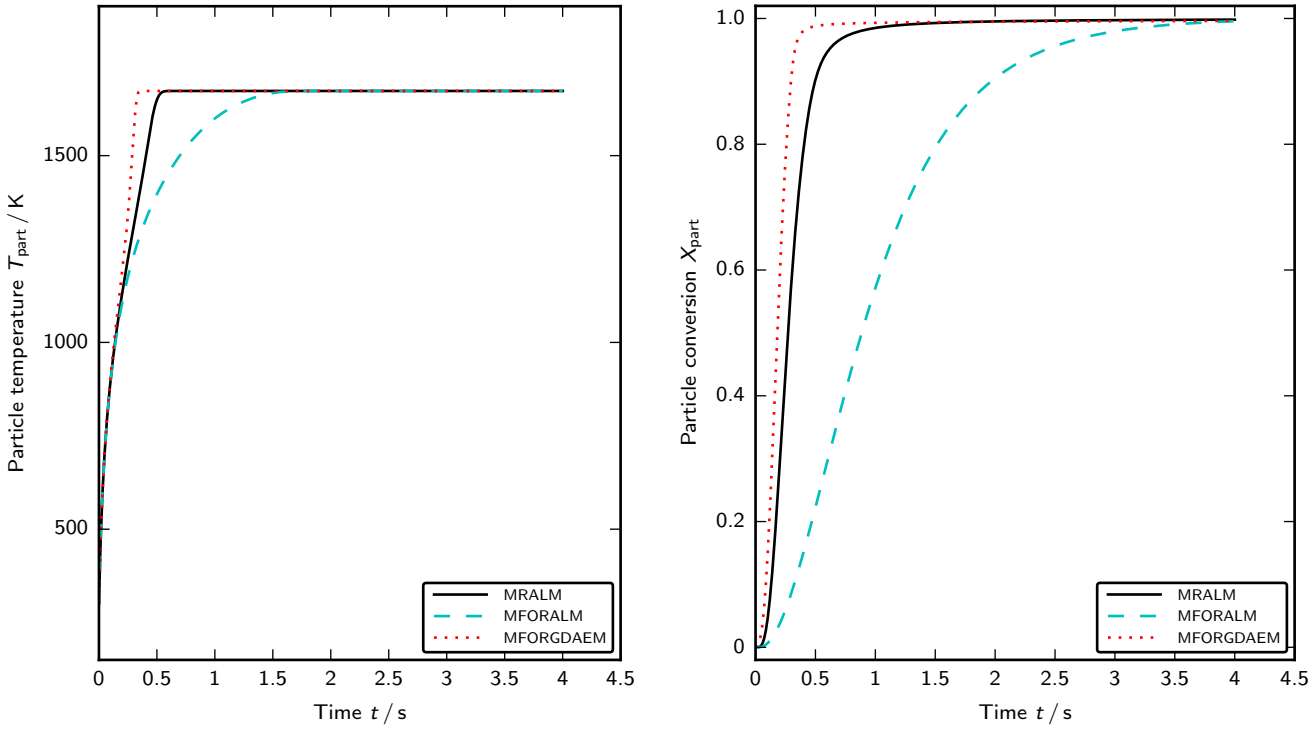

Figure S2: Predicted particle temperatures T_{part} (left) and predicted particle conversions X_{part} (right) using the multi-reaction Arrhenius law model (MRALM), the multi first-order reaction Arrhenius law model (MFORALM) and the multi first-order reaction Gauss distributed activation energy model (MFORGDAEM) for test case 2 but with 200 µm as particle diameter.

S2. Fractional distillation curves

S2.1. Fractional distillation curves

Fractional distillation curves were determined using the GC-MS data and boiling temperatures based on the databases of Aspen Properties [34] and on the group estimation method of Nannoolal et al. [35].

S2.2. Fractional distillation curves

Fractional distillation curves based on the GC-MS data of the beech wood pyrolysis oil samples are shown in Fig. S3. Even though restricted by the accuracy of the measured or estimated boiling temperatures, the curves are similar and demonstrate that the GC-MS data could be reproduced with good accuracy.

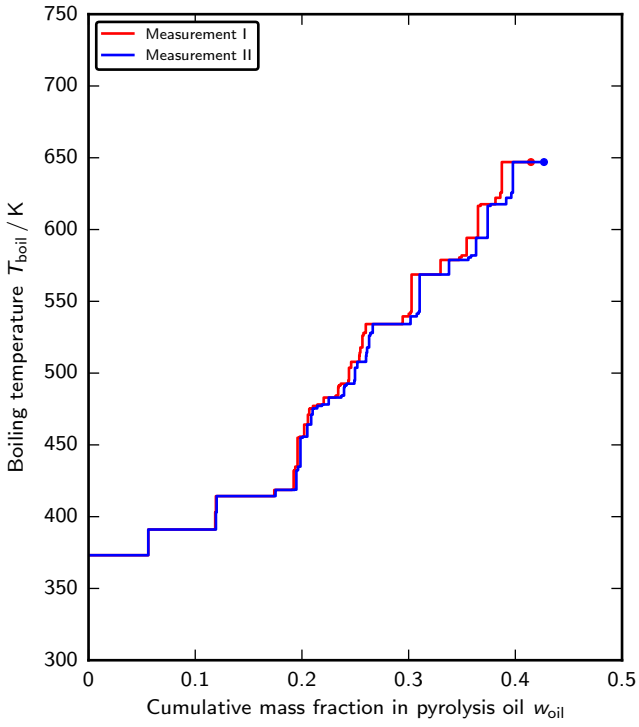

Figure S3: Flash distillation curves of the beech wood pyrolysis oil based on the GC-MS analyses: predictions for two single measurements.

S3. Physical properties of derivative products

S3.1. Methods

Simplified models are typically applied to calculate physical properties at intermediate conversion states. For example, the generic physical property p can be determined by [36]

$$p = p|_{X=0}\,(1 - X) + p|_{X=1}\,X\,, \tag{S1}$$

where the generic physical properties before conversion $p|_{X=0}$ and after complete conversion $p|_{X=1}$ are described by the properties of the raw material and the completely converted material, respectively. This approach can be adopted for the physical properties of the derivate products of the beech wood pyrolysis oil in a first approximation. The physical properties of the raw material are given by the physical properties of the beech wood pyrolysis oil (see Section 4.8), while the physical properties of the material after complete conversion at high heating rates and high temperatures are described by the physical properties of graphite [37], assuming similar compositions of the solid residues [16].

S3.2. Results

The specific heat capacity $\hat{C}_p$ at intermediate conversion states was calculated assuming significant conversion between 530 K and 890 K (based on a regularised incomplete beta function for the conversion X) and is shown in Fig. S4. The specific heat capacity $\hat{C}_p$ thus might increase up to 630 K during conversion before it decreases to the specific heat capacity of graphite.

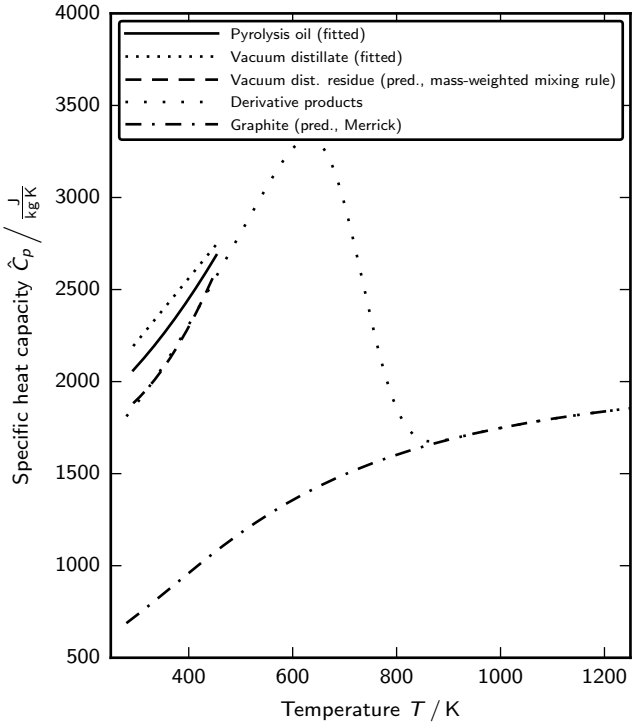

Figure S4: Specific heat capacity of the derivate products of the beech wood pyrolysis oil. Note the abbreviation: pred.: predicted.

S4. Surrogates

Four surrogates were defined for the vacuum distillate using the GC-MS data (see Table S10). The surrogates S1, S2 and S3 were specified accounting for representative species of each of the seven major chemical classes (see Fig. 2 and Table S10). The compositions of the surrogates S1, S2 and S3 are given in Table S13. In addition to that, the surrogate S4 was defined based on the normalised GC-MS data (see Table S10).

Table S13: Compositions of the surrogates S1, S2 and S3 in mass fractions $\boldsymbol{w} = (w_i)$.

i		$w_{i,\mathrm{S1}}$	$w_{i,\mathrm{S2}}$	$w_{i,\mathrm{S3}}$
CAS number	Name			
7732-18-5	water	0.149034	0.148324	0.148605
64-19-7	acetic acid	0.312140	0.311232	0.310924
90-05-1	guaiacol	–	0.082959	0.082820
91-10-1	syringol	0.298034	–	–
97-53-0	eugenol	0.083615	0.300506	–
97-54-1	isoeugenol	–	–	0.300914
98-01-1	furfural	0.025724	0.025454	0.025366
108-95-2	phenol	0.037099	0.037133	0.037116
116-09-6	acetol	0.094354	0.094392	0.094255

Engler distillation curves and thermo-physical properties of the surrogates were subsequently determined to analyse the representativeness of the surrogates through comparison with the measured data of the vacuum distillate (see Sections 4.5 and 4.8). The Engler distillation curves are compared in Section S4.1, while the thermo-physical properties are presented in Section S4.2.

S4.1. Engler distillations

Engler distillation curves were determined for the surrogates S1, S2 and S3 following ASTM D86-20a [38] (see Section 3.6). The Engler distillation curves are shown alongside the Engler distillation curve of the vacuum distillate in Fig. S5.

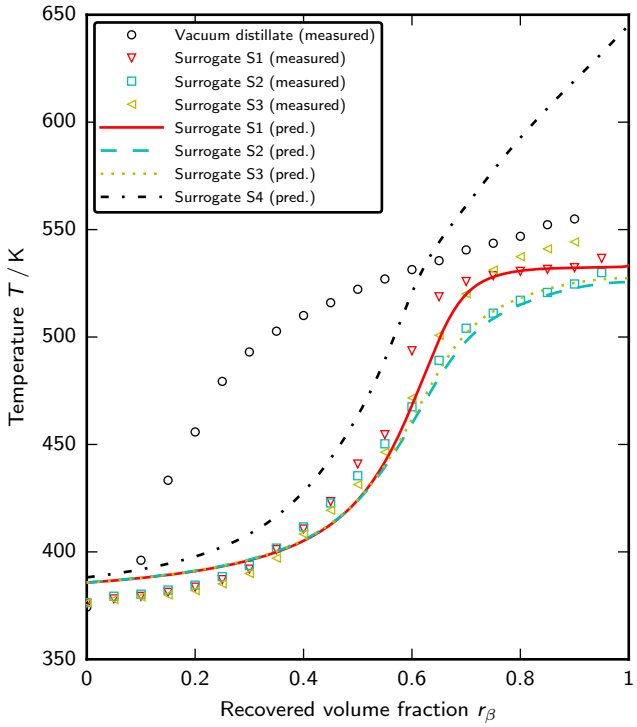

Figure S5: Engler distillation curves of the vacuum distillate and the surrogates. Note the abbreviation: pred.: predicted.

The curves of the surrogates S1, S2 and S3 have similar shapes but differ from the curve of the vacuum distillate. For further analysis, numerical equilibrium distillation curves were calculated using the methods and databases of Aspen Properties [34], the group contribution methods of Constantionou and Gani [39], the Lee-Kessler equation [40], the Racket equation [41] and the Raoult model. The curves calculated for the surrogates S1, S2, S3 and S4 are

shown in Fig. S5. Firstly, the curves predicted for the surrogates S1, S2 and S3 have similar shapes, whereas the curve calculated for the surrogate fuel S4 shows faster boiling behaviour. In addition, the boiling temperatures of the surrogate fuel S4 are higher above recovered mass fractions of 60 % compared to the boiling temperatures of the surrogates S1, S2 and S3. Secondly, the curves predicted for the surrogates S1, S2 and S3 are only in fair agreement with the experimental ones. The deviations are due to the deficiencies of both the Engler distillation method [42, 43] and the physical property models. The deviations can partially be reduced for recovered volume fractions below 50 % if numerical equilibrium distillation curves are determined using the UNIFAC model [44, 45, 46]. Thirdly, the Engler distillation curve of the vacuum distillate strongly deviates from the numerical equilibrium distillation curves of the surrogates. This is because of (i) the deficiencies of both the Engler distillation method [42, 43] and the physical property models, (ii) the limitations of the GC-MS analysis (see Sections 3.3 and 4.2) and (iii) the loss of volatiles during vacuum distillation (see Section 4.4). Future studies may reduce this knowledge gap.

S4.2. Thermo physical properties

Densities ρ, thermal conductivities λ and specific heat capacities $\hat{C}_p$ of the surrogates S1, S2, S3 and S4 were determined using the methods and databases of Aspen Properties [34], the group contributions methods of Constantinou and Gani [39], the Tee correlations [47], the Chapman-Enkskog equations [41], the corresponding-states equation of Bondi [48] and the common mixing rules. The thermo-physical properties of the surrogates were calculated by

$$\rho_j = \left(\sum_i \frac{w_{i,j}}{\rho_i} \right)^{-1} , \tag{S2}$$

$$\lambda_j = \left(\sum_i \frac{w_{i,j}}{\lambda_i^2} \right)^{-1/2} , \tag{S3}$$

$$\hat{C}_{p,j} = \sum_i w_{i,j} \, \hat{C}_{p,i} \, , \tag{S4}$$

where $j = \mathrm{S1}, \mathrm{S2}, \mathrm{S3}, \mathrm{S4}$, $w_{i,j}$ is the mass fraction of species i in the surrogate j and ρ_i, λ_i and $\hat{C}_{p,i}$ are the liquid density, the liquid thermal conductivity and the liquid specific heat capacity of species i, respectively.

The calculated densities ρ, the calculated thermal conductivities λ and the calculated specific heat capacities $\hat{C}_p$ of the surrogates are compared with the measured density ρ, the measured thermal conductivity λ and the measured specific heat capacities $\hat{C}_p$ of the vacuum distillate in Figs. S6, S7 and S8. In addition, measured ambient densities of the surrogates S1, S2 and S3 based on ASTM D4052-18a [27] (see Section 3.9.2) are shown in Fig. S6.

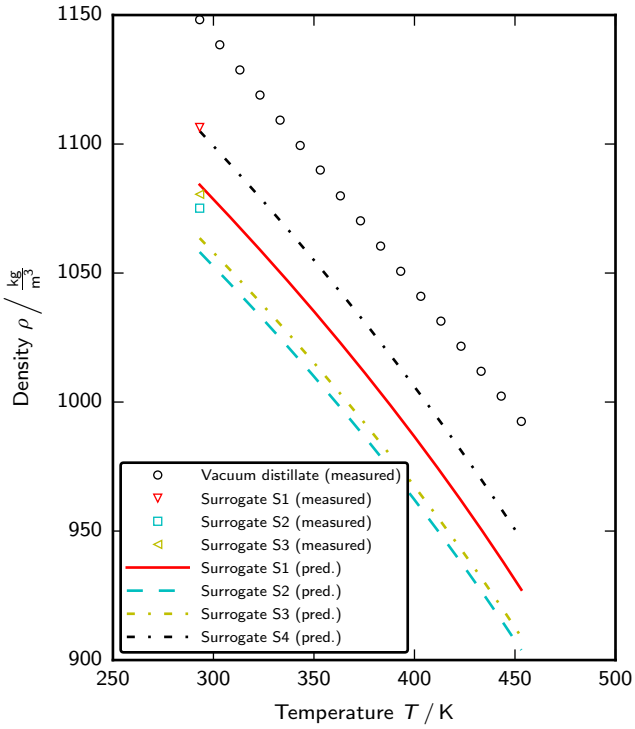

Figure S6: Densities of the vacuum distillate and the surrogates. Note the abbreviation: pred.: predicted.

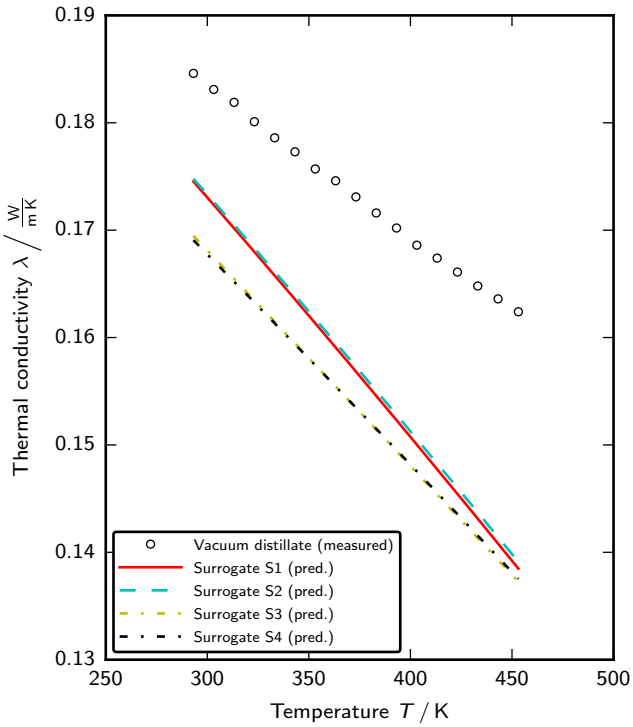

Figure S7: Thermal conductivities of the vacuum distillate and the surrogates. Note the abbreviation: pred.: predicted.

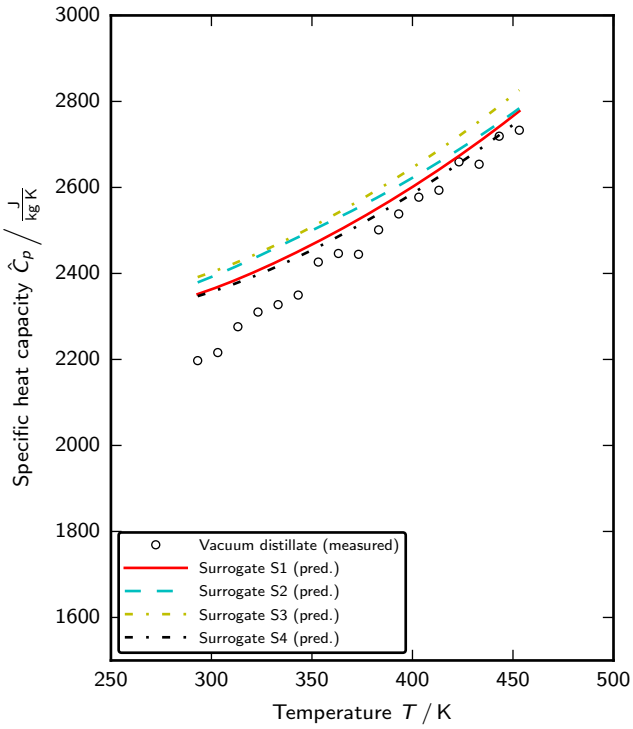

Figure S8: Specific heat capacities of the vacuum distillate and the surrogates. Note the abbreviation: pred.: predicted.

First, the relative deviations between the measured densities of the surrogates under ambient conditions and the calculated ones are up to 2 %. This indicates that the accuracy of the physical property models is partially not sufficient, as the measured densities have low uncertainties (see Section 4.8.1). Then, the calculated densities ρ and the calculated thermal conductivities λ are in poor agreement with the measured data. Moreover, larger deviations between the measured and the calculated specific heat capacities are found at temperatures below 350 K. The surrogate models cannot reflect the measured physical properties of the vacuum distillate. Future studies should revise both the physical property models and the definitions of the surrogates.

S5. Diffusion coefficients

Measurements of diffusion coefficients for the beech wood pyrolysis oil were beyond the objective of this study, in particular in the absence of accurate correlations for diffusion coefficients in multi-component liquids. Available approximations for diffusion coefficients D in liquids are usually based on [41]

$$D \propto \frac{(T/\mathrm{K})^m}{(\eta/\mathrm{mPa\,s})^n}\,\frac{\mathrm{m}^2}{\mathrm{s}}\,, \tag{S5}$$

where T is the temperature and η is the liquid dynamic viscosity and m and n are coefficients. m varies between 1 and 1.5, while n is typically between 0.5 and 1. For example, Hiss and Cussler [49] described the diffusion coefficient D of species i by

$$D_i = A_i \frac{T/\mathrm{K}}{(\eta/\mathrm{mPa\,s})^{2/3}}\,\frac{\mathrm{m}^2}{\mathrm{s}}\,, \tag{S6}$$

where A_i is a customised coefficient for species i. Similarly, Grimaldos Aguilar [50] recently correlated measured diffusion coefficients of toluene, n-pentane and n-heptane in viscous bitumen and maltenes under atmospheric-pressure conditions and suggested approximations based on

$$D_i = A_i\,\frac{(T/\mathrm{K})}{(\eta/\mathrm{mPa\,s})^{n_i}}\,\frac{\mathrm{m}^2}{\mathrm{s}}\,, \tag{S7}$$

where A_i and n_i are experimentally determined coefficients for species i.

Previous studies on droplet experiments with pyrolysis oils or heavy fuels [2, 51, 52] reported boiling phenomena, enrichment of heavy hydrocarbons, polymerisation and micro-explosions inside of droplets. This suggests that diffusion coefficients in pyrolysis oils are quite low. To affirm this hypothesis, diffusion coefficients were calculated using the Perkins-Geankoplis equation [41, 53]. This equation is based on the Wilke-Chang equation [54] and is given by

$$D_i = 7.4\cdot 10^{-12}\,\frac{\left(\sum_{j\neq i}\frac{\phi_j\,M_j}{\mathrm{kg/mol}}\right)^{1/2}\left(\frac{T}{\mathrm{K}}\right)}{\frac{\eta}{\mathrm{mPa\,s}}\,\frac{\overline{V}_{i,\mathrm{boil}}}{\mathrm{cm}^3/\mathrm{mol}}}\,\frac{\mathrm{m}^2}{\mathrm{s}}\,, \tag{S8}$$

where ϕ_j is an association factor of species j, M_j is the molar mass of species j, T is the temperature, η is the liquid dynamic viscosity and $\overline{V}_{i,\mathrm{boil}}$ is the molar liquid volume of species i at boiling temperature. The association factors depend on the solvent and have been determined for a few species only [41, 54] or have to be estimated [55].

Assuming that the vaporisable fraction of the pyrolysis oil can be approximated with the surrogate S1, diffusion coefficients were calculated using the dynamic viscosity of the beech wood pyrolysis oil η_{oil}. The results are shown in Fig. S9 and are compared with the effective diffusion coefficients of the species of the surrogate S1, obtained using the Grunberg-Nissan mixing rule [56] and the physical property methods and databases of Aspen Properties [34] for the liquid dynamic viscosities of the species. In addition, predictions based on the Hiss-Cussler correlation with two different proportionality factors and predictions based on correlations of Grimaldos Aguilar [50] are shown in Fig. S9.

The comparison of the different approximations suggests that the diffusion coefficients in the vacuum distillates are similar to diffusion coefficients in typical multi-component liquids, while the diffusion coefficients in pyrolysis oils might be similar to diffusion coefficients in bitumen or maltenes. Thus, the diffusion coefficients in pyrolysis oils are likely three magnitudes lower than in typical multi-component liquids. This affirms the hypothesis and previous experimental observations but challenges modelling efforts and simulations using simplified well-mixed and diffusion-limited approaches.

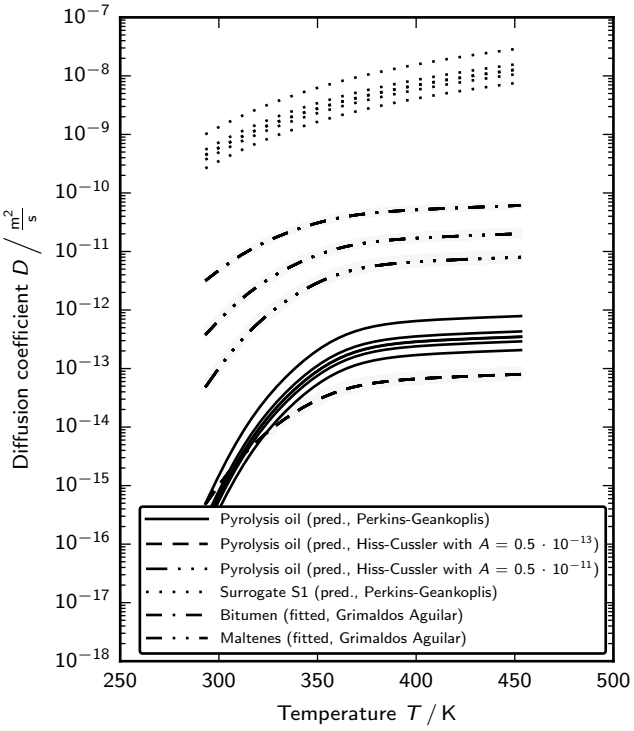

Figure S9: Diffusion coefficients in beech wood pyrolysis oils: comparison of various approximations. Note the abbreviation: pred.: predicted.

References

[1] S. Vitolo, P. Ghetti, Physical and combustion characterization of pyrolytic oils derived from biomass material upgraded by catalytic hydrogenation, Fuel 73 (11) (1994) 1810–1812. doi:10.1016/0016-2361(94)90175-9.
URL https://doi.org/10.1016/0016-2361(94)90175-9

[2] M. J. Wornat, B. G. Porter, N. Y. C. Yang, Single droplet combustion of biomass pyrolysis oils, Energy & Fuels 8 (5) (1994) 1131–1142. doi:10.1021/ef00047a018.
URL https://doi.org/10.1021/ef00047a018

[3] C. Branca, P. Giudicianni, C. Di Blasi, GC/MS characterization of liquids generated from low-temperature pyrolysis of wood, Industrial & Engineering Chemistry Research 42 (14) (2003) 3190–3202. doi:10.1021/ie030066d.
URL https://doi.org/10.1021/ie030066d

[4] C. Branca, C. Di Blasi, R. Elefante, Devolatilization and heterogeneous combustion of wood fast pyrolysis oils, Industrial & Engineering Chemistry Research 44 (4) (2005) 799–810. doi:10.1021/ie049419e.
URL https://doi.org/10.1021/ie049419e

[5] C. Branca, C. Di Blasi, Multistep mechanism for the devolatilization of biomass fast pyrolysis oils, Industrial & Engineering Chemistry Research 45 (17) (2006) 5891–5899. doi:10.1021/ie060161x.
URL https://doi.org/10.1021/ie060161x

[6] C. Branca, C. Di Blasi, C. Russo, Devolatilization in the temperature range 300-600 K of liquids derived from wood pyrolysis and gasification, Fuel 84 (1) (2005) 37–45. doi:10.1016/j.fuel.2004.07.007.
URL https://doi.org/10.1016/j.fuel.2004.07.007

[7] C. Branca, C. D. Blasi, R. Elefante, Devolatilization of conventional pyrolysis oils generated from biomass and cellulose, Energy & Fuels 20 (5) (2006) 2253–2261. doi:10.1021/ef0601059.
URL https://doi.org/10.1021/ef0601059

[8] M. García-Pérez, P. Lappas, P. Hughes, L. Dell, A. Chaala, D. Kretschmer, C. Roy, Evaporation and combustion characteristics of biomass vacuum pyrolysis oils, IFRF Combustion Journal (200601).
URL https://ifrf.net/research/archive/evaporation-and-combustion-characteristics-of-biomass-vacuum-pyrolysis-oils/

[9] R. Calabria, F. Chiariello, P. Massoli, Combustion fundamentals of pyrolysis oil based fuels, Experimental Thermal and Fluid Science 31 (5)

(2007) 413–420. doi:10.1016/j.expthermflusci.2006.04.010.
URL https://doi.org/10.1016/j.expthermflusci.2006.04.010

[10] G. van Rossum, Steam reforming and gasification of pyrolysis oil: reactor and process development for syngas production from biomass, Ph.D. Thesis, College voor Promoties, University of Twente, Enschede, The Netherlands (2009). doi:10.3990/1.9789036528894.
URL https://doi.org/10.3990/1.9789036528894

[11] G. van Rossum, B. M. Güell, B. R. P. Ramachandran, K. Seshan, L. Lefferts, W. P. M. Van Swaaij, S. R. A. Kersten, Evaporation of pyrolysis oil: product distribution and residue char analysis, AIChE Journal (2010) 2200–2210doi:10.1002/aic.12126.
URL https://doi.org/10.1002/aic.12126

[12] R. P. B. Ramachandran, G. van Rossum, W. P. M. van Swaaij, S. R. A. Kersten, Evaporation of biomass fast pyrolysis oil: evaluation of char formation, Environmental Progress & Sustainable Energy 28 (3) (2009) 410–417. doi:10.1002/ep.10388.
URL https://doi.org/10.1002/ep.10388

[13] C. Branca, C. Di Blasi, Combustion kinetics of secondary biomass chars in the kinetic regime, Energy & Fuels 24 (10) (2010) 5741–5750. doi:10.1021/ef100952x.
URL https://doi.org/10.1021/ef100952x

[14] Y. Chhiti, S. Salvador, J.-M. Commandré, F. Broust, Thermal decomposition of bio-oil: focus on the products yields under different pyrolysis conditions, Fuel 102 (2012) 274–281. doi:10.1016/j.fuel.2012.06.098.
URL https://doi.org/10.1016/j.fuel.2012.06.098

[15] M. Beran, L.-U. Axelsson, Development and experimental investigation of a tubular combustor for pyrolysis oil burning, Journal of Engineering for

Gas Turbines and Power 137 (3) (2015) 031508. doi:10.1115/1.4028450.
URL https://doi.org/10.1115/1.4028450

[16] P. Stoesser, J. Ruf, R. Gupta, N. Djordjevic, T. Kolb, Contribution to the understanding of secondary pyrolysis of biomass-based slurry under entrained-flow gasification conditions, Energy & Fuels 30 (8) (2016) 6448–6457. doi:10.1021/acs.energyfuels.6b00935.
URL https://doi.org/10.1021/acs.energyfuels.6b00935

[17] DIN Deutsches Institut für Normung, DIN 51732:2007-08. Prüfung fester Brennstoffe. Bestimmung des Gesamtgehaltes an Kohlenstoff, Wasserstoff und Stickstoff. Instrumentelle Methoden (Aug. 2007).

[18] DIN Deutsches Institut für Normung, DIN EN 15289:2011-04. Feste Biobrennstoffe. Bestimmung des Gesamtgehaltes an Schwefel und Chlor (Apr. 2011).

[19] DIN Deutsches Institut für Normung, DIN 51727:2001-06. Prüfung fester Brennstoffe. Bestimmung des Chlorgehaltes (Jun. 2001).

[20] DIN Deutsches Institut für Normung, DIN 51777:2020-04. Mineralölerzeugnisse. Bestimmung des Wassergehaltes durch Titration nach Karl Fischer (Apr. 2020).

[21] DIN Deutsches Institut für Normung, DIN 51719:1997-07. Prüfung fester Brennstoffe. Bestimmung des Aschegehaltes (Jul. 1997).

[22] DIN Deutsches Institut für Normung, DIN 51900-2:2003-03. Prüfung fester und flüssiger Brennstoffe. Bestimmung des Brennwertes mit dem Bomben-Kalorimeter und Berechnung des Heizwertes. Teil 2: Verfahren mit isoperibolem oder static-jacket Kalorimeter (Mar. 2003).

[23] DIN Deutsches Institut für Normung, DIN EN ISO 16948:2015-09. Biogene Festbrennstoffe. Bestimmung des Gesamtgehaltes an Kohlenstoff, Wasserstoff und Stickstoff (ISO 16948:2015) (Sep. 2015).

[24] DIN Deutsches Institut für Normung, DIN EN 15104:2011-04. Feste Biobrennstoffe. Bestimmung des Gesamtgehaltes an Kohlenstoff, Wasserstoff und Stickstoff. Instrumentelle Verfahren (Apr. 2011).

[25] DIN Deutsches Institut für Normung, DIN EN ISO 16994:2016-12. Biogene Festbrennstoffe. Bestimmung des Gesamtgehaltes an Schwefel und Chlor (ISO 16994:2016) (Dec. 2016).

[26] DIN Deutsches Institut für Normung, DIN ISO 3733:2003-02. Mineralölerzeugnisse und bituminöse Bindemittel. Bestimmung des Wassergehaltes. ISO 3733:1999 (Feb. 2003).

[27] ASTM International, ASTM D4052-18a. Standard test method for density, relative density, and API gravity of liquids by digital density meter (2018). doi:10.1520/D4052-18A.
URL https://doi.org/10.1520/D4052-18A

[28] DIN Deutsches Institut für Normung, DIN EN ISO 1183-1:2019-09. Kunststoffe. Verfahren zur Bestimmung der Dichte von nicht verschäumten Kunststoffen. Teil 1: Eintauchverfahren, Verfahren mit Flüssigkeitspyknometer und Titrationsverfahren (ISO 1183-1:2019, korrigierte Fassung 2019-05) (Sep. 2019).

[29] ASTM International, ASTM D2766-95. Standard test method for specific heat of liquids and solids (2017). doi:10.1520/D2766-95.
URL https://doi.org/10.1520/D2766-95

[30] ASTM International, ASTM D7896-19. Standard test method for thermal conductivity, thermal diffusivity, and volumetric heat capacity of engine coolants and related fluids by transient hot wire liquid thermal conductivity method (2019). doi:10.1520/D7896-19.
URL https://doi.org/10.1520/D7896-19

[31] DIN Deutsches Institut für Normung, DIN EN ISO 3219:1994-10. Kunststoffe/Polymere/Harze in flüssigem, emulgiertem oder dispergiertem

Zustand. Bestimmung der Viskosität mit einem Rotationsviskosimeter bei definiertem Geschwindigkeitsgefälle (Oct. 1994).

[32] DIN Deutsches Institut für Normung, DIN 51900-1:2000-04. Prüfung fester und flüssiger Brennstoffe. Bestimmung des Brennwertes mit dem Bomben-Kalorimeter und Berechnung des Heizwertes. Teil 1: Allgemeine Angaben, Grundgeräte, Grundverfahren (Apr. 2000).

[33] W. Boie, Vom Brennstoff zum Rauchgas: feuerungstechnisches Rechnen mit Brennstoffkenngrössen und seine Vereinfachung mit Mitteln der Statistik, Teubner, Leipzig, Germany, 1957.

[34] Aspen Properties. Release V10 (2017).
URL https://www.aspentech.com/products/aspen-properties.aspx

[35] Y. Nannoolal, J. Rarey, D. Ramjugernath, W. Cordes, Estimation of pure component properties. Part 1: estimation of the normal boiling point of non-electrolyte organic compounds via group contributions and group interactions, Fluid Phase Equilibria 226 (2004) 45–63. doi:10.1016/j.fluid.2004.09.001.
URL https://doi.org/10.1016/j.fluid.2004.09.001

[36] O. Senneca, M. Urciuolo, P. Bareschino, G. Diglio, F. Pepe, R. Chirone, Pyrolysis, combustion, and fragmentation model of coal particles: preliminary results, Combustion Science and Technology 188 (4-5) (2016) 759–768. doi:10.1080/00102202.2016.1138763.
URL https://doi.org/10.1080/00102202.2016.1138763

[37] D. Merrick, Mathematical models of the thermal decomposition of coal. 2. Specific heats and heats of reaction, Fuel 62 (5) (1983) 540–546. doi:10.1016/0016-2361(83)90223-5.
URL https://doi.org/10.1016/0016-2361(83)90223-5

[38] ASTM International, ASTM D86-20a. Standard test method for distillation of petroleum products and liquid fuels at atmospheric pressure (2020). doi:

10.1520/D0086-20A.
URL https://doi.org/10.1520/D0086-20A

[39] L. Constantinou, R. Gani, New group contribution method for estimating properties of pure compounds, AIChE Journal 40 (10) (1994) 1697–1710. doi:10.1002/aic.690401011.
URL https://doi.org/10.1002/aic.690401011

[40] B. I. Lee, M. G. Kesler, A generalized thermodynamic correlation based on three-parameter corresponding states, AIChE Journal 21 (3) (1975) 510–527. doi:10.1002/aic.690210313.
URL https://doi.org/10.1002/aic.690210313

[41] B. E. Poling, J. M. Prausnitz, J. P. O'Connell, The properties of gases and liquids, 5th Edition, McGraw-Hill, New York, NY, USA, 2001.

[42] T. J. Bruno, Improvements in the measurement of distillation curves. 1. A composition-explicit approach, Industrial & Engineering Chemistry Research 45 (12) (2006) 4371–4380. doi:10.1021/ie051393j.
URL https://doi.org/10.1021/ie051393j

[43] A. M. Ferris, D. A. Rothamer, Methodology for the experimental measurement of vapor-liquid equilibrium distillation curves using a modified ASTM D86 setup, Fuel 182 (2016) 467–479. doi:10.1016/j.fuel.2016.05.099.
URL https://doi.org/10.1016/j.fuel.2016.05.099

[44] A. Fredenslund, R. L. Jones, J. M. Prausnitz, Group-contribution estimation of activity coefficients in nonideal liquid mixtures, AIChE Journal 21 (6) (1975) 1086–1099. doi:10.1002/aic.690210607.
URL https://doi.org/10.1002/aic.690210607

[45] A. Fredenslund, Vapor-liquid equilibria using UNIFAC: a group contribution method, 1st Edition, Elsevier Scientific Publishers, Amsterdam, The Netherlands [et al.], 1977.

[46] A. Fredenslund, J. Gmehling, M. L. Michelsen, P. Rasmussen, J. M. Prausnitz, Computerized design of multicomponent distillation columns using the UNIFAC group contribution method for calculation of activity coefficients, Industrial & Engineering Chemistry Process Design and Development 16 (4) (1977) 450–462. doi:10.1021/i260064a004.
URL https://doi.org/10.1021/i260064a004

[47] L. S. Tee, S. Gotoh, W. E. Stewart, Molecular parameters for normal fluids. Lennard-Jones 12-6 potential, Industrial & Engineering Chemistry Fundamentals 5 (3) (1966) 356–363. doi:10.1021/i160019a011.
URL https://doi.org/10.1021/i160019a011

[48] A. Bondi, Physical properties of molecular crystals, liquids, and glasses, 1st Edition, John Wiley & Sons, New York, NY, USA [et al.], 1968.

[49] T. G. Hiss, E. L. Cussler, Diffusion in high viscosity liquids, AIChE Journal 19 (4) (1973) 698–703. doi:10.1002/aic.690190404.

[50] F. A. Grimaldos Aguilar, Measurement of liquid-liquid diffusion in solvent-bitumen systems, Master's Thesis, University of Calgary, Alberta, Calgary, AB, Canada (Nov. 2018).
URL https://www.ucalgary.ca/ENCH/AER/theses/2018MScThesis_FranklinGrimaldos.pdf

[51] J. D'Alessio, M. Lazzaro, P. Massoli, V. Moccia, Thermo-optical investigation of burning biomass pyrolysis oil droplets, Symposium (International) on Combustion 27 (2) (1998) 1915–1922. doi:10.1016/s0082-0784(98)80035-0.

[52] C. R. Shaddix, P. J. Tennison, Effects of char content and simple additives on biomass pyrolysis oil droplet combustion, Symposium (International) on Combustion 27 (2) (1998) 1907–1914. doi:10.1016/s0082-0784(98)80034-9.

[53] L. R. Perkins, C. J. Geankoplis, Molecular diffusion in a ternary liquid system with the diffusing component dilute, Chemical Engineering Science 24 (7) (1969) 1035–1042. doi:10.1016/0009-2509(69)80075-8.
URL https://doi.org/10.1016/0009-2509(69)80075-8

[54] C. R. Wilke, P. Chang, Correlation of diffusion coefficients in dilute solutions, AIChE Journal 1 (2) (1955) 264–270. doi:10.1002/aic.690010222.
URL https://doi.org/10.1002/aic.690010222

[55] Y. Stark, Modellierung der Kondensation von Pyrolysedämpfen unter Berücksichtigung der Aerosolbildung, Ph.D. Thesis, Fakultät für Chemieingenieurwesen und Verfahrenstechnik, Karlsruher Institut für Technologie, Karlsruhe, Germany (May 2020).

[56] L. Grunberg, A. H. Nissan, Mixture law for viscosity, Nature 164 (4175) (1949) 799–800. doi:10.1038/164799b0.
URL https://doi.org/10.1038/164799b0